Anderson Transitions

Ferdinand Evers[1,2] and Alexander D. Mirlin[1,2,3]

[1] *Institut für Nanotechnologie, Forschungszentrum Karlsruhe, 76021 Karlsruhe, Germany*
[2] *Institut für Theorie der Kondensierten Materie, Universität Karlsruhe, 76128 Karlsruhe, Germany*
[3] *Petersburg Nuclear Physics Institute, 188300 St. Petersburg, Russia*

(Dated: February 1, 2008)

The physics of Anderson transitions between localized and metallic phases in disordered systems is reviewed. The term "Anderson transition" is understood in a broad sense, including both metal-insulator transitions and quantum-Hall-type transitions between phases with localized states. The emphasis is put on recent developments, which include: multifractality of critical wave functions, criticality in the power-law random banded matrix model, symmetry classification of disordered electronic systems, mechanisms of criticality in quasi-one-dimensional and two-dimensional systems and survey of corresponding critical theories, network models, and random Dirac Hamiltonians. Analytical approaches are complemented by advanced numerical simulations.

Contents

I. INTRODUCTION

It is known since the seminal work of Anderson (1958) that disorder can localize a quantum particle inspite of quantum tunneling processes and even if the particle is not localized classically. For a given energy and disorder strength the quantum states are either all localized or all delocalized. This implies the existence of transitions between localized and metallic phases in disordered electronic systems, known as *Anderson transitions*. A great progress in understanding of the corresponding physics was achieved in the seventies and the eighties, due to the developments of scaling theory and field-theoretical approaches to localization, which demonstrated connections between the Anderson transition and conventional second-order phase transitions. These results were summarized in several review articles: (Kramer and MacKinnon, 1993; Lee and Ramakrishnan, 1985), and, in the context of the quantum Hall transitions, (Huckestein, 1995), as well as in the book (Efetov, 1997).

During the last ten years considerable progress in the field has been made in several research directions. This has strongly advanced the understanding of the Anderson localization phenomenon and the associated quantum phase transition physics in disordered electronic systems and allows us to view it nowadays in a considerably broader and more general context. These important advances have motivated us in writing the present review. While the article will also include a brief overview of basic earlier results, the main emphasis will be put on recent

developments and, in particular, on novel types of critical systems. In this review we understand the term "Anderson transition" in a broad sense, including not only metal-insulator transitions but also critical points separating phases with localized states (most prominently, quantum-Hall-type transitions).

We now list the key developments in the field that took place during the last decade and constitute the main subject of the review.

A. Symmetry classification and universality classes

Within the early classification scheme, three universality classes for the Anderson transition were identified – orthogonal, unitary, and symplectic – in correspondence with the Wigner-Dyson classification of random matrix theory ensembles. Two basic symmetries of this scheme are the invariance of the Hamiltonian under time reversal and spin rotations. More recent research has shown, however, that this picture is in fact by far incomplete, for two reasons: (i) there exist more symmetry classes of disordered systems, and (ii) in many cases, the symmetry class does not uniquely determine the universality class of the transition.

1. Additional symmetries.

It has been understood that a complete set of random matrix theories includes, in addition to the three Wigner-Dyson classes, three chiral ensembles and four Bogoliubov-de Gennes ensembles. The additional ensembles are characterized by one of the additional symmetries – the *chiral* or the *particle-hole* one. The field theories (σ-models) associated with these new symmetry classes have in fact been considered already in the eighties (Hikami, 1983; Wegner, 1989). However, it was only after their physical significance had been better understood that the new symmetry classes were studied systematically. For the chiral ensembles, important contributions in this direction were made in Gade (1993); Gade and Wegner (1991); Slevin and Nagao (1993); Verbaarschot and Zahed (1993). The particle-hole symmetric ensembles were called into life several years later (Altland and Zirnbauer, 1997). Zirnbauer has also established a relation between random matrix theories, σ-models and Cartan's classification of symmetric spaces (Sec. IV), which provides the mathematical basis for the statement of completeness of the new random matrix classification (Heinzner *et al.*, 2005; Zirnbauer, 1996).

Amongst other things, these developments have led the theorists to predict two novel quantum Hall effects, the spin quantum Hall effect (SQHE) (Kagalovsky *et al.*, 1999; Senthil *et al.*, 1998), Sec. VI.D, and the thermal quantum Hall effect (TQHE) (Chalker *et al.*, 2002; Senthil *et al.*, 1999), Sec. VI.E. Both should occur in materials with paired fermions where the particle-hole

symmetry is realized.

2. From symmetry classes to universality classes

The classification of fixed points governing the localization transitions in disordered metals has turned out to be much richer than that of symmetries of random matrix ensembles (or field theories). The first prominent example of this was in fact given more than 20 years ago by Pruisken (1984) who showed that the quantum Hall transition is described by a σ-model with an additional, topological, term. However, it is only recently that the variety of types of criticality – particularly rich in 2D systems – was fully appreciated:

(i) In several symmetry classes, the field theory (σ-model) allows for inclusion of the topological θ-term (responsible for the quantum Hall criticality) or of the Wess-Zumino (WZ) term.

(ii) The phase diagram may depend on the type of disorder. The class D represents a prominent example, with three different network-model realizations yielding vastly different phase diagrams, Sec. VI.E.

(iii) In some cases, the field theory may possess a line of fixed points, since the coupling constant corresponding to the conductivity is truly marginal. This situation is in particular realized in the chiral symmetry classes BDI, AIII, and CII, Sec. VI.F.

(iv) In some cases, the symmetry of the σ-model may get enhanced under renormalization, so that the ultimate fixed-point theory may have a different form. A paradigm for this behavior is provided by the S^2 sphere σ-model with $\theta = \pi$ topological term (describing a spin-$\frac{1}{2}$ antiferromagnet) which flows into a SU(2) Wess-Zumino-Witten (WZW) model. It was conjectured that a similar mechanism may be relevant to some σ-models of localization, including the critical theory of the integer quantum Hall effect (IQHE).

(v) It is possible that the same critical theory is shared by systems belonging to different symmetry classes. This type of "super-universality" has been proposed to occur in disordered wires with critical states, Sec. V.E, V.F.

(vi) It was recently discovered that Griffiths effects can render the conventional RG analysis of a σ-model insufficient. In the framework of the RG calculations the result can be recovered if infinitely many relevant couplings are kept, Sec. VI.F.2.

3. Many-channel disordered wires

Common wisdom has it that all states in one-dimensional disordered systems are localized. However, for several symmetry classes wires with critical states and even such with perfectly transmitting eigenchannels were identified recently. The emergence of criticality depends crucially on whether the number of channels is even or odd. These developments make a survey of disordered wires (Sec. V) a natural part of this review.

B. Multifractality of wave functions

It was appreciated by the beginning of nineties that wavefunctions at the Anderson transition exhibit strong amplitude fluctuations that can be characterized as wave function multifractality. The corresponding results are summarized in the review papers (Huckestein, 1995; Janßen, 1994) published about a decade ago. In more recent years a considerable progress in the understanding of wave function statistics in metallic samples (Mirlin, 2000b) and at criticality (Evers *et al.*, 2001; Evers and Mirlin, 2000; Mudry *et al.*, 1996) has been achieved. The multifractality implies the presence of infinitely many relevant operators, which is a peculiarity of the Anderson transition critical point, and the spectrum of multifractal exponents constitutes a crucially important characteristics of the fixed point governing the transition. The understanding of general properties of the statistics of critical wave functions and their multifractality (see Sec. II.C) was complemented by a detailed study – analytical as well as numerical – for a number of localization critical points, such as conventional Anderson transition in various dimensionalities, Dirac fermions in a random vector potential, IQHE, SQHE, and symplectic-class Anderson transition in 2D, as well as the power-law random banded matrix model.

In several situations, the characterization of a critical point by its multifractality spectrum has turned out to be particularly important. Specifically, a great deal of recent research activity has been devoted to conformal theories governing Anderson critical points in 2D systems. Further, in systems of the new symmetry classes, peculiar critical points have been found that correspond to strong disorder (Carpentier and LeDoussal, 2001; Motrunich *et al.*, 2002), such that critical wavefunctions show at the same time some kind of localization. Entrance of a system into such a strong-coupling regime manifests itself as a phase transition in the multifractality spectrum (the "freezing transition").

Finally, the notion of multifractality was very recently extended onto a boundary of a critical system, yielding a novel independent set of surface critical exponents. The importance of this notion has been confirmed by analytical and numerical studies of the surface multifractality for several models at criticality (Sec. II.C.8).

C. Quantitative understanding of critical behavior

For several types of Anderson transitions, very detailed studies using both analytical and numerical tools have been performed during the last few years. As a result, a fairly comprehensive quantitative understanding of the localization critical phenomena has been achieved. The

following developments played a particularly important role in this context:

1. Power-law random banded matrix model

An ensemble of power-law random banded matrices (PRBM), which can be viewed as a 1D system with long-range hopping, has been analytically solved on its critical line (Mirlin and Evers, 2000). This allowed, in particular, a detailed study of the statistics of wave functions (in particular, multifractality) and energy levels at criticality. The PRBM model serves as a "toy model" for the Anderson criticality. This model possesses a truly marginal coupling, thus yielding a line of critical points and allowing to study the evolution of critical properties in the whole range from weak- to strong-coupling fixed points.

2. Network models

Formulations of quantum dynamics in terms of network models, pioneered in Chalker and Coddington (1988) in the IQHE context, have been developed and systematically exploited for both analytical studies and computer simulations. Such network models have played a key role in advancement of understanding of Quantum Hall critical points, including the conventional IQHE and the systems of unconventional symmetries – SQHE and TQHE (Chalker et al., 2002; Cho and Fisher, 1997a; Gruzberg et al., 1999; Read and Ludwig, 2001). In particular, the investigation of the network model of SQHE has led to an analytical understanding of the critical behavior of a number of most important physical observables, Sec. VI.D.

3. Progress in numerical simulations

During the last ten years numerical mathematicians have developed highly efficient routines for diagonalizing sparse matrices. Combined with the increase in computer power and an improved understanding of finite size effects, this development has recently paved the way for highly accurate numerical studies of critical behavior for a variety of Anderson critical points.

4. Field theories: σ-models and Dirac fermions

The development of the symmetry classification of disordered systems has allowed to classify also the corresponding field theories having a form of nonlinear σ-models defined on different symmetric spaces. The renormalization-group (RG) method was used to analyze them at and near two dimensions. A complementary approach is based on the analysis of 2D disordered Dirac fermions subjected to different types of dis-

order (Ludwig et al., 1994; Nersesyan et al., 1995). Analytical methods have allowed to identify fixed points and determine the critical behavior for some types of disorder corresponding to unconventional symmetry classes. The interest to the random Dirac fermion models has been largely motivated by their applications to disordered d-wave superconductors, see Altland et al. (2002) for review. Recent breakthrough in the fabrication of monoatomic graphene sheets and corresponding transport measurements (Novoselov et al., 2005, 2004; Zhang et al., 2005) has greatly boosted the theoretical activity in this field.

II. ANDERSON TRANSITIONS IN CONVENTIONAL SYMMETRY CLASSES

A. Scaling theory, observables, and critical behavior

Quantum interference can completely suppress the diffusion of a particle in random potential, a phenomenon known as *Anderson localization* (Anderson, 1958). When the energy or the disorder strength is varied, the system can thus undergo a transition from the metallic phase with delocalized eigenstates to the insulating phase, where eigenfunctions are exponentially localized,

$$|\psi^2(\mathbf{r})| \sim \exp(-|\mathbf{r} - \mathbf{r_0}|/\xi), \qquad (2.1)$$

and ξ is the localization length. The character of this transition remained, however, unclear for roughly 20 years, until Wegner conjectured, developing earlier ideas of Thouless (1974), a close connection between the Anderson transition and the scaling theory of critical phenomena (Wegner, 1976). Three years later, Abrahams, Anderson, Licciardello, and Ramakrishnan formulated a *scaling theory* of localization (Abrahams et al., 1979), which describes the flow of the dimensionless conductance g with the system size L,

$$d \ln g / d \ln L = \beta(g). \qquad (2.2)$$

This phenomenological theory was put on a solid basis after Wegner's discovery of the field-theoretical description of the localization problem in terms of a nonlinear σ-model (Wegner, 1979), Sec. II.B. This paved the way for the resummation of singularities in perturbation theory at or near two dimensions (Gor'kov et al., 1979; Vollhardt and Wölfle, 1980) and allowed to cast the scaling in the systematic form of a field-theoretical RG. A microscopic derivation of the σ-model worked out in a number of papers (Efetov et al., 1980; Jüngling and Oppermann, 1980; Schaefer and Wegner, 1980) has completed a case for it as the field theory of the Anderson localization.

To analyze the transition, one starts from the Hamiltonian $\hat{H}$ consisting of the free part $\hat{H}_0$ and the disorder potential $U(\mathbf{r})$:

$$\hat{H} = \hat{H}_0 + U(\mathbf{r}) ; \qquad \hat{H}_0 = \hat{\mathbf{p}}^2/2m. \qquad (2.3)$$

The disorder is defined by the correlation function $\langle U(\mathbf{r})U(\mathbf{r'})\rangle$; we can assume it to be of the white-noise type for definiteness,

$$\langle U(\mathbf{r})U(\mathbf{r'})\rangle = (2\pi\rho\tau)^{-1}\delta(\mathbf{r}-\mathbf{r'}). \qquad (2.4)$$

Here, ρ is the density of states, τ the mean free time and $\langle\ldots\rangle$ denote the disorder average. It may be shown that models with finite-range and/or anisotropic disorder correlations are equivalent with respect to the long-time and long-distance behavior (hydrodynamics) to the white noise model with renormalized parameters (tensor of diffusion coefficients) (Wölfle and Bhatt, 1984).

More convenient for numerical simulations is the lattice version of (2.3), (2.4) known as the Anderson tight-binding model,

$$\hat{H} = t\sum_{\langle ij\rangle} c_i^\dagger c_j + \sum_i u_i c_i^\dagger c_i \ , \qquad (2.5)$$

where the sum $\langle ij\rangle$ goes over nearest neighbor sites and the random site energies u_i are chosen from some distribution $\mathcal{P}(u)$; the standard choice is the uniform distribution over an interval $[-W/2; W/2]$ ("box distribution").

The physical observables whose scaling at the transition point is of primary importance is the localization length ξ on the insulating side (say, $E < E_c$) and the DC conductivity σ on the metallic side ($E > E_c$),

$$\xi \propto (E_c - E)^{-\nu}, \qquad (2.6)$$
$$\sigma \propto (E - E_c)^s. \qquad (2.7)$$

The corresponding critical indices ν and s satisfy the scaling relation $s = \nu(d-2)$, first derived in Wegner (1976).

On a more technical level, the localization transition manifests itself in a change of the behavior of the diffusion propagator,

$$\Pi(\mathbf{r_1},\mathbf{r_2};\omega) = \langle G_{E+\omega/2}^R(\mathbf{r_1},\mathbf{r_2})G_{E-\omega/2}^A(\mathbf{r_2},\mathbf{r_1})\rangle, \quad (2.8)$$

where $\langle\ldots\rangle$ denotes the disorder averaging and G^R, G^A are retarded and advanced Green functions,

$$G_E^{R,A}(\mathbf{r},\mathbf{r'}) = \langle\mathbf{r}|(E-\hat{H}\pm i\eta)^{-1}|\mathbf{r'}\rangle, \qquad \eta\to+0. \ (2.9)$$

In the delocalized regime Π has the familiar diffusion form (in the momentum space),

$$\Pi(\mathbf{q},\omega) = 2\pi\rho(E)/(Dq^2 - i\omega), \qquad (2.10)$$

where ρ is the density of states and D is the diffusion constant, related to the conductivity via the Einstein relation $\sigma = e^2\rho D$. In the insulating phase, the propagator ceases to have the Goldstone form (2.10) and becomes massive,

$$\Pi(\mathbf{r_1},\mathbf{r_2};\omega) \simeq \frac{2\pi\rho}{-i\omega}\mathcal{F}(|\mathbf{r_1}-\mathbf{r_2}|/\xi), \qquad (2.11)$$

with the function $\mathcal{F}(\mathbf{r})$ decaying exponentially on the scale of the localization length, $\mathcal{F}(r/\xi) \sim \exp(-r/\xi)$.

It is worth emphasizing that the localization length ξ obtained from the averaged correlation function $\Pi = \langle G^R G^A\rangle$, Eq. (2.8), is in general different from the one governing the exponential decay of the typical value $\Pi_{\text{typ}} = \exp\langle\ln G^R G^A\rangle$. For example, in quasi-1D systems the two lengths differ by a factor of 4. However, this is usually not important for the definition of the critical index ν.[1] We will return to observables that are related to critical fluctuations of wave functions and discuss the corresponding family of critical exponents in Sec. II.C.

B. Field-theoretical description

1. Effective field theory: Non-linear σ-model

In the original derivation of the σ-model (Efetov et al., 1980; Jüngling and Oppermann, 1980; Schaefer and Wegner, 1980; Wegner, 1979), the replica trick was used to perform the disorder averaging. Within this approach, n copies of the system are considered, with fields ϕ_α, $\alpha = 1, \ldots, n$ describing the particles, and the replica limit $n \to 0$ is taken in the end. The resulting σ-model is defined on the $n \to 0$ limit of either non-compact or compact symmetric space, depending on whether the fields ϕ_α are considered as bosonic or fermionic. As an example, for the unitary symmetry class (A), which corresponds to a system with broken time-reversal invariance, the σ-model target manifold is $U(n,n)/U(n) \times U(n)$ in the first case and $U(2n)/U(n) \times U(n)$ in the second case, with $n \to 0$. A supersymmetric formulation given by Efetov (1983) combines fermionic and bosonic degrees of freedom, with the field Φ becoming a supervector. The resulting σ-model is defined on a supersymmetric coset space, e.g. $U(1,1|2)/U(1|1) \times U(1|1)$ for the unitary class. This manifold combines compact and non-compact features and represents a product of the hyperboloid $H^2 = U(1,1)/U(1) \times U(1)$ and the sphere $S^2 = U(2)/U(1) \times U(1)$ "dressed" by anticommuting (Grassmannian) variables. For a detailed presentation of the supersymmetry formalism and its applications to mesoscopic systems, see Efetov (1983, 1997); Fyodorov (1995); Fyodorov and Sommers (1997); Guhr et al. (1998); Mirlin (2000a,b); Verbaarschot et al. (1985); Zirnbauer (2004). While being equivalent to the replica version on the level of the perturbation theory (including its RG resummation), the supersymmetry formalism allows also for a non-perturbative treatment of the theory, which is particularly important for the analysis of the energy level and eigenfunction statistics, properties of quasi-1D systems, topological effects, etc.

We briefly sketch the key steps in the conventional

---

[1] A remarkable exception is the behavior of ξ in disordered wires of the chiral symmetry, see Eqs. (5.21), (5.22).

derivation of the σ-model; to be specific, we consider the unitary symmetry class. One begins by expressing the product of the retarded and advanced Green functions in terms of the integral over a supervector field $\Phi = (S_1, \chi_1, S_2, \chi_2)$:

$$G^R_{E+\omega/2}(\mathbf{r_1}, \mathbf{r_2}) G^A_{E-\omega/2}(\mathbf{r_2}, \mathbf{r_1})$$

$$= \int D\Phi \, D\Phi^\dagger S_1(\mathbf{r_1}) S_1^*(\mathbf{r_2}) S_2(\mathbf{r_2}) S_2^*(\mathbf{r_1})$$

$$\times \exp\left\{ i \int d\mathbf{r} \Phi^\dagger(\mathbf{r}) [(E - \hat{H})\Lambda + \frac{\omega}{2} + i\eta] \Phi(\mathbf{r}) \right\} \quad (2.12)$$

where $\Lambda = \text{diag}\{1, 1, -1, -1\}$. After disorder averaging, the resulting quartic term is decoupled via the Hubbard-Stratonovich transformation, by introducing a 4×4 supermatrix variable $\mathcal{R}_{\mu\nu}(\mathbf{r})$ conjugate to the tensor product $\Phi_\mu(\mathbf{r}) \Phi_\nu^\dagger(\mathbf{r})$. Integrating out the Φ fields, one gets the action in terms of the $\mathcal{R}$ fields,

$$S[\mathcal{R}] = \pi\rho\tau \int d^d\mathbf{r} \, \text{Str}\mathcal{R}^2 + \text{Str} \ln[E + (\frac{\omega}{2} + i\eta)\Lambda - \hat{H}_0 - \mathcal{R}], \quad (2.13)$$

where Str denotes the supertrace. The next step is to use the saddle-point approximation, which leads to the following equation for $\mathcal{R}$:

$$\mathcal{R}(\mathbf{r}) = (2\pi\rho\tau)^{-1} \langle \mathbf{r} | (E - \hat{H}_0 - \mathcal{R})^{-1} | \mathbf{r} \rangle \quad (2.14)$$

The relevant set of the solutions (the saddle-point manifold) has the form:

$$\mathcal{R} = \Sigma \cdot I - (i/2\tau)Q \quad (2.15)$$

where I is the unity matrix, Σ is certain constant, and the 4×4 supermatrix $Q = T^{-1}\Lambda T$ satisfies the condition $Q^2 = 1$ and belongs to the σ-model target space described above. Finally, one performs the gradient expansion of the second term in (2.13), for $\mathcal{R}$ having the form (2.15) with a slowly varying $Q(\mathbf{r})$. The expression for the propagator Π, Eq. (2.8), then reads,

$$\Pi(\mathbf{r_1}, \mathbf{r_2}; \omega) = \int DQ \, Q_{12}^{bb}(\mathbf{r_1}) Q_{21}^{bb}(\mathbf{r_2}) e^{-S[Q]}, \quad (2.16)$$

where $S[Q]$ is the σ-model action

$$S[Q] = \frac{\pi\rho}{4} \int d^d\mathbf{r} \, \text{Str} \left[-D(\nabla Q)^2 - 2i\omega\Lambda Q \right], \quad (2.17)$$

The size 4 of the matrix is due to (i) two types of the Green functions (advanced and retarded), and (ii) necessity to introduce bosonic and fermionic degrees of freedom to represent these Green's function in terms of a functional integral. The matrix Q consists thus of four 2×2 blocks according to its advanced-retarded structure, each of them being a supermatrix in the boson-fermion space. In particular, Q_{12}^{bb} is the boson-boson element of the RA block, and so on. One can also consider an average of the product of n retarded and n advanced Green functions, which will generate a σ-model defined

on a larger manifold, with the base being a product of $U(n, n)/U(n) \times U(n)$ and $U(2n)/U(n) \times U(n)$ (these are the same structures as in the replica formalism, but now *without* the $n \to 0$ limit).

For other symmetry classes, the symmetry of the σ-model is different but the general picture is the same. For example, for the orthogonal class (AI) the 8×8 Q-matrices span the manifold whose base is the product of the non-compact space $O(2, 2)/O(2) \times O(2)$ and the compact space $\text{Sp}(4)/\text{Sp}(2) \times \text{Sp}(2)$. The σ-model symmetric spaces for all the classes (Wigner-Dyson as well as unconventional) are listed in Sec. IV.

2. RG in $2 + \epsilon$ dimensions; ϵ-expansion

The σ-model is the effective low-momentum, low-frequency theory of the problem, describing the dynamics of interacting soft modes – diffusons and cooperons. Its RG treatment yields a flow equation of the form (2.2), thus justifying the scaling theory of localization. The β-function $\beta(t) \equiv -dt/d \ln L$ can be calculated perturbatively in the coupling constant t inversely proportional to the dimensional conductance, $t = 1/2\pi g$.[2] This allows one to get the ϵ-expansion for the critical exponents in $2 + \epsilon$ dimensions, where the transition takes place at $t_* \ll 1$. In particular, for the orthogonal symmetry class (AI) one finds (Wegner, 1989)

$$\beta(t) = \epsilon t - 2t^2 - 12\zeta(3)t^5 + O(t^6). \quad (2.18)$$

The transition point t_* is given by the zero of the β-function,

$$t_* = \frac{\epsilon}{2} - \frac{3}{8}\zeta(3)\epsilon^4 + O(\epsilon^5). \quad (2.19)$$

The localization length exponent ν is determined by the derivative

$$\nu = -1/\beta'(t_*) = \epsilon^{-1} - \frac{9}{4}\zeta(3)\epsilon^2 + O(\epsilon^3), \quad (2.20)$$

and the conductivity exponent s is

$$s = \nu\epsilon = 1 - \frac{9}{4}\zeta(3)\epsilon^3 + O(\epsilon^4). \quad (2.21)$$

Numerical simulations of localization on fractals with dimensionality slightly above 2 give the behavior of ν that is in good agreement with Eq. (2.20) (Schreiber and Grussbach, 1996). For the unitary symmetry class (A), the corresponding results read

$$\beta(t) = \epsilon t - 2t^3 - 6t^5 + O(t^7); \quad (2.22)$$

$$t_* = \left(\frac{\epsilon}{2}\right)^{1/2} - \frac{3}{2}\left(\frac{\epsilon}{2}\right)^{3/2} + O(\epsilon^{5/2}); \quad (2.23)$$

$$\nu = \frac{1}{2\epsilon} - \frac{3}{4} + O(\epsilon); \qquad s = \frac{1}{2} - \frac{3}{4}\epsilon + O(\epsilon^2). \quad (2.24)$$

---

[2] For spinful systems, g here does not include summation over spin projections.

In 2D ($\epsilon = 0$) the fixed point t_* in both cases becomes zero: the β-function is negative for any $t > 0$, implying that all states are localized. The situation is qualitatively different for the third Wigner-Dyson class – the symplectic one. The corresponding β-function is related to that for the orthogonal class via $\beta_{\mathrm{Sp}}(t) = -2\beta_{\mathrm{O}}(-t/2)$, yielding[3]

$$\beta(t) = \epsilon t + t^2 - \frac{3}{4}\zeta(3)t^5 + O(t^6). \qquad (2.25)$$

In 2D the β-function (2.25) is positive at sufficiently small t, implying the existence of a truly metallic phase at $t < t_*$, with an Anderson transition at certain $t_* \sim 1$, Sec. VI.B. This peculiarity of the symplectic class represents one of possible mechanisms of the emergence of criticality in 2D, see Sec. VI.A. The results for the β-functions in all the symmetry classes will be given in Sec. IV.F.

3. Additional comments

A few interrelated comments are in order here.

(i) ϵ-*expansion vs 3D exponents.* The ϵ-expansion is of asymptotic character, yielding numerically accurate values of the critical exponents only in the limit of small ϵ. It is thus not surprising that, if Eqs. (2.20), (2.21) are used to estimate the indices in 3D ($\epsilon = 1$), the best thing to do is to keep just the leading (one-loop) term, yielding a quite substantial error ($\nu = 1$ instead of $\nu \simeq 1.57 \pm 0.02$ (Slevin and Ohtsuki, 1999) known from numerical simulations). Rather unexpectedly, the agreement turns out to be remarkably good for the multifractal exponents, see Sec. II.C.6. Independently of the accuracy of these numbers, the ϵ-expansion plays a major role in understanding of qualitative properties of the transition.

(ii) *Composite operators.* The RG can also be used to calculate scaling dimensions of composite operators. In particular, the operators of the type $(Q\Lambda)^n$ determine multifractal fluctuations of wave functions at criticality that will be discussed in Sec. II.C. Another class of operators – those with high derivatives, $(\nabla Q)^{2n}$ – were studied in Kravtsov *et al.* (1988); Lerner and Wegner (1990) and found to have the scaling dimensions

$$y_n = d - 2n + 2t_* n(n-1) + O(t_*^2), \qquad (2.26)$$

where t_* is given by Eq. (2.19) for the orthogonal class and Eq. (2.23) for the unitary class. The fact that the one-loop result (2.26) becomes positive for a sufficiently large number of gradients, $n > t_*^{-1}$ (suggesting that the corresponding operators are relevant and might drive the system into an unknown fixed point) has

launched a debate about the stability of the σ-model and the one-parameter scaling. This question is not specific to the localization problem but is equally applicable to a broader class of σ-models, including the O(n) model of a Heisenberg ferromagnet (Castilla and Chakravarty, 1993; Wegner, 1990). It was, however, pointed out in Brezin and Hikami (1997); Derkachov and Manashov (1997) that since the expansion (2.26) is asymptotic and its true parameter is $t_* n$, the behavior of the one-loop result at $t_* n \gtrsim 1$ does not allow to make any reliable conclusions.

(iii) *Order parameter.* In view of the analogy with continuous thermodynamic phase transitions, it is natural to ask what is the order parameter for the Anderson transition. While naively Eq. (2.17) suggests that it is the expectation value of Q, the latter is in fact uncritical. To describe the transition in terms of symmetry breaking, one has to introduce an order parameter *function* (OPF) $F(Q)$ resulting from integrating out Q-fields at all points except one ($\mathbf{r_0}$), with given $Q(\mathbf{r_0}) \equiv Q$ (Efetov, 1987; Zirnbauer, 1986a,b). One can introduce an OPF $F(\Phi)$ with similar properties also within the supervector formalism (Mirlin and Fyodorov, 1991). It was shown (Mirlin and Fyodorov, 1994a,b) that the OPF is closely related to the distribution of one-site Green functions, in particular local density of states (LDOS), and wave function amplitudes. In the framework of scattering theory, this suggests an inerpretation of the Anderson transition as a phenomenon of spontaneous breakdown of $S-$matrix unitarity (Fyodorov, 2003).

(iv) *Upper critical dimension.* For conventional critical phenomena, there exists an upper critical dimension d_c above which the transition is governed by a Gaussian fixed point, with exponents being d-independent and given by their mean-field values. As a consequence, an ϵ-expansion near d_c (in the most standard case, in $4 - \epsilon$ dimensions) exists, alternative to $2 + \epsilon$ expansion. One can ask whether this is also the case for the Anderson localization transition. The answer is negative: there is no conventional mean field theory for the Anderson transition, and it was argued that the the upper critical dimension is $d_c = \infty$ (Mirlin and Fyodorov, 1994a,b). The closest existing analog of the mean-field theory is the model on the Bethe lattice corresponding to $d = \infty$; we will discuss it in more detail in Sec. II.D.

C. Critical wave functions: Multifractality

1. Scaling of inverse participation ratios

Multifractality of wave functions, describing their strong fluctuations at criticality, is a striking feature of the Anderson transitions (Castellani and Peliti, 1986; Wegner, 1980). Multifractality as a concept has been introduced by Mandelbrot (1974). Multifractal structures are characterized by an infinite set of critical exponents describing the scaling of the moments of some distribu-

---

[3] Here $t = 1/\pi g$, where g is the total conductance of the spinful system.

tion. This feature has been observed in various complex objects, such as the energy dissipating set in turbulence, strange attractors in chaotic dynamical systems, and the growth probability distribution in diffusion-limited aggregation. For the present problem, the underlying normalized measure is just $|\psi^2(\mathbf{r})|$ and the corresponding moments are the inverse participation ratios (IPR) [4]

$$P_q = \int d^d\mathbf{r}|\psi(\mathbf{r})|^{2q}. \qquad (2.27)$$

At criticality, P_q show an anomalous scaling with the system size L,

$$\langle P_q \rangle = L^d\langle|\psi(\mathbf{r})|^{2q}\rangle \sim L^{-\tau_q}, \qquad (2.28)$$

governed by a continuous set of exponents τ_q. One often introduces fractal dimensions D_q via $\tau_q = D_q(q-1)$. In a metal $D_q = d$, in an insulator $D_q = 0$, while at a critical point D_q is a non-trivial function of q, implying wave function multifractality. Splitting off the normal part, one defines the anomalous dimensions Δ_q,

$$\tau_q \equiv d(q - 1) + \Delta_q, \qquad (2.29)$$

which distinguish the critical point from the metallic phase and determine the scale dependence of the wave function correlations. Among them, $\Delta_2 \equiv -\eta$ plays the most prominent role, governing the spatial correlations of the "intensity" $|\psi|^2$,

$$L^{2d}\langle|\psi^2(\mathbf{r})\psi^2(\mathbf{r}')|\rangle \sim (|\mathbf{r} - \mathbf{r}'|/L)^{-\eta}. \qquad (2.30)$$

Equation (2.30) can be obtained from (2.28) by using the fact that the wave function amplitudes become essentially uncorrelated at $|\mathbf{r} - \mathbf{r}'| \sim L$. Scaling behavior of higher order spatial correlations, $\langle|\psi^{2q_1}(\mathbf{r_1})\psi^{2q_2}(\mathbf{r_2})\ldots\psi^{2q_n}(\mathbf{r_n})|\rangle$ can be found in a similar way, e.g.

$$L^{d(q_1+q_2)}\langle|\psi^{2q_1}(\mathbf{r_1})\psi^{2q_2}(\mathbf{r_2})|\rangle$$
$$\sim L^{-\Delta_{q_1}-\Delta_{q_2}}(|\mathbf{r_1} - \mathbf{r_2}|/L)^{\Delta_{q_1+q_2}-\Delta_{q_1}-\Delta_{q_2}} \quad (2.31)$$

Correlations of two different (but close in energy) eigenfunctions possess the same scaling properties,

$$\left.\begin{array}{l} L^{2d}\langle|\psi_i^2(\mathbf{r})\psi_j^2(\mathbf{r}')|\rangle \\ L^{2d}\langle\psi_i(\mathbf{r})\psi_j^*(\mathbf{r})\psi_i^*(\mathbf{r}')\psi_j(\mathbf{r}')\rangle \end{array}\right\} \sim \left(\frac{|\mathbf{r} - \mathbf{r}'|}{L_\omega}\right)^{-\eta},$$
$$\qquad (2.32)$$

where $\omega = \epsilon_i - \epsilon_j$, $L_\omega \sim (\rho\omega)^{-1/d}$, ρ is the density of states, and $|\mathbf{r} - \mathbf{r}'| < L_\omega$. For conventional classes,

---

[4] Strictly speaking, P_q as defined by Eq. (2.27), diverges for sufficiently negative q ($q \leq -1/2$ for real ψ and $q \leq -3/2$ for complex ψ), because of zeros of wave functions related to their oscillations on the scale of the wave length. To find τ_q for such negative q, one should first smooth $|\psi^2|$ by averaging over some microscopic volume (block of several neighboring sites in the discrete version).

where the DOS is uncritical, the diffusion propagator (2.8) scales in the same way.

In the field-theoretical language (Sec. II.B), Δ_q are the leading anomalous dimensions of the operators $\text{Tr}(Q\Lambda)^q$ (or, more generally, $\text{Tr}(Q\Lambda)^{q_1}\ldots\text{Tr}(Q\Lambda)^{q_m}$ with $q_1+\ldots+q_m = q$) (Wegner, 1980). The strong multifractal fluctuations of wave functions at criticality are related to the fact that $\Delta_q < 0$ for $q > 1$, so that the corresponding operators increase under RG. In this formalism, the scaling of correlation functions [Eq. (2.30) and its higher-order generalizations] results from an operator product expansion (Duplantier and Ludwig, 1991; Mudry *et al.*, 1996; Wegner, 1985).

2. Singularity spectrum $f(\alpha)$

The average IPR $\langle P_q \rangle$ are (up to the normalization factor L^d) the moments of the distribution function $\mathcal{P}(|\psi|^2)$ of the eigenfunction intensities. The behavior (2.28) of the moments corresponds to the intensity distribution function of the form

$$\mathcal{P}(|\psi^2|) \sim \frac{1}{|\psi^2|}L^{-d+f(-\frac{\ln|\psi^2|}{\ln L})} \qquad (2.33)$$

Indeed, calculating the moments $\langle|\psi^{2q}|\rangle$ with the distribution function (2.33), one finds

$$\langle P_q \rangle = L^d\langle|\psi^{2q}|\rangle \sim \int d\alpha\, L^{-q\alpha+f(\alpha)} , \qquad (2.34)$$

where we have introduced $\alpha = -\ln|\psi^2|/\ln L$. Evaluation of the integral by the saddle-point method (justified in the limit of large L) reproduces the result (2.28), with the exponent τ_q related to the singularity spectrum $f(\alpha)$ via the Legendre transformation,

$$\tau(q) = q\alpha - f(\alpha) , \qquad q = f'(\alpha) , \qquad \alpha = \tau_q'. \quad (2.35)$$

The meaning of the function $f(\alpha)$ is as follows: it is the fractal dimension of the set of those points $\mathbf{r}$ where the eigenfunction intensity is $|\psi^2(\mathbf{r})| \sim L^{-\alpha}$. In other words, in a lattice version of the model the number of such points scales as $L^{f(\alpha)}$ (Halsey *et al.*, 1986).

General properties of the functions τ_q and $f(\alpha)$ follow from their definitions and the wave function normalization:

(i) τ_q is a non-decreasing, convex function ($\tau_q' \geq 0$, $\tau_q'' \leq 0$), with $\tau_0 = -d$, $\tau_1 = 0$;

(ii) $f(\alpha)$ is a convex function ($f''(\alpha) \leq 0$) defined on the semiaxis $\alpha \geq 0$ with a maximum at some point α_0 (corresponding to $q = 0$ under the Legendre transformation) and $f(\alpha_0) = d$. Further, for the point α_1 (corresponding to $q = 1$) we have $f(\alpha_1) = \alpha_1$ and $f'(\alpha_1) = 1$.

If one formally defines $f(\alpha)$ for a metal, it will be concentrated in a single point $\alpha = d$, with $f(d) = d$ and $f(\alpha) = -\infty$ otherwise. On the other hand, at criticality this "needle" broadens and the maximum shifts to a position $\alpha_0 > d$, see Fig. 1.

FIG. 1 Schematic plot of the multifractal spectrum, $f(\alpha)$. A metal is represented by a "needle", i.e. $f(\alpha)$ having zero width, at $\alpha = d$. At criticality $f(\alpha)$ acquires a finite width and the apex, α_0, shifts to a value larger than d. The negative parts of $f(\alpha)$ (grey area) correspond to rare events – values of the wavefunction amplitude that typically do not occur in a single sample.

3. Weak multifractality: approximately parabolic spectrum

One of the situations in which the τ_q spectrum can be evaluated analytically is the regime of weak multifractality, when the critical point is, in a sense, close to a metal. This happens, in particular, for the Anderson transition in $2+\epsilon$ dimensions with $\epsilon \ll 1$, see Sec. II.C.6, and in the PRBM model with $b \gg 1$, Sec. III.B. In this situation, one finds generically a spectrum of the form

$$\tau_q \simeq d(q-1) - \gamma q(q-1), \qquad \gamma \ll 1, \qquad (2.36)$$

i.e. the anomalous dimension $\Delta_q \simeq \gamma q(1-q)$. (We remind that $\Delta_0 = \Delta_1 = 0$ by definition.) The approximation (2.36) is valid in general as long as the second term (Δ_q) is small compared to the first one, i.e. for $q \ll d/\gamma$. After the Legendre transformation Eq. (2.36) yields

$$f(\alpha) \simeq d - \frac{(\alpha-\alpha_0)^2}{4(\alpha_0-d)}; \qquad \alpha_0 = d + \gamma. \qquad (2.37)$$

In some specific cases, the parabolic form of the spectrum (2.36), (2.37) is not just an approximation but rather an exact result. This happens, in particular, for the random vector potential model, see Sec. VI.G.3. There is a conjecture corroborated by numerical simulations that this is also the case for the IQHE transition, see Sec. VI.C.7. Note that exact parabolicity cannot extend to all q: at $q_c = (d+\gamma)/2\gamma$ the derivative τ_q' becomes zero (i.e. the corresponding $\alpha = 0$), so that τ_q should stay constant for larger q. We will discuss this issue, known as "termination" of the multifractal spectra, in Sec. II.C.7.

4. Symmetry of the multifractal spectra

As was recently shown (Mirlin *et al.*, 2006), the multifractal exponents for the Wigner-Dyson classes satisfy
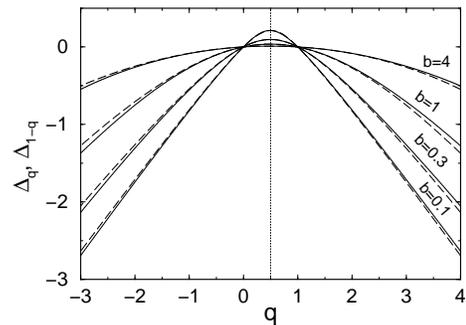
FIG. 2 Multifractal exponents Δ_q for the PRBM model with $b = 4, 1, 0.3, 0.1$. The symmetry (2.38) with respect to the point $q = 1/2$ is evident. A small difference between Δ_q (full line) and Δ_{1-q} (dashed) is due to numerical errors. (Mildenberger *et al.*, 2007b).
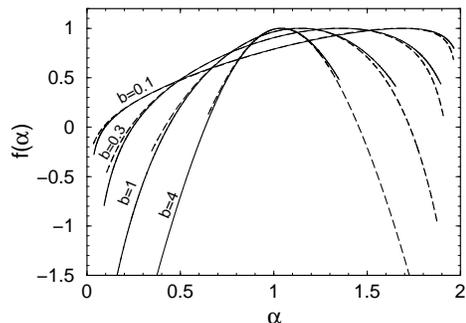
FIG. 3 The data of Fig. 2 in terms of the singularity spectrum $f(\alpha)$. Dashed lines represent $f(2-\alpha)+\alpha-1$, demonstrating the validity of Eq. (2.39). (Mildenberger *et al.*, 2007b).

an exact symmetry relation[5]

$$\Delta_q = \Delta_{1-q} , \qquad (2.38)$$

connecting exponents with $q < 1/2$ (in particular, with negative q) to those with $q > 1/2$. In terms of the singularity spectrum, this implies

$$f(2d-\alpha) = f(\alpha) + d - \alpha. \qquad (2.39)$$

The analytical derivation of Eqs. (2.38), (2.39) is based on the supersymmetric σ-model; it has been confirmed by numerical simulations on the PRBM model at criticality (Mildenberger *et al.*, 2007b), see Figs. 2, 3 and Sec. III, and the 2D Anderson transition of the symplectic class (Mildenberger and Evers, 2007; Obuse *et al.*, 2007b), Sec. III.

5. Role of ensemble averaging

a. Average vs. typical spectra. It should be stressed that the definition (2.28) of τ_q is based on the ensemble-

---

[5] If the multifractal spectrum possesses a termination (non-analyticity) point q_c, Sec. II.C.7, the status of the relation (2.38) beyond this point is not clear.

averaged IPRs, $\langle P_q \rangle$. On the other hand, until recently most numerical studies of multifractality were dealing with properties of a single (representative) wave function. Formally, this corresponds to an analysis of the typical IPR,

$$P_q^{\text{typ}} = \exp\langle \ln P_q \rangle. \qquad (2.40)$$

Similarly to Eq. (2.28), one can define the exponents τ_q^{typ},

$$P_q^{\text{typ}} \sim L^{-\tau_q^{\text{typ}}}, \qquad (2.41)$$

and introduce the spectrum $f^{\text{typ}}(\alpha)$ as the Legendre transform of τ_q^{typ}. The relation between τ_q, $f(\alpha)$, on one side, and τ_q^{typ}, $f^{\text{typ}}(\alpha)$, on the other side, was analyzed in detail in Evers and Mirlin (2000); Mirlin and Evers (2000).[6] The function τ_q^{typ} has the form

$$\tau_q^{\text{typ}} = \begin{cases} q\alpha_- , & q < q_- \\ \tau_q , & q_- < q < q_+ \\ q\alpha_+ , & q > q_+ , \end{cases} \qquad (2.42)$$

where $\alpha_\pm$ are determined by the condition $f(\alpha) = 0$, and $q_\pm$ are the corresponding values of q, with $q_- < q_+$.[7] The singularity spectrum $f^{\text{typ}}(\alpha)$ is defined on the interval $[\alpha_+, \alpha_-]$, where it is equal to $f(\alpha)$. The information about the negative part of $f(\alpha)$ (on $\alpha < \alpha_+$ and $\alpha > \alpha_-$), or, equivalently, about the part of τ_q with q outside the range $[q_-, q_+]$, gets lost when one considers a single wave function. This is because the average number of points with such a singularity α for a single eigenfunction is $L^{f(\alpha)} \ll 1$, so that the ensemble averaging is of crucial importance for determination of this part of the multifractal spectrum, see Fig. 1.

b. IPR distribution and tail exponents. A closely related issue is that of the distribution function of the IPR P_q. It was conjectured in Fyodorov and Mirlin (1995) and shown in Evers and Mirlin (2000); Mirlin and Evers (2000) that the distribution function of the IPR normalized to its typical value P_q^{typ} has a scale invariant form $\mathcal{P}(P_q/P_q^{\text{typ}})$ at criticality. In other words, the distribution function of the IPR logarithm, $\mathcal{P}(\ln P_q)$, preserves its form and only shifts along the x axis with increasing L. On the large-P_q side, this distribution develops a power-law tail,

$$\mathcal{P}(P_q/P_q^{\text{typ}}) \propto (P_q/P_q^{\text{typ}})^{-1-x_q}, \qquad P_q \gg P_q^{\text{typ}}. \quad (2.43)$$

The upper cutoff of this tail, $(P_q/P_q^{\text{typ}})_{\max}$ depends on the system size L, moving to infinity with $L \to \infty$. It is clear that the relation between τ_q^{typ} and τ_q depends crucially on the power-law exponent x_q. If $x_q > 1$, the two definitions of the fractal exponents are identical, $\tau(q) = \tau^{\text{typ}}(q)$. On the other hand, if $x_q < 1$, the average $\langle P_q \rangle$ is determined by the upper cut-off of the power-law tail, which depends on L. As a result, $\langle P_q \rangle$ shows scaling with an exponent τ_q^{typ} different from τ_q. In this situation the average value $\langle P_q \rangle$ is not representative and is determined by rare realizations of disorder. Thus, $x_q = 1$ for $q = q_\pm$, $x_q > 1$ for $q_- < q < q_+$, and $x_q < 1$ otherwise. Furthermore, it was found (Mirlin and Evers, 2000) that the power-law-tail index x_q is related to the fractal exponents as follows:

$$x_q \tau_q^{\text{typ}} = \tau_{qx_q} . \qquad (2.44)$$

More precisely, Eq. (2.44) was proven for the case when x_q is an integer. Also, it was shown to hold for the small-b limit of the PRBM model, at $q > 1/2$. The generic validity of this formula remains a conjecture. In the range of non-self-averaging IPR it yields

$$x_q = q_+/q , \qquad q > q_+, \qquad (2.45)$$

and similarly for $q < q_-$. As to the range $q_- < q < q_+$, the behavior of x_q depends on the specific form of τ_q. In the particular case of the weak multifractality, Eq. (2.36), the solution of Eq. (2.44) reads

$$x_q \simeq (q_+/q)^2 , \qquad q_- < q < q_+ , \qquad (2.46)$$

with

$$q_\pm = \pm(d/\gamma)^{1/2}. \qquad (2.47)$$

6. Dimensionality dependence of the wave function statistics at the Anderson transition

In this subsection, which is largely based on Mildenberger *et al.* (2002), we summarize the results for the Anderson transition in d dimensions, obtained by analytical and numerical means. This allows us to analyze the evolution of the critical statistics from the weak-multifractality regime in $d = 2 + \epsilon$ dimensions to the strong multifractality at $d \gg 1$.

In $2+\epsilon$ dimensions with $\epsilon \ll 1$ the multifractality exponents can be obtained within the ϵ-expansion, Sec. II.B.2. The 4-loop results for the orthogonal and unitary symmetry classes read (Wegner, 1987)

$$\Delta_q^{(O)} = q(1-q)\epsilon + \frac{\zeta(3)}{4}q(q-1)(q^2-q+1)\epsilon^4$$
$$+ O(\epsilon^5); \quad (2.48)$$
$$\Delta_q^{(U)} = q(1-q)(\epsilon/2)^{1/2} - \frac{3}{8}q^2(q-1)^2\zeta(3)\epsilon^2$$
$$+ O(\epsilon^{5/2}). \quad (2.49)$$

---

[6] In Evers and Mirlin (2000); Mirlin and Evers (2000) different notations were used: τ_q, $f(\alpha)$ for the typical spectra, and $\tilde{\tau}_q$, $\tilde{f}(\alpha)$ for the averaged spectra.

[7] It is tacidly assumed here, that $q_\pm$ and α_- actually exist, i.e. are not infinite. To the best of our knowledge, an example to the opposite has never been encountered in the context of the Anderson transitions.
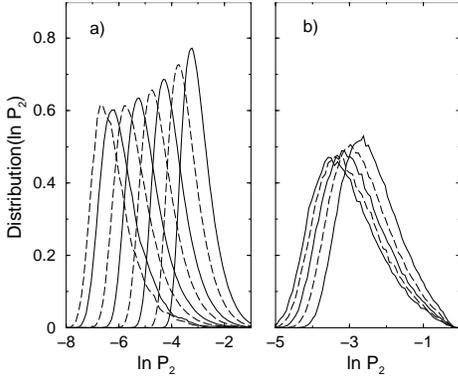
FIG. 4 IPR distribution at the Anderson transition (GOE) (a) 3D (system sizes $L = 8, 11, 16, 22, 32, 44, 64, 80$) and (b) 4D ($L = 8, 10, 12, 14, 16$). (Mildenberger *et al.*, 2002)

Keeping only the leading (one-loop) term on the r.h.s. of Eqs. (2.48) and (2.49), we get the parabolic approximation for τ_q, Eq. (2.36), and $f(\alpha)$, Eq. (2.37), with $\gamma = \epsilon$ for the orthogonal class and $\gamma = (\epsilon/2)^{1/2}$ for the unitary class. The IPR fluctuations (Sec. II.C.5) can be studied analytically as well. In particular, in the orthogonal symmetry class, the variance σ_q of the distribution $\mathcal{P}(\ln P_q)$ is given, to the leading order in $\epsilon \ll 1$, by

$$\sigma_q = 8\pi^2 a \epsilon^2 q^2 (q-1)^2 , \qquad |q| \ll q_+ , \qquad (2.50)$$

where $a \simeq 0.00387$ for the periodic boundary conditions. The values $q_\pm$ of q beyond which the typical and the average IPR scale differently are given by Eq. (2.47) with $d \simeq 2$ and the above values of γ. The power-law exponent x_q of the IPR distribution is given by Eqs. (2.45), (2.46). At $q \gg q_+$ the variance σ_q is governed by the slowly decaying power-law tail, yielding

$$\sigma_q \simeq x_q^{-1} \simeq q/q_+ . \qquad (2.51)$$

Results of numerical simulations of the wave function statistics in 3D and 4D for the orthogonal symmetry class are shown in Figs. 4–7, in comparison with the one-loop analytical results of the $2 + \epsilon$ expansion. Figure 4 demonstrates that the critical IPR distribution $\mathcal{P}(\ln P_q)$ acquires the scale-invariant form (as also found in (Cuevas *et al.*, 2002)). The corresponding variance is shown in Fig. 5; in 3D it is described very well by the analytical formulas with $\epsilon = 1$. The evolution from the weak- to strong-multifractality with increasing d is nicely seen in Fig. 6 for $f(\alpha)$. As is demonstrated in the inset, the one-loop result of the $2 + \epsilon$ expansion with $\epsilon = 1$ describes the 3D singularity spectrum with a remarkable accuracy (though with detectable deviations). In particular, the position of the maximum, $\alpha_0 = 4.03 \pm 0.05$, is very close to its value $\alpha_0 = d + \epsilon$ implied by Eq. (2.37). As expected, in 4D the deviations from parabolic shape are much more pronounced and $\alpha_0 = 6.5 \pm 0.2$ differs noticeably from 6.

Evolution of the fractal dimension $D_q \equiv \tau_q/(q-1)$ with d is shown in Fig. 7. It is seen that the fractal
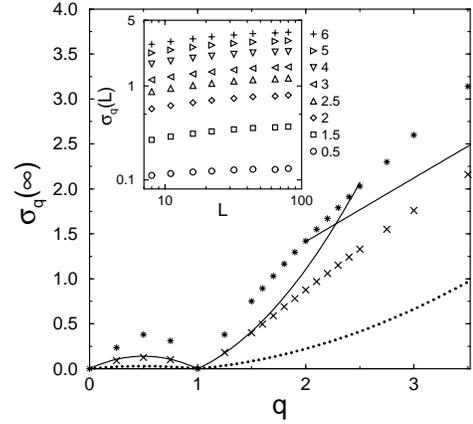
FIG. 5 The rms deviation σ_q of $\ln P_q$ extrapolated to $L \to \infty$ in 3D ($\times$) and 4D ($*$). The dotted line is the analytical result (2.50) for $\epsilon = 0.2$; the full lines represent Eqs. (2.50), (2.51) with $\epsilon = 1$. Inset: evolution of σ_q with L in 3D for values of $q = 0.5, 1.5, 2, 2.5, 3, 4, 5, 6$. The leading finite size correction of all data has the form L^{-y} with $y = 0.25 \div 0.5$ for 3D and $y = 0.1 \div 0.4$ in 4D. (Mildenberger *et al.*, 2002)
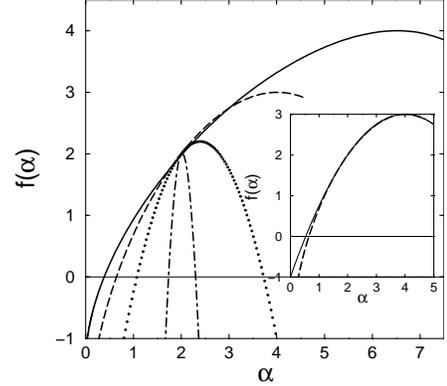
FIG. 6 Singularity spectrum $f(\alpha)$ in 3D (dashed) and 4D (full line). To illustrate the evolution of the spectrum from $d = 2$ to $d = 4$, analytical results for $d = 2 + \epsilon$ are shown for $\epsilon = 0.2$ (dotted) and $\epsilon = 0.01$ (dot-dashed). Inset: comparison between $f(\alpha)$ for 3D and the one-loop result of the $2 + \epsilon$ expansion with $\epsilon = 1$ (solid). (Mildenberger *et al.*, 2002)

dimensions D_q with $q \gtrsim 1$ decrease with increasing d. As an example, for $q = 2$ we have $D_2 \simeq 2 - 2\epsilon$ in $2 + \epsilon$ dimensions, $D_2 = 1.3 \pm 0.05$ in 3D, and $D_2 = 0.9 \pm 0.15$ in 4D. This confirms the expectation based on the Bethe-lattice results (Sec. II.D) that $\tau_q \to 0$ at $d \to \infty$ for $q > 1/2$. Such a behavior of the multifractal exponents is a manifestation of a very sparse character of critical eigenstates at $d \gg 1$, formed by rare resonance spikes. In combination with the symmetry relation (2.38) this implies the limiting form of the multifractal spectrum at $d \to \infty$,

$$\tau_q = \begin{cases} 0 , & q \geq 1/2 \\ 2d(q - 1/2) , & q \leq 1/2 . \end{cases} \qquad (2.52)$$
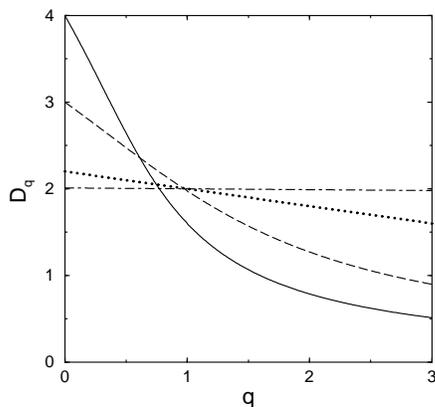
FIG. 7 Fractal dimensions $D_q/q(q-1)$ in 3D (dashed) and 4D (full line). Analytical results for $d = 2 + \epsilon$ with $\epsilon = 0.2$ (dotted) and $\epsilon = 0.01$ (dot-dashed) are also shown. (Mildenberger *et al.*, 2002)

This corresponds to $f(\alpha)$ of the form

$$f(\alpha) = \alpha/2 \ , \qquad 0 < \alpha < 2d \ , \qquad (2.53)$$

dropping to $-\infty$ at the boundaries of the interval $[0, 2d]$. In Mildenberger *et al.* (2002) arguments were given that the way the multifractality spectrum approaches this limiting form with increasing d is analogous to the behavior found in the PRBM model with $b \ll 1$, Sec. III.C.

7. Possible singularities in multifractal spectra: termination and freezing

In this subsection, we discuss what kinds of singularities may be typically encountered in the multifractality spectra $f(\alpha)$ and τ_q. First of all, we recall that the spectrum τ_q^{typ} of a typical eigenfunction has non-analyticity points at $q_\pm$, corresponding to the termination of $f^{\text{typ}}(\alpha)$ at its zero $\alpha_\pm$, see Sec. II.C.5. However, the ensemble-averaged spectra τ_q and $f(\alpha)$ (that we are considering throughout) do not have any singularity there.

Singularities in τ_q and $f(\alpha)$ may arise, depending on the behavior of $f(\alpha)$ at $\alpha = 0$ in the particular critical system under investigation. One possibility is that $f(\alpha)$ approaches the $\alpha = 0$ axis continuously, with $f(\alpha) \to -\infty$ as $\alpha \to 0$ (Fig. 8a). Then τ_q increases monotonically with q, without any non-analyticities. Such a situation is realized e.g. in the PRBM model, see Sec. III.C. An alternative option is that $f(0)$ is finite, see Fig. 8b. This generically implies that τ_q has a discontinuity in the second derivative at certain $q_c \equiv f'(\alpha)|_{\alpha \to 0}$ and is strictly constant, $\tau_q = -f(0)$ at $q \geq q_c$. Such a behavior of the multifractality spectrum at $q = q_c$ is called "termination". In particular, it takes place unavoidably if the spectrum is exactly parabolic, as is the case, e.g., for the random vector potential problem, Sec. VI.G.3. From the point of view of the underlying field theory, termination implies that there is a qualitative change in properties of the operators $\mathcal{O}_q$ describing the moments of the density
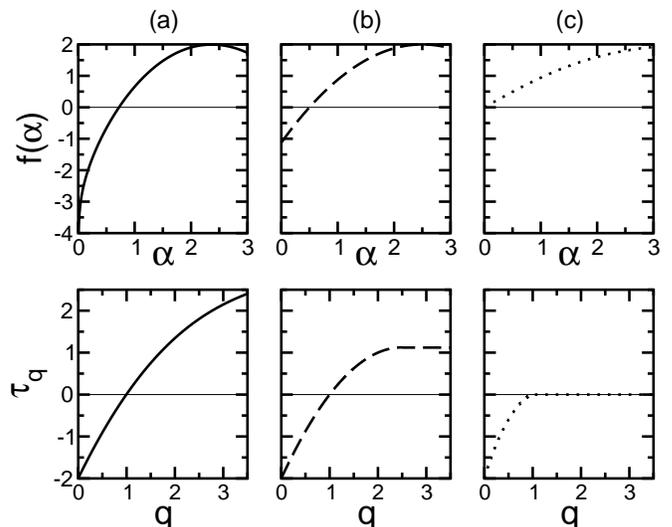

FIG. 8 Possible behavior of the singularity spectrum $f(\alpha)$ at $\alpha \to 0$: (a) no singularity, (b) termination, (c) freezing. The corresponding behavior of τ_q is shown as well.

of states. An explicit example of how this may happen is provided by the 2D Liouville field theory (Kogan *et al.*, 1996; Seiberg, 1990; Zamolodchikov and Zamolodchikov, 1996) (closely related to the random vector potential problem), where the operators $\mathcal{O}_q$ cease to be local for $q > q_c$.

A spectrum with termination may show another peculiarity. While normally $f(0)$ is negative, one can also imagine a situation with $f(0) = 0$, Fig. 8c (corresponding to $q_c \leq 1$). In fact, this is exactly what happens in the random vector potential problem, Sec. VI.G.3, when the disorder strength exceeds a certain critical value. The transition into this phase is termed "freezing transition". In the "frozen" phase the wave functions combine properties of localized and critical states: while the wave function normalization is governed by a vicinity of one or few (of order unity) points, the tails away from these points show multifractal fluctuations and correlations.

8. Surface vs. bulk multifractality

Recently, the concept of wave function multifractality was extended (Subramaniam *et al.*, 2006) to the surface of a system at the critical point of an Anderson transition. It was shown that the fluctuations of critical wave functions at the surface are characterized by a new set of exponent τ_q^{s} (or, equivalently, anomalous exponents Δ_q^{s}), which are in general independent from their bulk counterparts,

$$L^{d-1}\langle |\psi(\mathbf{r})|^{2q}\rangle \sim L^{-\tau_q^{\text{s}}}, \qquad (2.54)$$

$$\tau_q^{\text{s}} = d(q-1) + q\mu + 1 + \Delta_q^{\text{s}}. \qquad (2.55)$$

Here μ is introduced for generality, in order to account for a possibility of non-trivial scaling of the average value,

$\langle|\psi(\mathbf{r})|^2\rangle \propto L^{-d-\mu}$, at the boundary in unconventional symmetry classes. For the Wigner-Dyson classes, $\mu = 0$. The normalization factor L^{d-1} is chosen such that Eq. (2.54) yields the contribution of the surface to the inverse participation ratios $\langle P_q\rangle = \int d^d\mathbf{r}|\psi(\mathbf{r})|^{2q}\rangle$. The exponents Δ_q^s as defined in Eq. (2.55) vanish in a metal and govern statistical fluctuations of wave functions at the boundary, $\langle|\psi(\mathbf{r})|^{2q}\rangle/\langle|\psi(\mathbf{r})|^2\rangle^q \sim L^{-\Delta_q^s}$, as well as their spatial correlations, e.g. $L^{2(d+\mu)}\langle|\psi^2(\mathbf{r})\psi^2(\mathbf{r}')|\rangle \sim (|\mathbf{r} - \mathbf{r}'|/L)^{\Delta_2^s}$.

Wave function fluctuations are much stronger at the edge than in the bulk. As a result, surface exponents are important even if one performs a multifractal analysis for the whole sample, without separating it into "bulk" and "surface", despite the fact that the weight of surface points is down by a factor $1/L$. This was analytically demonstrated in Subramaniam et al. (2006), using a model of a 2D weakly localized metallic system (large dimensionless conductance $g \gg 1$), which shows weak multifractality on length scales below the localization length $\xi \sim e^{(\pi g)^\beta}$, where $\beta = 1$ (2) for systems with preserved (resp. broken) time-reversal symmetry. With minor modifications, the formulas below describe also the Anderson transition in $2 + \epsilon$ dimensions.

For the bulk multifractal spectrum one gets the result (2.36) with $\gamma = (\beta\pi g)^{-1} \ll 1$ (Altshuler et al., 1986; Fal'ko and Efetov, 1995a,b; Wegner, 1980); generalization of this result to the surface case reads:

$$\tau_q^s = 2(q - 1) + 1 + 2\gamma q(1 - q). \qquad (2.56)$$

The corresponding $f(\alpha)$-spectra have the form:

$$f^b(\alpha) = 2 - (\alpha - 2 - \gamma)^2/4\gamma, \qquad (2.57)$$
$$f^s(\alpha) = 1 - (\alpha - 2 - 2\gamma)^2/8\gamma. \qquad (2.58)$$

These results are illustrated in Fig. 9. When the multifractality in the whole sample is analyzed, the lowest of the τ_q exponents "wins". The surface effects become dominant outside the range $q_-^{bs} < q < q_+^{bs}$, where $q_\pm^{bs} \simeq \pm\gamma^{-1/2}$ are the roots of the equation $\tau_q^b = \tau_q^s$. The lower panel of Fig. 9 shows how this is translated into the $f(\alpha)$ representation. The total singularity spectrum is given by the bulk function $f^b(\alpha)$ only for $\alpha_+^b < \alpha < \alpha_-^b$, where $\alpha_\pm^b - 2 \simeq \mp 2\gamma^{1/2}$. Outside this range the surface effects are important. Specifically, $f(\alpha)$ is equal to the surface spectrum $f^s(\alpha)$ for $\alpha < \alpha_+^s$ and $\alpha > \alpha_-^s$, where $\alpha_\pm^s - 2 \simeq \mp 4\gamma^{1/2}$, while in the intermediate intervals $\alpha_+^s < \alpha < \alpha_+^b$ and $\alpha_-^b < \alpha < \alpha_-^s$ its dependence on α becomes linear (shown by dashed lines). The latter behavior is governed by intermediate (between "bulk" and "surface") points with a distance from the surface $r \sim L^\beta$, $0 < \beta < 1$; their $f(\alpha)$ spectrum is found to be $f_\beta(\alpha) = \beta f^b(\alpha) + (1 - \beta)f^s(\alpha)$. Note that in this case the surface effects modify $f(\alpha)$ in the whole range below $f(\alpha) \simeq 1$. Therefore, the surface exponents affect the multifractal spectrum of the sample not only for rare realizations of disorder (governing the negative part of $f(\alpha)$) but already in a typical sample.
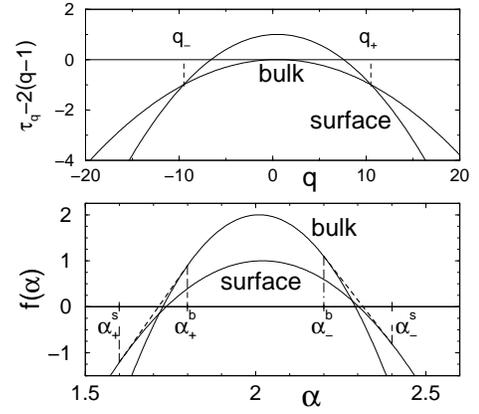
FIG. 9 Surface and bulk multifractal spectra τ_q and $f(\alpha)$ for a 2D metal with $\gamma = 0.01$. For details see text. (Subramaniam et al., 2006).

The boundary multifractality was also explicitly studied, analytically as well as numerically, for several other systems at criticality: the 2D spin quantum Hall transition (Subramaniam et al., 2006), the Anderson transition in a 2D system with spin-orbit coupling (Obuse et al., 2007b), and the PRBM model (Mildenberger et al., 2007b), see Sec. VI.D.5, VI.B.4, and III.E, respectively.

In Obuse et al. (2007b) the notion of surface multifractality was further generalized to a corner of a critical system. It was shown that for a 2D system at criticality conformal invariance leads to the following dependence of the corresponding anomalous exponent Δ_q^θ on the opening angle θ,

$$\Delta_q^\theta = (\pi/\theta)\Delta_q^s. \qquad (2.59)$$

More carefully, for $\theta < \pi$ the spectrum will terminate at some q_θ (see Sec. II.C.7, Fig. 8b), even if the surface spectrum showed no singularity, as in Fig. 8a. Equation (2.59) holds then for $q \leq q_\theta$; for larger q the exponent τ_q is constant.

9. Manifestations of multifractality in other observables.

The multifractal structure of wave functions at criticality manifests itself also in other physical characteristics of the system. In particular, one can open the system by attaching a local lead at some point $\mathbf{r}$. The system can then be characterized by the Wigner delay time t_W (energy derivative of the scattering phase shift), whose statistical properties in chaotic and disordered systems have become a subject of research activity in recent years (Fyodorov and Sommers, 1997; Kottos, 2005). At criticality, the moments of the inverse delay time show a scaling behavior (Fyodorov, 2003; Mendez-Bermudez and Kottos, 2005; Mirlin et al., 2006; Ossipov and Fyodorov, 2005),

$$\langle t_W^{-q}\rangle \propto L^{-\gamma_q}. \qquad (2.60)$$

It was shown that for all Wigner-Dyson classes the exponents γ_q are linked to the wave function exponents τ_q by an exact relation (Mirlin *et al.*, 2006; Ossipov and Fyodorov, 2005),

$$\gamma_q = \tau_{1+q}. \qquad (2.61)$$

If a second local lead is attached to the system, the statistics of the two-point conductance $g(\mathbf{r}, \mathbf{r}')$ can be studied. Specifically, one can analyze the scaling of the moments $\langle g^q(\mathbf{r}', \mathbf{r}) \rangle$ with the distance $|\mathbf{r} - \mathbf{r}'|$ between the contacts (Janßen *et al.*, 1999; Zirnbauer, 1994, 1999),

$$\langle g^q(\mathbf{r}, \mathbf{r}') \rangle \sim |\mathbf{r} - \mathbf{r}'|^{-X_q}. \qquad (2.62)$$

For the case of the unitary symmetry class (A), a relation linking the exponents X_q to the wave function anomalous dimensions Δ_q [and based on a result of Klesse and Zirnbauer (2001)] was obtained (Evers *et al.*, 2001),

$$X_q = \begin{cases} \Delta_q + \Delta_{1-q} , & q < 1/2 \\ 2\Delta_{1/2} , & q > 1/2. \end{cases} \qquad (2.63)$$

In view of (2.38), the first line of Eq. (2.63) can be equivalently written as $X_q = 2\Delta_q$, which has also been proposed in (Janßen *et al.*, 1999).

A relation between the exponents X_q and Δ_q was also derived for the case of the spin quantum Hall transition (Sec. VI.D.5), belonging to the unconventional symmetry class C. In contrast to critical points of the Wigner-Dyson classes, the density of states ρ in this case is critical, i.e. it has a non-trivial scaling dimensions $\rho \propto L^{-x_\rho}$ with $x_\rho > 0$. It was shown in Mirlin *et al.* (2003) (see also Bernard and LeClair (2002b)) that in this case

$$X_q = \begin{cases} 2qx_\rho + 2\Delta_q , & q \leq q_0 , \\ X_{q_0} , & q > q_0 , \end{cases} \qquad (2.64)$$

where q_0 is the point at which $2qx_\rho + 2\Delta_q$ reaches its maximum. It is plausible that the relation (2.64) (which reduces to (2.63) for the Wigner-Dyson classes) holds in fact for critical points of all symmetry classes.

D. Anderson transition in $d = \infty$: Bethe lattice

The Bethe lattice (BL) is a tree-like lattice with a fixed coordination number. Since the number of sites at a distance r increases exponentially with r on the BL, it effectively corresponds to the limit of high dimensionality d. As has been already mentioned in Sec. II.B.3, the BL models are the closest existing analogs of the mean-field theory for the case of the Anderson transition.

The Anderson tight-binding model (lattice version of Eqs. (2.3), (2.4)) on the BL was studied for the first time in Abou-Chacra *et al.* (1973), where the existence of the metal-insulator transition was proven and the position of the mobility edge was determined. The analytical results were confirmed by numerical simulations

(Abou-Chacra and Thouless, 1974; Girvin and Jonson, 1980). In later works the BL versions of the σ-model (2.17) (Efetov, 1985, 1987; Zirnbauer, 1986a,b) and of the tight-binding model (Mirlin and Fyodorov, 1991) were studied within the supersymmetry formalism, which allowed to determine the critical behavior. It was found that the localization length diverges in the way usual for BL models, $\xi \propto |E - E_c|^{-1}$, where E is a microscopic parameter driving the transition. When reinterpreted within the effective-medium approximation (Efetov, 1990; Fyodorov *et al.*, 1992), this yields the conventional mean-field value of the localization length exponent, $\nu = 1/2$. On the other hand, the critical behavior of other observables is very peculiar. The inverse participation ratios P_q with $q > 1/2$ have a finite limit at $E \to E_c$ when the critical point is approached from the localized phase and then jump to zero. By comparison with the scaling formula, $P_q \propto \xi^{-\tau_q}$, this can be interpreted as $\tau_q = 0$ for all $q \geq 1/2$. Further, in the delocalized phase the diffusion coefficient vanishes exponentially when the critical point is approached,

$$D \propto \Omega^{-1} \ln^3 \Omega ; \qquad (2.65)$$

$$\Omega \sim \exp\{\text{const} \, |E - E_c|^{-1/2}\}, \qquad (2.66)$$

which can be thought as corresponding to the infinite value, $s = \infty$, of the critical index s. The distribution function of the LDOS $v \equiv \rho(r)/\langle \rho \rangle$ (normalized to its average value for convenience) was found to be of the form

$$\mathcal{P}(v) \propto \Omega^{-1/2} v^{-3/2} , \qquad \Omega^{-1} \ll v \ll \Omega , \qquad (2.67)$$

and exponentially small outside this range. Equation (2.67) implies the following behavior of the LDOS moments:

$$\langle v^q \rangle \propto \Omega^{|q-1/2|-1/2}. \qquad (2.68)$$

The physical reason for the unconventional critical behavior was unravelled in Mirlin and Fyodorov (1994a,b). It was shown that the exponential largeness of the factor Ω reflects the spatial structure of the BL: the "correlation volume" V_ξ (number of sites within a distance ξ from the given one) on such a lattice is exponentially large. On the other hand, for any finite dimensionality d the correlation volume has a power-law behavior, $V_d(\xi) \propto \xi^d \propto |E - E_c|^{\nu d}$, where $\nu \simeq 1/2$ at large d. Thus, the scale Ω cannot appear for finite d and, assuming some matching between the BL and large-d results, will be replaced by $V_d(\xi)$. Then Eq. (2.68) yields the following high-d behavior of the anomalous exponents Δ_q governing the scaling of the LDOS moments (Sec. II.C),

$$\Delta_q \simeq d(1/2 - |q - 1/2|) , \qquad (2.69)$$

or, equivalently, the results (2.52), (2.53) for the multifractal spectra τ_q, $f(\alpha)$. These formulas describe the strongest possible multifractality.
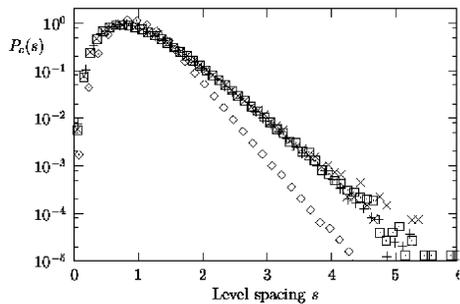
FIG. 10 Critical level spacing distribution of 2D symplectic systems for periodic (PBC) and Dirichlet (DBC) boundary conditions and various system sizes L. PBC: $L=20$ ($\diamond$); DBC: $L=40, 80, 120$ ($+$, $\square$, $\times$). Adapted from Schweitzer and Potempa (1999); see also Schweitzer and Zharekeshev (1997).

The critical behavior of the conductivity, Eq. (2.65), is governed by the same exponentially large factor Ω. When it is replaced by the correlation volume $V_d(\xi)$, the power-law behavior at finite $d \gg 1$ is recovered, $\sigma \propto |E - E_c|^s$ with $s \simeq d/2$. The result for the exponent s agrees (within its accuracy, i.e. to the leading order in d) with the scaling relation $s = \nu(d - 2)$.

E. Level statistics at criticality

We restrict ourselves here to a brief account of key results on the critical level statistics; more detailed exposition and list of references can be found in the review (Mirlin, 2000b). The primary quantity is the two-level correlation function (the superscript "c" standing for the connected part)

$$R_2^{(c)}(s) = \langle\rho\rangle^{-2}\langle\rho(E - \omega/2)\rho(E + \omega/2)\rangle - 1 , \quad (2.70)$$

where $\rho(E) = V^{-1}\mathrm{Tr}\,\delta(E - \hat{H})$ is the fluctuating DOS, V the system volume, $s = \omega/\Delta$, and $\Delta = 1/\langle\rho\rangle V$ the mean level spacing. In a metallic system $R_2^{(c)}(s)$ is given, as a first approximation, by the RMT (Wigner-Dyson statistics; see Mirlin (2000b) for analysis of deviation and limits of applicability), while in the insulating limit the levels are uncorrelated, $R_2^{(c)}(s) = \delta(s)$ (Poisson statistics). In a critical point the level statistics takes an intermediate scale-invariant form. Specifically, $R_2^{(c)}(s)$ (and higher-order correlation functions) is independent under rescaling of the sample, although it does depend on the sample shape and the boundary conditions, see Fig. 10. A closely related quantity is the variance $\langle\delta N(E)^2\rangle$ of the number of levels $N(E)$ in a spectral window of the width E,

$$\langle\delta N(E)^2\rangle = \int_{-\langle N(E)\rangle}^{\langle N(E)\rangle} ds(\langle N(E)\rangle - |s|)R_2^{(c)}(s) . \quad (2.71)$$

In the RMT limit the level number variance increases logarithmically, $\langle\delta N^2\rangle = (2/\pi^2\beta)\ln\langle N\rangle$ at $\langle N\rangle \gg 1$, while

in the Poisson limit $\langle\delta N^2\rangle = \langle N\rangle$. At criticality, $\langle\delta N^2\rangle$ shows an intermediate linear behavior

$$\langle\delta N^2\rangle = \chi\langle N\rangle , \quad (2.72)$$

with a coefficient $0 < \chi < 1$ called "spectral compressibility". The parameter χ is a universal characteristics of the critical theory, i.e. it has a status analogous to critical indices. Evolution of χ from the "quasi-metallic" ($\chi \ll 1$) to the "quasi-insulating" (χ close to 1) criticality can be explicitly analyzed for the family of critical PRBM theories, Sec. III. It is expected that similar evolution takes place for the Anderson transition in d dimensions when d is changed from $d = 2 + \epsilon$ to $d \gg 1$, see a related discussion of the wave function statistics in Sec. II.C.6. The "quasi-metallic" $d = 2 + \epsilon$ limit can be studied analytically with the result $\chi = t^*/\beta$, where the critical coupling t^* is given by Eqs. (2.19) or (2.23), depending on the symmetry class. The approach of the critical statistics to the Poisson limit at large d was clearly demonstrated in the recent numerical work (Garcia-Garcia and Cuevas, 2006), where systems of dimensionality up to $d = 6$ were studied (with χ reaching the value $\simeq 0.8$ in 6D).

In systems of unconventional symmetry classes already the one-point correlation function (average DOS) is nontrivial and acquires, in analogy with the two-level correlation function discussed above, a scale-invariant form at criticality. In particular, this will be shown in Sec. VI.D.6 for the case of the SQH transition (class C).

III. CRITICALITY IN THE POWER-LAW RANDOM BANDED MATRIX (PRBM) MODEL

A. Definition and generalities

The PRBM model is defined (Mirlin *et al.*, 1996) as the ensemble of random $L \times L$ Hermitean matrices $\hat{H}$ (real for $\beta = 1$ or complex for $\beta = 2$). The matrix elements H_{ij} are independently distributed Gaussian variables with zero mean $\langle H_{ij}\rangle = 0$ and with variance

$$\langle|H_{ij}|^2\rangle \equiv J_{ij} = a^2(|i - j|) , \quad (3.1)$$

where $a(r)$ is given by

$$a^2(r) = [1 + (r/b)^{2\alpha}]^{-1} . \quad (3.2)$$

At $\alpha = 1$ the model undergoes an Anderson transition from the localized ($\alpha > 1$) to the delocalized ($\alpha < 1$) phase. Below, we concentrate on the critical value $\alpha = 1$, when $a(r)$ falls down as $a(r) \propto 1/r$ at $r \gg b$.

In a straightforward interpretation, the PRBM model describes a 1D sample with random long-range hopping, the hopping amplitude decaying as $1/r^\alpha$ with the distance. Also, such an ensemble arises as an effective description in a number of physical contexts, see Evers and Mirlin (2000) for relevant references. At $\alpha = 1$ the PRBM model is critical for arbitrary value of b and shows all the key features of the Anderson critical point,

including multifractality of eigenfunctions and non-trivial spectral compressibility. The existence of the parameter b which labels the critical point is a distinct feature of the PRBM model: Eq. (3.1) defines a whole family of critical theories parametrized by b. The limit $b \gg 1$ represents a regime of weak multifractality, analogous to the conventional Anderson transition in $d = 2 + \epsilon$ with $\epsilon \ll 1$. This limit allows for a systematic analytical treatment via a mapping onto a supermatrix σ-model and a weak-coupling expansion (Evers and Mirlin, 2000; Mirlin, 2000b; Mirlin and Evers, 2000; Mirlin et al., 1996). The opposite limit $b \ll 1$ is characterized by very strongly fluctuating eigenfunctions, similarly to the Anderson transition in $d \gg 1$, where the transition takes place in the strong disorder ("strong coupling" in the field-theoretical language) regime. It is also accessible to an analytical treatment using a real-space renormalization-group (RG) method (Mirlin and Evers, 2000) introduced earlier for related models by Levitov (1990).

In addition to the feasibility of the systematic analytical treatment of both the weak-coupling and strong-coupling regimes, the PRBM model is very well suited for numerical simulations in a broad range of couplings. For these reasons, it has attracted a considerable interest in the last few years as a model for the investigation of various properties of the Anderson critical point, see Sec. III.E, III.F.

B. Weak multifractality, $b \gg 1$

The quasi-metallic regime $b \gg 1$ can be studied (Evers and Mirlin, 2000; Mirlin, 2000b; Mirlin and Evers, 2000; Mirlin et al., 1996) via mapping onto the supermatrix σ-model, cf. Sec. II.B.1,

$$S[Q] = \frac{\pi\rho\beta}{4}\text{Str}\left[\pi\rho\sum_{rr'}J_{rr'}Q(r)Q(r') - i\omega\sum_r Q(r)\Lambda\right],$$
$$(3.3)$$

In momentum (k) space and in the low-k limit, the action takes the form

$$S[Q] = \beta\,\text{Str}\left[-\frac{1}{t}\int\frac{dk}{2\pi}|k|Q_kQ_{-k} - \frac{i\pi\rho\omega}{4}Q_0\Lambda\right]\ ,\ (3.4)$$

where $Q_k = \sum_r e^{ikr}Q(r)$ and $Q(r)$ is a 4×4 ($\beta = 2$) or 8×8 ($\beta = 1$) supermatrix field constrained by $Q^2(r) = 1$, see Sec. II.B.1, ρ is the density of states given by the Wigner semicircle law

$$\rho(E) = (1/2\pi^2 b)(4\pi b - E^2)^{1/2}\ ,\qquad |E| < 2\sqrt{\pi b}\ ,\ (3.5)$$

and $t \ll 1$ is the coupling constant,

$$1/t = (\pi/4)(\pi\rho)^2 b^2 = (b/4)(1 - E^2/4\pi b)\ .\qquad (3.6)$$

The main difference between the action (3.4) and that of the diffusive σ-model, Eq. (2.17) is in the replacement of
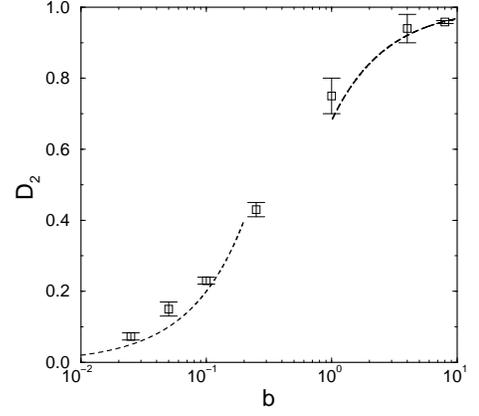
FIG. 11 Fractal dimension D_2 as a function of the parameter b of the PRBM ensemble. The data points are the results of the numerical simulations, while the lines represent the $b \gg 1$ and $b \ll 1$ analytical asymptotics, $D_2 = 1 - 1/\pi b$ [Eq. (3.7)] and $D_2 = 2b$ [Eq. (3.20)]. (Mirlin and Evers, 2000).

the diffusion operator $\frac{\pi\rho}{8}Dk^2$ by $\frac{1}{t}|k|$. Consequently, all calculations within the weak coupling expansion of the σ-model are generalized to the PRBM case by substituting $\Pi(k) = t/8|k|$ for the diffusion propagator $\Pi(k) = 1/\pi\rho Dk^2$. The $1/|k|$ behavior of $\Pi(k)$ implies that the kinetics is superdiffusive, also known as Lévy flights, and leads to criticality in 1D (Bouchaud and Georges, 1990). In particular, calculating the average IPR $\langle P_q\rangle$, one finds the following result for the fractal dimensions

$$\tau_q \simeq (q-1)(1 - qt/8\pi\beta)\ ,\qquad q \ll 8\pi\beta/t\ ,\qquad (3.7)$$

i.e. the weak-multifractality-results (2.36), (2.37) for τ_q and $f(\alpha)$ with $d = 1$ and $\gamma = t/8\pi\beta$. For definiteness, we focus below on the band center, $E = 0$, where $\gamma = 1/2\pi\beta b$.

These results are in good agreement with numerical simulations, Figs. 11, 12. The deviations from the asymptotic (parabolic) form in Fig. 12, which are particularly pronounced at $b = 1$, are a precursor of the crossover to the small-b regime (Sec. III.C), where the parabolic approximation breaks down completely.

The IPR fluctuations are also found (Evers and Mirlin, 2000; Mirlin and Evers, 2000) by generalizing the results obtained for metallic samples (Fyodorov and Mirlin, 1995; Mirlin, 2000b; Prigodin and Altshuler, 1998). In particular, the IPR variance is given for $q \ll q_+(b) \equiv (2\beta\pi b)^{1/2}$ by

$$\text{var}(P_q)/\langle P_q\rangle^2 = q^2(q-1)^2/24\beta^2 b^2\ ,\qquad (3.8)$$

cf. Eq. (2.50). Calculating higher cumulants, one can restore the corresponding scale-invariant distribution function,

$$\mathcal{P}(\tilde{P}) = e^{-\tilde{P}-\mathbf{C}}\exp(-e^{-\tilde{P}-\mathbf{C}})\ ,\qquad (3.9)$$

where

$$\tilde{P} = \left[\frac{P_q}{\langle P_q\rangle} - 1\right]\frac{2\pi\beta b}{q(q-1)}\ ,\qquad (3.10)$$
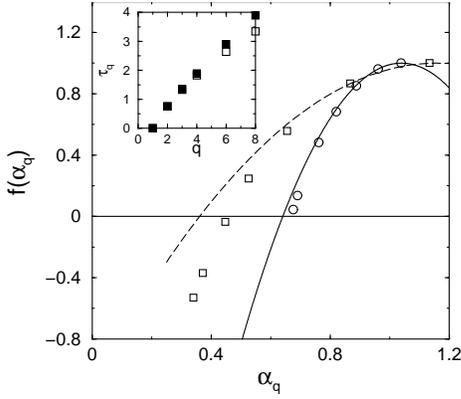
FIG. 12 Multifractal spectrum $f(\alpha)$ for $b = 1$ ($\square$) and $b = 4$ ($\circ$). Solid line indicates the parabolic approximation Eq. (2.37). Inset: exponent τ_q ($\square$) and τ_q^{typ} ($\blacksquare$) for $b = 1$. (Mirlin and Evers, 2000).
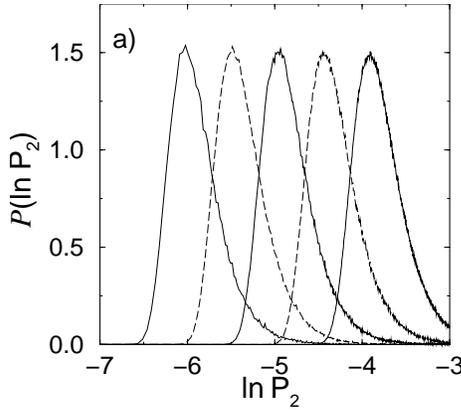
FIG. 13 Evolution of the distribution $\mathcal{P}(\ln P_2)$ for $b = 1$ with the system size L (from left to right: $L = 4096, 2048, 1024, 512, (256)$). The scale invariance of the IPR distribution is clearly seen. (Mirlin and Evers, 2000).

and $\mathbf{C} \simeq 0.5772$ is the Euler constant. Equation (3.9) is valid for $P_q/\langle P_q \rangle - 1 \ll 1$. At $P_q/\langle P_q \rangle - 1 \sim 1$ the exponential falloff (3.9) crosses over to a power-law tail

$$\mathcal{P}(P_q) \sim (P_q/\langle P_q \rangle)^{-1-x_q} \ . \tag{3.11}$$

with

$$x_q = 2\pi\beta b/q^2 \ , \qquad q^2 < 2\pi\beta b \ , \tag{3.12}$$

see the discussion of general properties of the IPR distribution in Sec. II.C.5.

The analytical results on the IPR distribution are confirmed by numerical simulations. Figure 13 demonstrates the scale invariance of the distribution. Figure 14 shows results for the distribution of the IPRs P_q with $q = 2$, 4, and 6 at $b = 4$ (the corresponding value of q_+ being $q_+ = (8\pi)^{1/2} \simeq 5$). It is seen that at $q = 2$ the analytical formula (3.9) nicely describes the "main body" of the distribution, with the upward deviations at large $\tilde{P}$ indicating the crossover to the power-law tail (3.11).
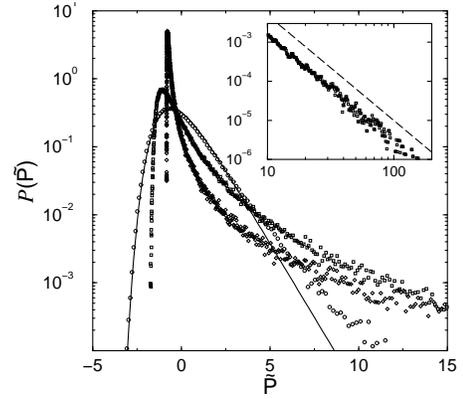
FIG. 14 Distribution function $\mathcal{P}(\tilde{P}_q)$ at $q = 2$ ($\circ$), 4 ($\square$), and 6 ($\diamond$) at $b = 4$ for systems of size $L = 4096$. The solid line represents the analytical result Eq. (3.9). Inset: Asymptotic of $\mathcal{P}(\tilde{P}_4)$. Dashed line indicates power law with exponent $x_4 = 1.7$. (Mirlin and Evers, 2000).

The asymptotic behavior (3.11) is outside the reach of the numerical simulations for $q = 2$, however, since the condition of its validity $\tilde{P} \gg 2\pi\beta/q(q-1) \simeq 12.5$ corresponds to very small values of the distribution function $\mathcal{P}(\tilde{P}) \ll 10^{-5}$, and its clear resolution would require a much larger statistical ensemble. The situation changes, however, with increasing q (see the data for $q = 4$, 6 in Fig. 14). Equation (3.9) becomes inapplicable (since the condition of its validity $q \ll q_+$ is no longer met), and the power-law asymptotic behavior (3.11) becomes clearly seen. In particular, the inset of Fig. 14 shows the tail for $q = 4$; the extracted value of the index $x_4 \simeq 1.7$ is in good agreement with the prediction of the $b \gg 1$ theory, $x_4 = \pi/2$.

C. Strong multifractality, $b \ll 1$

In the quasi-insulating case $b \ll 1$ the problem can be studied (Mirlin and Evers, 2000) via the RG method earlier developed for related problems by Levitov (1990, 1999). The idea of the method is as follows. One starts from the diagonal part of the matrix $\hat{H}$, each eigenstate with an energy $E_i = H_{ii}$ being localized on a single site i. Then one includes into consideration non-diagonal matrix elements H_{ij} with $|i-j| = 1$. Most of these matrix elements are essentially irrelevant, since their typical value is $\sim b$, while the energy difference $|E_i - E_j|$ is typically of order unity. Only with a small probability ($\sim b$) is $|E_i - E_j|$ also of the order of b, so that the matrix element mixes strongly the two states, which are then said to be in resonance. In this case one is led to consider a two-level problem

$$\hat{H}_{\text{two-level}} = \begin{pmatrix} E_i & V \\ V & E_j \end{pmatrix} \ ; \qquad V = H_{ij} \ . \tag{3.13}$$

The corresponding eigenfunctions and eigenenergies are

$$\psi^{(+)} = \begin{pmatrix} \cos\theta \\ \sin\theta \end{pmatrix} ; \qquad \psi^{(-)} = \begin{pmatrix} -\sin\theta \\ \cos\theta \end{pmatrix} (3.14)$$

$$E_\pm = (E_i + E_j)/2 \pm |V|\sqrt{1+\tau^2} , \qquad (3.15)$$

where $\tan\theta = -\tau + \sqrt{1+\tau^2}$ and $\tau = (E_i - E_j)/2V$.

In the next RG step the matrix elements H_{ij} with $|i-j| = 2$ are taken into account, then those with $|i-j| = 3$, and so forth. Each time a resonance is encountered, the Hamiltonian is re-expressed in terms of the new states. Since the probability of a resonance at a distance r is $\sim b/r$, the typical scale r_2 at which a resonance state formed at a scale r_1 will be again in resonance satisfies

$$\ln(r_2/r_1) \sim 1/b , \qquad (3.16)$$

so that r_2 is much larger than r_1. Therefore, when considering the resonant two-level system at the scale r_2, one can treat the r_1-resonance state as point-like.

This leads to the following evolution equation for the IPR distribution (for $\beta = 1$):

$$\frac{\partial}{\partial \ln r} f(P_q, r) = \frac{2b}{\pi} \int_0^{\pi/2} \frac{d\theta}{\sin^2\theta \cos^2\theta}$$

$$\times [-f(P_q, r) + \int dP_q^{(1)} dP_q^{(2)} f(P_q^{(1)}, r) f(P_q^{(2)}, r)$$

$$\times \delta(P_q - P_q^{(1)} \cos^{2q}\theta - P_q^{(2)} \sin^{2q}\theta)] . \qquad (3.17)$$

Eq. (3.17) is a kind of kinetic equation (in the fictitious time $t = b\ln r$), with the two terms in the square brackets describing the scattering-out and scattering-in processes, respectively.

Multiplying Eq. (3.17) by P_q and then integrating over P_q, we get the evolution equation for $\langle P_q \rangle$

$$\partial \langle P_q \rangle / \partial \ln r = -2bT(q)\langle P_q \rangle \qquad (3.18)$$

with

$$T(q) = \frac{1}{\pi} \int_0^{\pi/2} \frac{d\theta}{\sin^2\theta \cos^2\theta} (1 - \cos^{2q}\theta - \sin^{2q}\theta)$$

$$= \frac{2}{\sqrt{\pi}} \frac{\Gamma(q-1/2)}{\Gamma(q-1)} \equiv \frac{1}{2^{2q-3}} \frac{\Gamma(2q-1)}{\Gamma(q)\Gamma(q-1)} . (3.19)$$

Integrating (3.18) from $r = 1$ to $r \sim L$, we find the multifractal behavior $\langle P_q \rangle \sim L^{-\tau_q}$ with the exponents

$$\tau_q = 2bT(q) . \qquad (3.20)$$

It is assumed here that $q > 1/2$, which is the condition of the existence of the integral in Eq. (3.19). For $q < 1/2$ the resonance approximation breaks down; the exponents can be found then from the symmetry relation (2.38). The function $T(q)$ is shown in Fig. 15. Its asymptotics are

$$T(q) \simeq -1/[\pi(q-1/2)] , \qquad q \to 1/2 ; \quad (3.21)$$
$$T(q) \simeq (2/\sqrt{\pi})q^{1/2} , \qquad q \gg 1 . \quad (3.22)$$
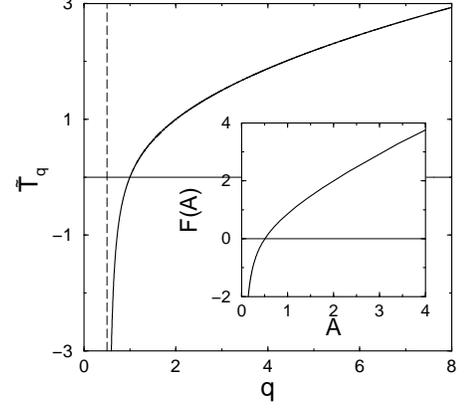
FIG. 15 Universal function $T(q)$ characterizing the exponents $\tau(q)$ via $\tau(q) = 2bT(q)$ at $b \ll 1$. Dashed line indicates the pole position. Inset: Legendre transform $F(A)$ describing the multifractal spectrum via $f(\alpha) = 2bF(\alpha/2b)$. (Mirlin and Evers, 2000).

We see that the fractal exponents are proportional to the small parameter b. This is characteristic of wave functions that are very small, typically, with rare and strong peaks (resonances). In the limit $b \to 0$ the fractal exponents tend to their insulator value $\tau_q = 0$ for all $q > 1/2$.

Legendre transformation of (3.20) produces the $f(\alpha)$-spectrum of the form

$$f(\alpha) = 2bF(A) ; \qquad A = \alpha/2b , \qquad (3.23)$$

where $F(A)$ is the Legendre transform of $T(q)$. The function $F(A)$ is shown in the inset of Fig. 15, its asymptotics are

$$F(A) \simeq -1/\pi A , \qquad A \to 0 ; \qquad (3.24)$$
$$F(A) \simeq A/2 , \qquad A \to \infty . \qquad (3.25)$$

Furthermore, it changes sign at $A_- \simeq 0.5104$, corresponding to $q_c \simeq 2.4056$. These analytical findings are fully supported by numerical simulations, Fig. 16. The above results, Eqs. (3.20)–(3.25) are valid for $q > 1/2$, which corresponds to $\alpha < 1$. The other part of the spectrum can be obtained via the symmetry relation (2.38), (2.39), which is also confirmed by numerical results, see Figs. 2, 3, 23, 24.

We return now to the IPR distribution function. Figure 17 shows the results of the numerical integration of Eq. (3.17) for $q = 2$ with the initial condition $f(P_2) = \delta(P_2 - 1)$ at $t = 0$. It is seen that at sufficiently large t the distribution of $\ln P_2$ acquires a limiting form, shifting with t without changing its shape. This conclusion of scale-invariance of the IPR distribution is also supported
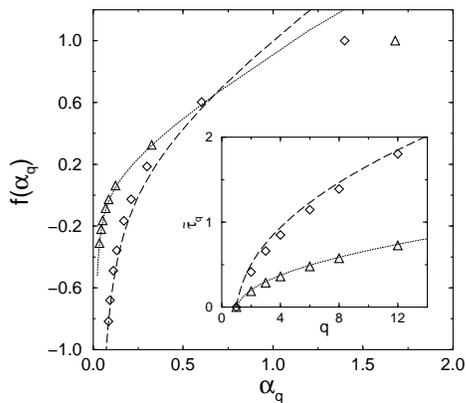
FIG. 16 Multifractal spectrum $f(\alpha)$ for $b = 0.25$ ($\diamond$) and $b = 0.1$ ($\triangle$). Inset: exponent $\tau(q)$. Dashed and dotted lines indicate the analytical results Eqs. (3.23) and (3.20). (Mirlin and Evers, 2000).
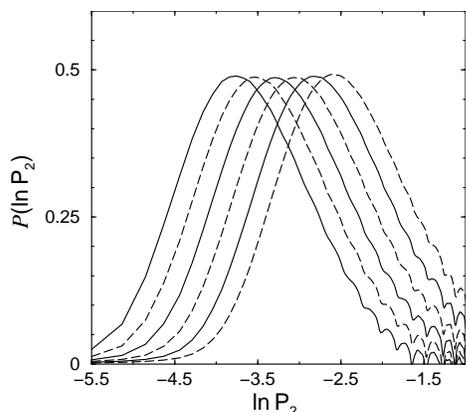
FIG. 17 Flow of the distribution of $\ln P_2$ calculated from the kinetic equation (3.17) at $t = b\ln r = 1.2 \ldots 1.7$ (from right to left). The oscillations near $\ln P_2 = -1.5$ are numerical artifacts due to rounding errors. (Mirlin and Evers, 2000).

by analytical arguments: it is found that the fixed-point distribution has the form

$$f(P_q, r) = r^{\tau_q^{\text{typ}}} f_0(P_q r^{\tau_q^{\text{typ}}}) \qquad (3.26)$$

with τ_q^{typ} as defined in Sec. II.C.5. In agreement with a general discussion in Sec. II.C.5 the distribution is found to have a power-law tail, $f_0(\tilde{P}_q) \sim \tilde{P}^{-x_q-1}$, with the index x_q given by Eqs. (2.44), (2.45).

All the formulas of this subsection remain valid for the case $\beta = 2$, with a replacement $b \longrightarrow (\pi/2\sqrt{2})b$.

D. Levels statistics

In the $b \gg 1$ regime the two-level correlation function (2.70) is obtained by an appropriate generalization of the earlier findings for the diffusive samples. In particular, considering for simplicity the $\beta = 2$ ensemble at the band center, the level correlation function has

the form[8] (Kravtsov and Muttalib, 1997; Mirlin, 2000b; Mirlin and Evers, 2000)

$$R_2^{(c)}(s) = \delta(s) - \frac{\sin^2(\pi s)}{(\pi s)^2}\frac{(\pi s/4b)^2}{\sinh^2(\pi s/4b)} \ . \qquad (3.27)$$

The correlation function (3.27) follows the RMT result $R_2^{(c)}(s) = \delta(s) - \sin^2(\pi s)/(\pi s)^2$ up to the scale $s \sim b$ (playing the role of the Thouless energy here), and then begins to decay exponentially. The spectral compressibility at $b \gg 1$ is given by

$$\chi \simeq 1/2\pi\beta b \ , \qquad b \gg 1 \ . \qquad (3.28)$$

In the opposite limit, $b \ll 1$, the evolution equation for $R_2(\omega, r)$ can be written down in analogy with Eq. (3.17) (Mirlin and Evers, 2000), with the result (for $\beta = 1$)

$$R_2^{(c)}(s) = \delta(s) - \text{erfc}(|s|/2\sqrt{\pi}b) \ , \qquad (3.29)$$

where $\text{erfc}(x) = (2/\sqrt{\pi})\int_x^\infty \exp(-t^2)dt$ is the error function. This yields the spectral compressibility

$$\chi \simeq 1 - 4b \ , \qquad b \ll 1 \ . \qquad (3.30)$$

The results for the $\beta = 2$ case are qualitatively similar,

$$R_2^{(c)}(s) = \delta(s) - \exp(-s^2/2\pi b^2) \qquad (3.31)$$

$$\chi \simeq 1 - \pi\sqrt{2}\,b \ , \qquad b \ll 1 \ . \qquad (3.32)$$

Thus, in the limit of small b the level repulsion is efficient in a narrow region $|s| \lesssim b$ only, and the spectral compressibility tends to the Poisson value $\chi = 1$. The physical reason for the reduced range of the level repulsion is quite transparent. Consider two nearby in energy states separated by a typical distance $r \sim L$ in the coordinate space. If their energy difference $s \lesssim b$, such two states will form a resonance pair, so that their levels will repel. On the other hand, if $s \gg b$, these two states will not be in resonance, their wave functions remain weakly overlapping, and the level repulsion between them will be inefficient.

These results are fully supported by the numerical data. Figure 18 represents the level correlation function $R_2(s)$ at $b = 0.1$, in agreement with Eq. (3.29). The level number variance $\text{var}[n(\mathcal{E})]$ is plotted versus the average $\langle n(\mathcal{E})\rangle$ in Fig. 19; the data show an extended plateau region in $\text{var}[n(\mathcal{E})]/\langle n(\mathcal{E})\rangle$, determining χ. The upper bound for this region is set by the matrix size L, while the lower bound is $\sim b$. The numerically obtained spectral compressibility in a broad range of b is shown in Fig. 20; in the large-b and small-b regions it agrees well with the corresponding analytical asymptotics.

[8] The precise form of the level correlation function R_2 depends on the boundary conditions, which are chosen to be periodic in this subsection. The value of the spectral compressibility η is independent on the boundary conditions.
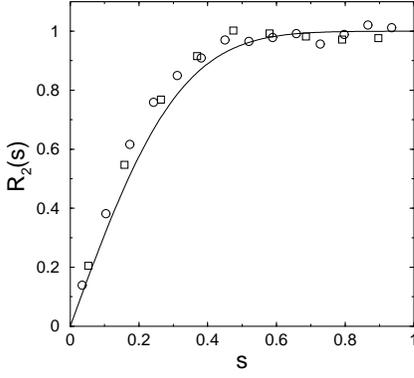
FIG. 18 Two-level correlation function $R_2(s)$ for two system sizes $L = 256$ (○) and $L = 512$ (□) at $b = 0.1$. The solid line indicates the theoretical result (3.29). (Mirlin and Evers, 2000).
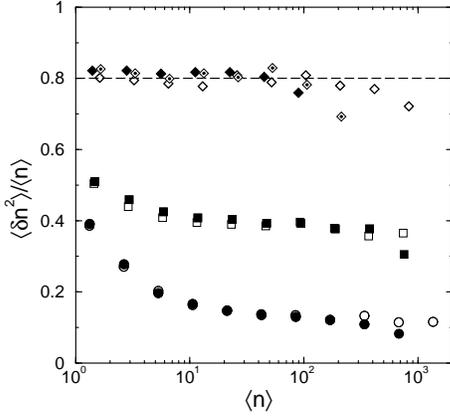
FIG. 19 Variance of the number of levels $\langle \delta n^2 \rangle$ as a function of the energy width of the interval parametrized by the mean level number $\langle n \rangle$. Traces correspond to $b = 1$ (open ○: $L = 4096$, filled: $L = 2048$), $b = 0.25$ (open □: $L = 4096$, filled: $L = 2048$) and $b = 0.05$ (open ◇: $L = 4096$, ◇ with dot: $L = 1024$, filled: $L = 512$). The dashed line indicates the analytical prediction Eq. (3.30). (Mirlin and Evers, 2000).
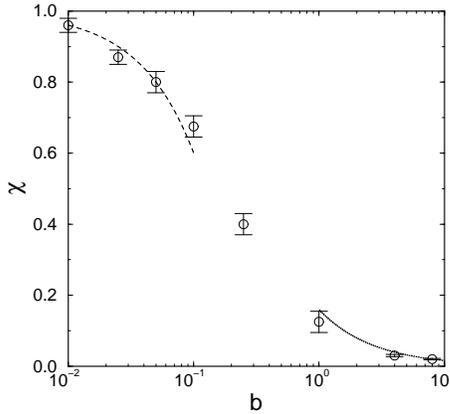
FIG. 20 Spectral compressibility χ as a function of b: crossover from the "quasi-metallic" ($b \gg 1$) to the "quasi-insulating" ($b \ll 1$) behavior. The lines indicate the analytical results for $b \gg 1$ and $b \ll 1$, Eqs. (3.28) and (3.30). (Mirlin and Evers, 2000).

E. Boundary criticality

The presentation in this subsection follows Mildenberger *et al.* (2007b). In spirit of Sec. II.C.8, we consider the critical PRBM model model with a boundary at $i = 0$, which means that the matrix element H_{ij} is zero whenever one of the indices is negative. The implementation of the boundary is, however, not unique. The important point is that this degree of freedom affects the boundary criticality. Specifically, one should specify what happens with a particle which "attempts to hop" from a site $i \geq 0$ to a site $j < 0$, which is outside of the Hilbert space. One possibility is that such hops are simply discarded, so that the matrix element variance $\langle |H_{ij}|^2 \rangle \equiv J_{ij}$ is simply given by $J_{ij} = [1 + (i-j)^2/b^2]^{-1}$ for $i, j \geq 0$. More generally, the particle may be reflected by the boundary with certain probability p and "land" on the site $-j > 0$. This leads to the following formulation of the model,

$$J_{ij} = \frac{1}{1 + |i-j|^2/b^2} + \frac{p}{1 + |i+j|^2/b^2}. \qquad (3.33)$$

While the above probability interpretation restricts p to the interval $[0, 1]$, the model is defined for all p in the range $-1 < p < \infty$. The newly introduced parameter p is immaterial in the bulk, where $i, j \gg |i-j|$ and the second term in Eq. (3.33) can be neglected. Therefore, the bulk exponents τ_q^b depend on b only (and not on p), and their analysis in Sec. III.B, III.C remains applicable without changes. On the other hand, as discussed below, the surface exponents τ_q^s are function of two parameters, b and p.

Equation (3.33) describes a semi-infinite system with one boundary at $i = 0$. For a finite system of a length L (implying that the relevant coordinates are restricted to $0 \leq i, j \leq L$) another boundary term, $p'/[1 + (i + j - 2L)^2/b^2]$, is to be included on the right-hand side of Eq. (3.33). In general, the parameter p' of this term may be different from p. This term, however, does not affect the boundary criticality at the $i = 0$ boundary, so it is discarded below.

The regime of weak criticality, $b \gg 1$, can be studied via a mapping onto the supermatrix σ-model as in the bulk case, Sec. III.B. This results again in an approximately parabolic spectrum, which, however, differs by a constant factor R_p from its bulk counterpart,

$$\Delta_q^s = [q(1-q)/2\pi\beta b]R_p \equiv \Delta_q^b R_p. \qquad (3.34)$$

This factor is determined from the solution of the classical Levy flight problem with boundary,

$$\frac{\partial W_i(t)}{\partial t} + \pi\rho \sum_{j=0}^{\infty} \left[\delta_{ij} J_0^{(i)} - J_{ij} \right] W_j(t) = 0, \qquad (3.35)$$

where $J_0^{(i)} = \sum_{k=0}^{\infty} J_{ik}$, with the initial condition $W_i(0) = \delta_{ir}$, where r is near the boundary. Specifically,
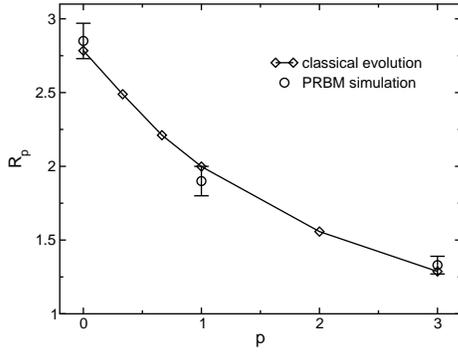
FIG. 21 The ratio $R_p = \Delta_q^{\mathrm{s}}(b,p)/\Delta_q^{\mathrm{b}}(b)$ of the surface and bulk anomalous exponents for large b, as a function of the reflection parameter p. Diamonds represent the results of the σ-model analysis with a numerical solution of the corresponding classical evolution equation (3.35). Circles represent a direct computer simulation of the PRBM model with $b = 8$. The ratio R_p has been evaluated for the range $0 < q < 1$, where the numerical accuracy of the anomalous exponents is the best. Within this interval the obtained R_p is q-independent (within numerical errors) in agreement with Eq. (3.34). (Mildenberger $et\ al.$, 2007b).

the return probability $W_r(t)$ decays with time as $1/t$, and the corresponding prefactor yields the fractal exponents,

$$\Delta_q^{\mathrm{s}}/q(1-q) = \beta^{-1} t W_r(t)|_{t\to\infty}. \qquad (3.36)$$

The evolution equation (3.35) was solved numerically; the obtained results for R_p are shown in Fig. 21. For $p = 1$ the evolution equation can be obtained from its bulk counterpart (defined on the whole axis, $-\infty < i < \infty$) by "folding the system" on the semiaxis $i > 0$ according to $W_i(t) + W_{-i}(t) \longrightarrow W_i(t)$, leading to the analytical result

$$R_1 = 2. \qquad (3.37)$$

As in the bulk case, the regime of small b can be studied via the real-space RG method (Sec. III.C). The multifractal exponents are found to be

$$\tau_q^{\mathrm{s}} = (1+p)^{1/2} b T(q) = [(1+p)^{1/2}/2]\tau_q^{\mathrm{b}}, \qquad (3.38)$$

with $T(q)$ given by Eq. (3.19), i.e. they differ from the bulk exponents by the factor $(1+p)^{1/2}$. In full analogy with the bulk formula (3.20), the result (3.38) is valid for $q > 1/2$, where the multifractal exponent τ_q is small. The results can, however be extended to the range of $q < 1/2$ by using the symmetry relation (2.38). For all q the obtained relation between the surface and the bulk multifractal spectra can be formulated in the following way:

$$\tau_q^{\mathrm{s}}(b,p) = \tau_q^{\mathrm{b}}(b \longrightarrow b(1+p)^{1/2}/2). \qquad (3.39)$$

These predictions were corroborated by numerical simulations of the PRBM model. Figure 22 shows the dependence of the anomalous dimension $\Delta_2 \equiv D_2 - 1$ on b
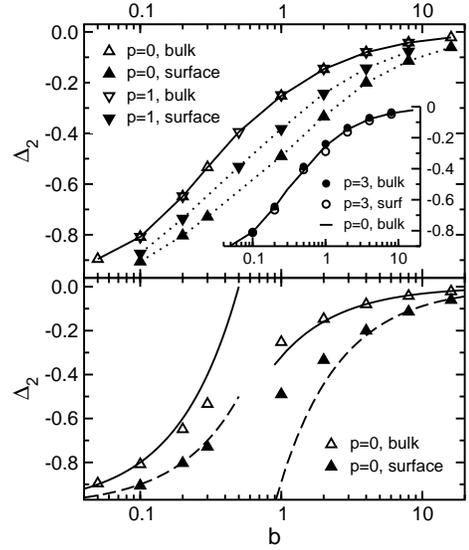
FIG. 22 $Upper\ panel:$ Anomalous exponent $\Delta_2 \equiv D_2 - 1$ as a function of b from numerical simulations in the bulk and at the boundary for the reflection parameter $p = 0$ and 1. The inset shows data for $p = 3$ compared to the $p = 0$ bulk values. $Lower\ panel:$ Surface and bulk data for $p = 0$ compared with analytical results for small and large b (using $R_0 = 2.78$), Eqs. (3.7), (3.34), (3.20), (3.38). (Mildenberger $et\ al.$, 2007b).

in the bulk and at the boundary, for three different values of the reflection parameter p. In Fig. 23 the whole multifractal spectra Δ_q are shown for fixed large values of b. Specifically, the anomalous dimensions Δ_q^{s} and Δ_q^{b} are presented for $b = 2$, 4 and 8, with the reflection parameter chosen to be $p = 1$. For all curves the q dependence is approximately parabolic, as predicted by the large-b theory, Eq. (3.34), with the prefactor inversely proportional to b. It is also seen in Fig. 23 that the bulk multifractality spectrum for $b = 4$ and the surface spectrum for $b = 8$ are almost identical, in agreement with Eq. (3.37). The same is true for the relation between the bulk spectrum for $b = 2$ and the surface spectrum for $b = 4$. The ratio of the large-b surface and bulk anomalous dimensions, $R_p = \Delta_q^{\mathrm{s}}/\Delta_q^{\mathrm{b}}$, is in good agreement with the σ-model predictions for R_p, as shown in Fig. 21. In Fig. 24 the surface and bulk multifractal spectra are shown for the case of small b. While the spectra are strongly non-parabolic in this limit, they clearly exhibit the symmetry $q \to 1 - q$, Eq. (2.38). The data are in good agreement with the real-space RG results.

F. Further related activities

As a model of the Anderson critical point, the PRBM ensemble has attracted a lot of interest during recent years. In view of space limitations, we can only briefly mention some of these works. The corresponding research directions in-
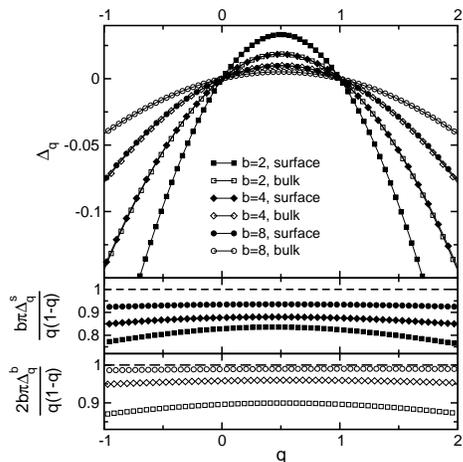
FIG. 23 *Upper panel:* Boundary and bulk multifractal spectra, Δ_q^{s} and Δ_q^{b}, at $b = 2, 4$, and 8 for the reflection parameter $p = 1$. In accordance with Eq. (3.37), the surface multifractality spectrum is enhanced by a factor close to two compared to the bulk. *Middle panel:* Surface spectrum divided by the analytical $b \gg 1$ result, Eq. (3.34). With increasing b, the numerical data converges towards the analytical result (dashed line). *Lower panel:* Analogous plot for the bulk spectrum. (Mildenberger *et al.*, 2007b).

FIG. 24 *Main panel:* Numerically determined boundary and bulk anomalous dimensions Δ_q at $b = 0.1$ for $p = 0, 1$, and 3. As expected, the bulk anomalous dimension is independent of the value of p. In accordance with Eq. (3.39), for $p = 3$ surface and bulk dimensions have the same values. *Inset:* The $p = 0$ data compared to the analytical results, surface [solid line, Eq. (3.38)] and bulk [dashed line, Eq. (3.20)]. Analytical data have been calculated for $q \geq 0.6$ and mirrored for $q \leq 0.4$ by using the symmetry relation $\Delta_q = \Delta_{1-q}$. In the vicinity of $q = 1/2$, at $|q - 1/2| \lesssim 1/\ln b^{-1}$, the analytical result (3.20) breaks down. (Mildenberger *et al.*, 2007b).

clude: relation to the system of interacting fermions in 1D (Luttinger liquid) (Kravtsov and Tsvelik, 2000); a generalization of the model to two dimensions (Potempa and Schweitzer, 2002); wave function statistics (Cuevas, 2003a,b; Cuevas *et al.*, 2002; Varga, 2002); level correlations (Cuevas, 2005; Garcia-Garcia, 2006); virial expansion for level statistics of almost diagonal random matrices (Kravtsov *et al.*, 2006; Yevtushenko and Kravtsov, 2003, 2004); chiral PRBM and possible applications to quantum chromodynamics (Garcia-Garcia and Takahashi, 2004), and manifestations of multifractality in scattering characteristics of an open system (Mendez-Bermudez and Kottos, 2005; Mendez-Bermudez and Varga, 2006). Rotationally-invariant random matrix ensembles with level statistics largely similar to that in the critical PRBM ensembles were studied in Moshe *et al.* (1994); Muttalib *et al.* (2001, 1993); a relation between these ensembles and the PRBM model is discussed in (Kravtsov and Muttalib, 1997; Mirlin, 2000b).

IV. SYMMETRIES OF DISORDERED SYSTEMS

In this section we briefly review the symmetry classification of disordered systems based on the relation to the classical symmetric spaces, which was established in Altland and Zirnbauer (1997); Zirnbauer (1996). For a detailed presentation of the scheme and the underlying mathematical structures the reader is referred to a recent review by Caselle and Magnea (2004). A mathematical

proof of the completeness of the classification was given in Heinzner *et al.* (2005).

A. Wigner-Dyson classes

The random matrix theory (RMT) was introduced into physics by Wigner (1951). Developing Wigner's ideas, Dyson (1962) put forward a classification scheme of ensembles of random Hamiltonians. This scheme takes into account the invariance of the system under time reversal and spin rotations, yielding three symmetry classes: unitary, orthogonal and symplectic.

If the time-reversal invariance (T) is broken, the Hamiltonians are just arbitrary Hermitian matrices,

$$H = H^\dagger \;, \tag{4.1}$$

with no further constraints. This set of matrices is invariant with respect to rotations by unitary matrices; hence the name "unitary ensemble". In this situation, the presence or absence of spin rotation invariance (S) is not essential: if the spin is conserved, H is simply a spinless unitary-symmetry Hamiltonian times the unit matrix in the spin space. In the RMT one considers most frequently an ensemble of matrices with independent, Gaussian-distributed random entries, which is called the Gaussian unitary ensemble (GUE). While disordered systems have, of course, much richer physics than the Gaussian ensembles, their symmetry classification is inherited from the RMT.

Let us now turn to the systems with preserved time-reversal invariance. The latter is represented by an antiunitary operator, $T = KC$, where C is the operator of complex conjugation and K is unitary. The time-reversal invariance thus implies $H = KH^{\mathrm{T}}K^{-1}$ (we used the Hermiticity, $H^* = H^{\mathrm{T}}$). Since acting twice with T should leave the physics unchanged, one infers that $K^*K = p$, where $p = \pm 1$. As was shown by Wigner, the two cases correspond to systems with integer ($p = +1$) and half-integer ($p = -1$) angular momentum. If $p = 1$, a representation can be chosen where $K = 1$, so that

$$H = H^{\mathrm{T}} . \tag{4.2}$$

The set of Hamiltonians thus spans the space of real symmetric matrices in this case. This is the orthogonal symmetry class; its representative is the Gaussian orthogonal ensemble (GOE). For disordered electronic systems this class is realized when spin is conserved, as the Hamiltonian then reduces to that for spinless particles (times unit matrix in the spin space).

If T is preserved but S is broken, we have $p = -1$. In the standard representation, K is then realized by the second Pauli matrix, $K = i\sigma_y$, so that the Hamiltonian satisfies

$$H = \sigma_y H^{\mathrm{T}} \sigma_y. \tag{4.3}$$

It is convenient to split the $2N \times 2N$ Hamiltonian in 2×2 blocks (quaternions) in spin space. Each of them then is of the form $q = q_0\sigma_0 + iq_1\sigma_x + iq_2\sigma_y + iq_3\sigma_z$ (where σ_0 is the unit matrix and $\sigma_{x,y,z}$ the Pauli matrices), with real q_μ, which defines a real quaternion. This set of Hamiltonians is invariant with respect to the group of unitary transformations conserving σ_y, $U\sigma_y U^T = \sigma_y$, which is the symplectic group $\mathrm{Sp}(2N)$. The corresponding symmetry class is thus called symplectic, and its RMT representative is the Gaussian symplectic ensemble (GSE).

B. Relation to symmetric spaces

Before discussing the relation to the families of symmetric spaces, we briefly remind the reader how the latter are constructed (Caselle and Magnea, 2004; Helgason, 1978). Let G be one of the compact Lie groups $\mathrm{SU}(N)$, $\mathrm{SO}(N)$, $\mathrm{Sp}(2N)$, and $\mathfrak{g}$ the corresponding Lie algebra. Further, let θ be an involutive automorphism $\mathfrak{g} \to \mathfrak{g}$ such that $\theta^2 = 1$ but θ is not identically equal to unity. It is clear that θ splits $\mathfrak{g}$ in two complementary subspaces, $\mathfrak{g} = \mathfrak{K} \oplus \mathfrak{P}$, such that $\theta(X) = X$ for $X \in \mathfrak{K}$ and $\theta(X) = -X$ for $X \in \mathfrak{P}$. It is easy to see that the following Lie algebra multiplication relations holds:

$$[\mathfrak{K}, \mathfrak{K}] \subset \mathfrak{K}, \qquad [\mathfrak{K}, \mathfrak{P}] \subset \mathfrak{P}, \qquad [\mathfrak{P}, \mathfrak{P}] \subset \mathfrak{K}. \tag{4.4}$$

This implies, in particular, that $\mathfrak{K}$ is a subalgebra, whereas $\mathfrak{P}$ is not. The coset space G/K (where K is the Lie group corresponding to $\mathfrak{K}$) is then a compact symmetric space. The tangent space to G/K is $\mathfrak{P}$. One can also construct an associated non-compact space. For this purpose, one first defines the Lie algebra $\mathfrak{g}^* = \mathfrak{K} \oplus i\mathfrak{P}$, which differs from $\mathfrak{g}$ in that the elements in $\mathfrak{P}$ are multiplied by i. Going to the corresponding group and dividing K out, one gets a non-compact symmetric space G^*/K.

The groups G themselves are also symmetric spaces and can be viewed as coset spaces $G \times G/G$. The corresponding non-compact space is $G^{\mathbb{C}}/G$, where $G^{\mathbb{C}}$ is the complexification of G (which is obtained by taking the Lie algebra $\mathfrak{g}$, promoting it to the algebra over the field of complex numbers, and then exponentiating).

The connection with symmetric spaces is now established in the following way (Altland and Zirnbauer, 1997; Zirnbauer, 1996). Consider first the unitary symmetry class. Multiplying a Hamiltonian matrix by i, we get an antihermitean matrix $X = iH$. Such matrices form the Lie algebra $\mathfrak{u}(N)$. Exponentiating it, one gets the Lie group $\mathrm{U}(N)$, which is the compact symmetric space of class A in Cartan's classification. For the orthogonal class, $X = iH$ is purely imaginary and symmetric. The set of such matrices is a linear complement $\mathfrak{P}$ of the algebra $\mathfrak{K} = \mathfrak{o}(N)$ of imaginary antisymmetric matrices in the algebra $\mathfrak{g} = \mathfrak{u}(N)$ of antihermitean matrices. The corresponding symmetric space is $G/K = \mathrm{U}(N)/\mathrm{O}(N)$, which is termed AI in Cartan's classification. For the symplectic ensemble the same consideration leads to the symmetric space $\mathrm{U}(N)/\mathrm{Sp}(N)$, which is the compact space of the class AII. If we don't multiply H by i but instead proceed with H in the analogous way, we end up with associated non-compact spaces G^*/K. To summarize, the linear space $\mathfrak{P}$ of Hamiltonians can be considered as a tangent space to the compact G/K and non-compact G^*/K symmetric spaces of the appropriate symmetry class.

This correspondence is summarized in Table I, where the first three rows correspond to the Wigner-Dyson classes, the next three to the chiral classes (Sec. IV.C) and last four to the Bogoliubov-de Gennes classes (Sec. IV.D). The last two columns of the table specify the symmetry of the corresponding σ-model. In the supersymmetric formulation, the base of the σ-model target space $\mathcal{M}_\mathcal{B} \times \mathcal{M}_\mathcal{F}$ is the product of a non-compact symmetric space $\mathcal{M}_\mathcal{B}$ corresponding to the bosonic sector and a compact ("fermionic") symmetric space $\mathcal{M}_\mathcal{F}$. (In the replica formulation, the space is $\mathcal{M}_\mathcal{B}$ for bosonic replicas or $\mathcal{M}_\mathcal{F}$ for fermionic replicas, supplemented with the replica limit $n \to 0$.) The Cartan symbols for these symmetric spaces are given in the sixth column, and the compact components $\mathcal{M}_\mathcal{F}$ are listed in the last column. It should be stressed that the symmetry classes of $\mathcal{M}_\mathcal{B}$ and $\mathcal{M}_\mathcal{F}$ are different from the symmetry class of the ensemble (i.e. of the Hamiltonian) and in most cases are also different from each other. Following the common convention, when we refer to a system as belonging to a particular class, we mean the symmetry class of the Hamiltonian.

It is also worth emphasizing that the orthogonal groups appearing in the expressions for $\mathcal{M}_\mathcal{F}$ are $\mathrm{O}(N)$ rather than $\mathrm{SO}(N)$. This difference (which was irrelevant when

Ham. class	RMT	T	S	compact symmetric space	non-compact symmetric space	σ-model B|F	σ-model compact sector $\mathcal{M}_F$
Wigner-Dyson classes							
A	GUE	$-$	$\pm$	$\mathrm{U}(N)\times\mathrm{U}(N)/\mathrm{U}(N)\equiv\mathrm{U}(N)$	$\mathrm{GL}(N,\mathbb{C})/\mathrm{U}(N)$	AIII|AIII	$\mathrm{U}(2n)/\mathrm{U}(n)\times\mathrm{U}(n)$
AI	GOE	$+$	$+$	$\mathrm{U}(N)/\mathrm{O}(N)$	$\mathrm{GL}(N,\mathbb{R})/\mathrm{O}(N)$	BDI|CII	$\mathrm{Sp}(4n)/\mathrm{Sp}(2n)\times\mathrm{Sp}(2n)$
AII	GSE	$+$	$-$	$\mathrm{U}(2N)/\mathrm{Sp}(2N)$	$\mathrm{U}^*(2N)/\mathrm{Sp}(2N)$	CII|BDI	$\mathrm{O}(2n)/\mathrm{O}(n)\times\mathrm{O}(n)$
chiral classes							
AIII	chGUE	$-$	$\pm$	$\mathrm{U}(p+q)/\mathrm{U}(p)\times\mathrm{U}(q)$	$\mathrm{U}(p,q)/\mathrm{U}(p)\times\mathrm{U}(q)$	A|A	$\mathrm{U}(n)$
BDI	chGOE	$+$	$+$	$\mathrm{SO}(p+q)/\mathrm{SO}(p)\times\mathrm{SO}(q)$	$\mathrm{SO}(p,q)/\mathrm{SO}(p)\times\mathrm{SO}(q)$	AI|AII	$\mathrm{U}(2n)/\mathrm{Sp}(2n)$
CII	chGSE	$+$	$-$	$\mathrm{Sp}(2p+2q)/\mathrm{Sp}(2p)\times\mathrm{Sp}(2q)$	$\mathrm{Sp}(2p,2q)/\mathrm{Sp}(2p)\times\mathrm{Sp}(2q)$	AII|AI	$\mathrm{U}(n)/\mathrm{O}(n)$
Bogoliubov - de Gennes classes							
C		$-$	$+$	$\mathrm{Sp}(2N)\times\mathrm{Sp}(2N)/\mathrm{Sp}(2N)\equiv\mathrm{Sp}(2N)$	$\mathrm{Sp}(2N,\mathbb{C})/\mathrm{Sp}(2N)$	DIII|CI	$\mathrm{Sp}(2n)/\mathrm{U}(n)$
CI		$+$	$+$	$\mathrm{Sp}(2N)/\mathrm{U}(N)$	$\mathrm{Sp}(2N,\mathbb{R})/\mathrm{U}(N)$	D|C	$\mathrm{Sp}(2n)$
BD		$-$	$-$	$\mathrm{SO}(N)\times\mathrm{SO}(N)/\mathrm{SO}(N)\equiv\mathrm{SO}(N)$	$\mathrm{SO}(N,\mathbb{C})/\mathrm{SO}(N)$	CI|DIII	$\mathrm{O}(2n)/\mathrm{U}(n)$
DIII		$+$	$-$	$\mathrm{SO}(2N)/\mathrm{U}(N)$	$\mathrm{SO}^*(2N)/\mathrm{U}(N)$	C|D	$\mathrm{O}(n)$

TABLE I Symmetry classification of disordered systems. First column: symbol for the symmetry class of the Hamiltonian. Second column: names of the corresponding RMT. Third column: presence ($+$) or absence ($-$) of the time-reversal (T) and spin-rotation (S) invariance. Fourth and fifth columns: families of the compact and non-compact symmetric spaces of the corresponding symmetry class. The Hamiltonians span the tangent space to these symmetric spaces. Sixth column: symmetry class of the σ-model; the first symbol corresponds to the non-compact ("bosonic") and the second to the compact ("fermionic") sector of the base of the σ-model manifold. The compact component $\mathcal{M}_F$ (which is particularly important for theories with non-trivial topological properties) is explicitly given in the last column.

we were discussing the symmetry of the Hamiltonians, as it does not affect the tangent space) is important here, since it influences topological properties of the manifold. As we will detail in Sec. V,VI, the topology of the σ-model target space often affects the localization properties of the theory in a crucial way.

C. Chiral classes

The Wigner-Dyson classes are the only allowed if one looks for a symmetry that is translationally invariant in energy, i.e. is not spoiled by adding a constant to the Hamiltonian. However, additional discrete symmetries may arise at some particular value of energy (which can be chosen to be zero without loss of generality), leading to novel symmetry classes. As the vicinity of a special point in the energy space governs the physics in many cases (i.e. the band center in lattice models at half filling, or zero energy in non-s-wave superconductors), these ensembles are of large interest. They can be subdivided into two groups – chiral and Bogoliubov - de Gennes ensembles – considered here and in Sec. IV.D, respectively.

The chiral ensembles appeared in both contexts of particle physics and physics of disordered electronic systems about fifteen years ago (Gade, 1993; Gade and Wegner, 1991; Slevin and Nagao, 1993; Verbaarschot and Zahed, 1993). The corresponding Hamiltonians have the form

$$H = \begin{pmatrix} 0 & h \\ h^\dagger & 0 \end{pmatrix} , \qquad (4.5)$$

i.e. they possess the symmetry

$$\tau_z H \tau_z = -H , \qquad (4.6)$$

where τ_z is the third Pauli matrix in a certain "isospin" space. In the condensed matter context, such ensembles arise, in particular, when one considers a tight-binding model on a bipartite lattice with randomness in hopping matrix elements only. In this case, H has the block structure (4.5) in the sublattice space.

In addition to the chiral symmetry, a system may possess time reversal symmetry and/or spin-rotation invariance. In full analogy with the Wigner-Dyson classes, IV.A, one gets therefore three chiral classes (unitary, orthogonal, and symplectic). The corresponding symmetric spaces, the Cartan notations for symmetry classes, and the σ-model manifolds are given in the rows 4–6 of the Table I.

D. Bogoliubov - de Gennes classes

As was found in Altland and Zirnbauer (1997), the Wigner-Dyson and chiral classes do not exhaust all possible symmetries of disordered electronic systems. The remaining four classes arise most naturally in superconducting systems. The quasiparticle dynamics in such systems can be described by the Bogoliubov-de Gennes Hamiltonian of the form

$$\hat{H} = \sum_{\alpha\beta}^{N} h_{\alpha\beta} c_\alpha^\dagger c_\beta + \frac{1}{2}\sum_{\alpha\beta}^{N}\left(\Delta_{\alpha\beta} c_\alpha^\dagger c_\beta^\dagger - \Delta_{\alpha\beta}^* c_\alpha c_\beta\right) \quad (4.7)$$

where $c^\dagger$ and c are fermionic creation and annihilation operators, and the $N \times N$ matrices h, Δ satisfy $h = h^\dagger$ and $\Delta^T = -\Delta$, in view of hermiticity. Combining $c_\alpha^\dagger, c_\alpha$ in a spinor $\psi_\alpha^\dagger = (c_\alpha^\dagger, c_\alpha)$, one gets a matrix representation of the Hamiltonian, $\hat{H} = \psi^\dagger H \psi$, where H has the structure

$$H = \begin{pmatrix} h & \Delta \\ -\Delta^* & -h^T \end{pmatrix}, \qquad h = h^\dagger, \quad \Delta = -\Delta^T . \quad (4.8)$$

The minus signs in the definition of H result form the fermionic commutation relations between $c^\dagger$ and c. The Hamiltonian structure (4.8) corresponds to the condition

$$H = -\tau_x H^T \tau_x \qquad (4.9)$$

(in addition to the Hermiticity $H = H^\dagger$), where τ_x is the Pauli matrix in the particle-hole space. Alternatively, one can perform a unitary rotation of the basis, defining $\tilde{H} = g^\dagger H g$ with $g = (1 + i\tau_x)/\sqrt{2}$. In this basis, the defining condition of class D becomes $\tilde{H} = -\tilde{H}^T$, so that $\tilde{H}$ is pure imaginary. The matrices $X = iH$ thus form the Lie algebra $\mathfrak{so}(2N)$, corresponding to the Cartan class D. This symmetry class described disordered superconducting systems in the absence of other symmetries.

Again, the symmetry class will be changed if the time reversal and/or spin rotation invariance are present. The difference with respect to the Wigner-Dyson and chiral classes is that now one gets four different classes rather than three. This is because the spin-rotation invariance has an impact even in the absence of time-reversal invariance, since it combines with the particle-hole symmetry in a non-trivial way. Indeed, if the spin is conserved, the Hamiltonian has the form

$$H = \sum_{ij}^N h_{ij}(c_{i\uparrow}^\dagger c_{j\uparrow} - c_{j\downarrow}c_{i,\downarrow}^\dagger) + \sum_{ij}^N \Delta_{ij} c_{i,\uparrow}^\dagger c_{j,\downarrow}^\dagger + \Delta_{ij}^* c_{i\downarrow}c_{j\uparrow}.$$
$$(4.10)$$

where h and Δ are $N \times N$ matrices satisfying $h = h^\dagger$ and $\Delta = \Delta^T$. Similar to (4.8), we can introduce the spinors $\psi_i^\dagger = (c_{i\uparrow}^\dagger, c_{i\downarrow})$ and obtain the following matrix form of the Hamiltonian

$$H = \begin{pmatrix} h & \Delta \\ \Delta^* & -h^T \end{pmatrix}, \qquad h = h^\dagger, \quad \Delta = \Delta^T . \quad (4.11)$$

It exhibits a symmetry property

$$H = -\tau_y H^T \tau_y. \qquad (4.12)$$

The matrices $H = iX$ now form the Lie algebra $\mathfrak{sp}(2N)$, which is the symmetry class C.

If the time reversal invariance is present, one gets two more classes (CI and DIII). The symmetric spaces for the Hamiltonians and the σ-models corresponding to the Bogoliubov–de Gennes classes are given in the last four rows of the Table I.

E. Additional comments

i) In addition to Table I, where the symmetry classes are ordered according to the discrete symmetries of the underlying physical systems, we include Table II with a more mathematical ordering. There, the first row is formed by compact symmetric spaces that are groups and the rest is a "matrix" of symmetric spaces G/K arranged according to the type (U, Sp, or O) of the groups G and K. This ordering illustrates the completeness of the classification scheme: all entries in the "matrix" are filled, except for two, as there is no symmetric spaces of the O/Sp and Sp/O types. Also, we will see in Sec. VI that this ordering is relevant to types of 2D critical behavior that the corresponding systems may show. In particular, the first row are the classes where different types of the QHE (IQHE, SQHE, and TQHE) take place. The second row is formed by the classes allowing for the Wess-Zumino type of criticality, while the third row are the systems which allow for a $\mathbb{Z}_2$ topological term. The diagonal of the "matrix" is occupied by three chiral classes.

ii) Strictly speaking, one should distinguish between the orthogonal group $\mathrm{SO}(N)$ with even and odd N, which form different Cartan classes: $\mathrm{SO}(2N)$ belongs to class D, while $\mathrm{SO}(2N+1)$ to class B. In the conventional situation of a disordered superconductor, the matrix size is even due to the particle-hole space doubling, see Sec. IV.D. It was found, however, that the class B can arise in p-wave vortices (Ivanov, 2002a,b). In the same sense, the class DIII should be split in DIII-even and DIII-odd; the last one represented by the symmetric space $\mathrm{SO}(4N + 2)/\mathrm{U}(2N + 1)$ can appear in vortices in the presence of time-reversal symmetry.

F. Perturbative β-functions for σ-models of different symmetry classes

Perturbative β-functions for σ-models on all the types of symmetric spaces were in fact calculated (Hikami, 1981; Wegner, 1989) long before the physical significance of the chiral and Bogoliubov-de Gennes classes has been fully appreciated. In Table III we have collected the results for all β-functions, $\beta(t) = -dt/d\ln L$, in $d = 2 + \epsilon$ dimensions up to four-loop order. Here t is the coupling constant inverse proportional to the dimensionless conductance g, and the Anderson localization problem corresponds to the replica limit $N = p = 0$. The corresponding results for the Wigner-Dyson classes have already been quoted in Sec. II.B.2. For each symmetry class of disordered electronic systems, the perturbative β-function can be equivalently obtained from either compact or non-compact σ-models on the appropriate manifolds. As an example, the β-function for the Wigner-Dyson orthogonal class can be found by using the replica limit of the compact σ-model of the type CII or of the non-compact σ-model of the type BDI.

It is seen that for the classes A, AI, C, CI the β-

U(N)	A	Sp($2N$)	C	SO(N)	BD
U($p+q$)/U(p)×U(q)	AIII	Sp($2N$)/U(N)	CI	$SO(2N)$/U(N)	DIII
U($2N$)/Sp($2N$)	AII	Sp($2p+2q$)/Sp($2p$)×Sp($2q$)	CII		
U(N)/O(N)	AI			SO($p+q$)/SO(p)×SO(q)	BDI

TABLE II Compact symmetric spaces arranged in a form of a "matrix", with the corresponding Cartan symbols. First row: U, Sp, and O groups. Second (third, fourth) row: symmetric spaces G/K (which are not groups themselves) with K being the unitary (resp. symplectic, orthogonal) group.

function is negative in 2D in the replica limit $N = p = 0$ (at least, for small t). This indicates that normally all states are localized in such systems in 2D. (This conclusion can in fact be changed in the presence of topological or Wess-Zumino terms, Sec. VI.A.) Above 2D, these systems undergo the Anderson transition that can be studied within the $2 + \epsilon$ expansion, Sec. II.B.2. For the classes AIII, BDI, and CII (chiral unitary, orthogonal and symplectic classes, respectively) the β-function is exactly zero in 2D, implying a line of fixed points, Sec. VI.F. Finally, in the classes AII, D, and DIII the β-function is positive at small t, implying the existence of a metal-insulator transition at strong coupling in 2D. The 2D Anderson transitions in the Wigner-Dyson symplectic class AII and in the Bogoliubov-de Gennes class D will be discussed in more detail in Sec. VI.B and VI.E, respectively.

V. QUASI-1D SYSTEMS: DISORDERED WIRES

Under usual conditions, electronic states in disordered wires are localized, with localization length $\xi \sim Nl$, where l is the mean free path and N the number of conducting channels (Berezinsky, 1974; Efetov and Larkin, 1983). This is, however, not the full story, and that is why we include a section about quasi-1D systems in this review devoted to localization-delocalization transitions and criticality. In fact, one route to delocalization and criticality in systems of one 1D geometry – long-range $1/r$ hopping – has already been discussed in Sec. III. In this section we consider possible types of delocalization in disordered wires which are related to the symmetries of the problem. We will see later that in many cases there are close connections between such phenomena in quasi-1D and 2D systems (Sec. VI).

Two approaches to quasi-1D disordered electronic systems have been developed. The first one is the supersymmetric σ-model approach, Sec. II.B.1. For the wire geometry, the σ-model field Q depends on the longitudinal coordinate only. As a result, the problem becomes a kind of imaginary-time quantum mechanics on the σ-model manifold, with the longitudinal coordinate playing the role of the (imaginary) time. This has allowed researchers to get a number of exact results for systems of Wigner-Dyson symmetry classes, including the asymptotics of the density-density correlation function and the value of the localization length (Efetov and Larkin, 1983), a detailed description of the wave function statistics (Fyodorov and Mirlin, 1994), average conductance and its variance (Mirlin *et al.*, 1994; Zirnbauer, 1992). For reviews of results for statistical properties of various quantities in disordered wires obtained within the σ-model approach the reader is referred to Efetov (1997); Mirlin (2000b).

The second approach is based on the description of a wire in terms of its transfer-matrix M. The evolution of the corresponding distribution $\mathcal{P}(M)$ with the wire length is described by the Dorokhov-Mello-Pereyra-Kumar (DMPK) equation (Dorokhov, 1982; Mello *et al.*, 1988). At variance with the σ-model approach, which allows to address any observable, the DMPK approach is designed to study the transport properties. On the other hand, the advantage of the DMPK approach is that it allows one to study wires with arbitrary number N of channels (not necessarily $N \gg 1$ as required for the derivation of the diffusive σ-model) and provides a very detailed information on the whole distribution of transmission eigenvalues. The two approaches are thus complementary; their equivalence for transport properties of many-channel wires (when both of them are applicable) was explicitly shown in Brouwer and Frahm (1996). A review of the results of the DMPK method for Wigner-Dyson symmetry classes was given in Beenakker (1997).

Peculiar transport properties of disordered wires of unconventional symmetry classes have been mainly studied within the DMPK approach. Below we briefly describe this method and present the key results. Whenever appropriate, we will also make contact to the results obtained within the σ-model formalism.

A. Transfer matrix and DMPK equations

In the transfer matrix approach, one imagines the wire attached to two clean electrodes, where one can define asymptotic states. This allows to formulate a scattering problem. The transfer matrix M relates the amplitudes in N incoming and N outgoing channels to the right of the wire to the corresponding amplitudes on the left side of the wire,

$$\begin{pmatrix} R^{\text{out}} \\ R^{\text{in}} \end{pmatrix} = M \begin{pmatrix} L^{\text{in}} \\ L^{\text{out}} \end{pmatrix} \quad (5.1)$$

σ-model class	compact σ-model manifold	Ham. c | n-c	t	t^2	t^3	t^4	t^5
AIII	$U(N)/U(p)\times U(N{-}p)$	A	ϵ	$-N$	$-2(1{+}p(N{-}p))$	$-\frac{1}{2}N(3p(N{-}p){+}7)$	$c_4(N,p)$
BDI	$O(N)/O(p)\times O(N{-}p)$	AII|AI	ϵ	$-(N{-}2)$	$-(2p(N{-}p){-}N)$	$-[\frac{3}{2}pN(N{-}p)-\frac{5}{4}N^2{+}p(N{-}p){+}\frac{1}{2}N]$	$c_5(N,p)$
CII	$Sp(2N)/Sp(2p)\times Sp(2N{-}2p)$	AI|AII	ϵ	$\frac{1}{2}(N{-}2)$	$-\frac{1}{4}(2p(N{-}p){-}N)$	$\frac{1}{8}[\frac{3}{2}pN(N{-}p)-\frac{5}{4}N^2{+}p(N{-}p){+}\frac{1}{2}N]$	$\frac{1}{16}c_5(N,p)$
AI	$U(N)/O(N)$	CII|BDI	ϵ	$-N$	$-N(\frac{1}{2}N+1)$	$-N(\frac{3}{8}N^2+\frac{5}{4}N+1)$	$-\frac{N}{2}c_2(-N/2)$
AII	$U(2N)/Sp(2N)$	BDI|CII	ϵ	$-2N$	$-2N(N-1)$	$-N(3N^2-5N+2)$	$Nc_2(N)$
CI	$Sp(2N)/U(N)$	C|BD	ϵ	$-(N{+}1)$	$-\frac{1}{2}(N^2{+}3N{+}4)$	$-\frac{1}{8}(3N^3{+}14N^2{+}35N{+}28)$	$c_3(N)$
DIII	$O(2N)/U(N)$	BD|C	ϵ	$-(2N-2)$	$-(2N^2-6N+8)$	$-(3N^3-14N^2+35N-28)$	$c_3(-2N)$
A	$U(N)\times U(N)/U(N)$	AIII	ϵ	$-N$	$-\frac{1}{2}N^2$	$-N^3(\frac{3}{8}+(\frac{19}{48}+a)N)$	$aN^2(N{-}2)(N{+}2)$
C	$Sp(2N)\times Sp(2N)/Sp(2N)$	CI|DIII	ϵ	$-(N+1)$	$-\frac{1}{2}(N+1)^2$	$-\frac{3}{8}(N+1)^3$	$-\frac{N+1}{8}c_1(-2N)$
BD	$O(N)\times O(N)/O(N)$	DIII|CI	ϵ	$-(N{-}2)$	$-\frac{1}{2}(N-2)^2$	$-\frac{3}{8}(N-2)^3$	$(N-2)c_1(N)$

TABLE III Perturbative β-functions, $\beta(t) = -dt/d\ln L$, up to the four-loop order for the σ-models in $d = 2 + \epsilon$ dimensions with symmetric spaces as target manifolds (Hikami, 1981; Wegner, 1989). First column: Cartan symbol for the σ-model symmetric space. Second column: compact σ-model manifold. (The associated non-compact spaces can be found in Table I.) Third column: symmetry class of random Hamiltonians described by the replica version of the compact σ-model (c) and of its non-compact counterpart (n-c). The last five columns give the coefficients of the terms from t to t^5 in the β-functions for compact σ-models. The β-functions for the corresponding non-compact σ-models are obtained by the substitution $\beta(t) \rightarrow -\beta(-t)$, i.e. by flipping the sign of the terms with even powers of t. Following notations are used: $a = \frac{3}{16}\zeta(3)$, $c_5(N,p) = -(\frac{2}{3}N^2(N-p) + 5p^2(N-p)^2 - \frac{5}{12}N^3 - (\frac{23}{6}+8a)pN(N-p) + (-\frac{2}{3}+16a)p(N-p) + (\frac{7}{6}+16a)N^2 + (\frac{1}{3}-64a)N + 64a)$; $c_4(N,p) = -(\frac{1}{3}pN^2(N{-}p){+}5p^2(N{-}p)^2{+}\frac{11}{6}N^2{+}11p(N{-}p){+}6)$; $c_3(N) = -(\frac{19}{48}N^4{+}\frac{119}{48}N^3{+}\frac{380}{48}N^2{+}\frac{578}{48}N{+}\frac{376}{48})$; $c_2(N) = -(\frac{19}{3}N^3 - (\frac{43}{3}-8a)N^2 + (9+8a)N - 1)$; $c_1(N) = -[(\frac{19}{48}+a)(N{-}2)^3{-}a(N{-}3)(N{-}4)(N{+}2)]$

(In fact, for symmetry classes A, C, and BD with broken time-reversal symmetry the number of incoming and outgoing channels can differ. We will discuss this peculiar situation in Sec. V.D.) The requirement of the current conservation

$$|R^{\text{out}}|^2 - |R^{\text{in}}|^2 = |L^{\text{in}}|^2 - |L^{\text{out}}|^2 \qquad (5.2)$$

implies that M is an element of the pseudounitary group $G = U(N, N)$. The transfer matrix can be presented in the form (Cartan decomposition)

$$M = \begin{pmatrix} u & 0 \\ 0 & u' \end{pmatrix} \begin{pmatrix} \cosh\hat{x} & \sinh\hat{x} \\ \sinh\hat{x} & \cosh\hat{x} \end{pmatrix} \begin{pmatrix} v & 0 \\ 0 & v' \end{pmatrix} \qquad (5.3)$$

where $\hat{x} = \text{diag}(x_1, \ldots, x_N)$ are "radial coordinates", while the left and right matrices ("angular coordinates") are the elements of $K = U(N)\times U(N)$. If the Hamiltonian of the system possesses some additional (time-reversal, spin-rotation, chiral, particle-hole) symmetries, the group G of the transfer matrices will change correspondingly, with K being the maximal compact subgroup of G. The coset spaces G/K (which play the central role for the DMPK equations, see below) are non-compact symmetric spaces; they are listed for all the symmetry classes of the Hamiltonian in Table IV. The dimensionless conductance of the wire is expressed in terms of the radial coordinates x_n as $G = d\sum_{n=1}^{N} T_n$, where $T_n = 1/\cosh^2 x_n$ are transmission eigenvalues and d is the degeneracy (1, 2, or 4) depending on the symmetry class.

When an additional thin slice with a transfer matrix T is attached to the wire, the new transfer matrix is obtained by simple multiplication $M' = TM$. For a given distribution function of the elementary transfer-matrices T, one then gets a stochastic process on the space of transfer matrices. It is assumed in the derivation of the DMPK equations that the distribution of T is fully invariant with respect to the subgroup K (isotropy assumption), which corresponds to a complete mixture of channels at each elementary step. (This model assumption is justified by the fact that the mixing of channels in a realistic wire takes place on a scale much shorter than the localization length.) As a result, the stochastic process develops in fact on the coset space G/K, describing a Brownian motion on this manifold. In view of the rotational symmetry, the distribution function depends on radial coordinates x_i only. The corresponding evolution equation — which is the DMPK equation — has the form

$$\frac{d\mathcal{P}}{dL} = \frac{1}{2\ell\gamma} \sum_{i=1}^{N} \frac{\partial}{\partial x_i} J(x) \frac{\partial}{\partial x_i} J^{-1}(x) \, \mathcal{P} \; . \qquad (5.4)$$

where the Jacobian $J(x)$ of transformation to the radial coordinates and the parameter γ are specified below.

For the Wigner-Dyson and Bogoliubov-de Gennes classes the radial coordinates x_i satisfy[9] $0 < x_1 < x_2 <$

---

[9] For the classes D and DIII the proper variation domain of x_i is slightly different, $|x_1| < x_2 < \ldots < x_N$ (Gruzberg et al., 2005).

$\ldots < x_N$ and the Jacobian $J(x)$ is

$$J(x) \;=\; \prod_{i<j}^{N} \prod_{\pm} |\sinh(x_i \pm x_j)|^{m_o} \prod_{k}^{N} |\sinh 2x_k|^{m_l}$$

$$\times \prod_{l}^{N} |\sinh x_l|^{m_s} . \tag{5.5}$$

Here m_o, m_s, and m_l are the multiplicities of the ordinary, short, and long roots for the corresponding symmetric space (Caselle and Magnea, 2004; Helgason, 1978). The root multiplicities for all the symmetry classes are listed in Table IV. The first factor in Eq. (5.5) is responsible for the repulsion between eigenvalues x_i, analogous to the energy level repulsion in RMT. The last two factors govern (when the corresponding multiplicities are non-zero) the repulsion between an eigenvalue x_i and its mirror $-x_i$, and the repulsion between x_i and zero, respectively. For the chiral classes, the variation domain of the coordinates x_i does not restrict their sign, $x_1 < x_2 < \ldots < x_N$, and the Jacobian is

$$J(x) = \prod_{i<j}^{N} |\sinh(x_i - x_j)|^{m_\circ} . \tag{5.6}$$

(For these classes $m_s = m_l = 0$.) For the Wigner-Dyson and the chiral classes the multiplicity $m_\circ$ of the ordinary roots is the familiar parameter β of the RMT, equal to 1,2, and 4 for the orthogonal, unitary, and symplectic symmetry classes, respectively. Further, the parameter γ in the DMPK equation is given by

$$\gamma = \begin{cases} m_o(N-1) + m_l + 1 , & \text{WD and BdG} ; \\ \frac{1}{2}[2 + m_o(N-1)] , & \text{chiral} . \end{cases} \tag{5.7}$$

In the short-wire regime, $L \ll \gamma\ell$, where the conductance is large, $g \gg 1$, the DMPK equation yields Ohm's law for the average conductance, the quasi-1D universal conductance fluctuations, and the weak-localization corrections in the form of a $1/g$ series. Our interest here is in the opposite, long-wire limit, $L \gg \gamma\ell$, where localization or critical properties of the problem manifest themselves. This will be the subject of the remaining part of Sec. V. We also briefly mention that at the crossover scale, $L \sim \gamma\ell$, an analytical treatment is most complicated. An approximate scheme has, however, been developed in Gopar et al. (2002); Muttalib and Wölfle (1999); Muttalib et al. (2003) that allows one to understand key properties of the conductance distribution in this regime.

B. Conventional localization in 1D geometry

We begin by considering the standard quasi-1D localization in Wigner-Dyson classes ($m_l = 1$, $m_o = \beta$, $m_s = 0$). In the long-wire limit the transmission eigenvalues satisfy the hierarchy $1 \gg T_1 \gg T_2 \gg \ldots$, i.e.

Ham. class	transfer matrix symmetric space		tr.matr. class	m_o	m_l	m_s
Wigner-Dyson classes						
A	$\mathrm{U}(p+q)/\mathrm{U}(p)\times\mathrm{U}(q)$		AIII	2	1	$2|p-q|$
AI	$\mathrm{Sp}(2N,\mathbb{R})/\mathrm{U}(N)$		CI	1	1	0
AII	$\mathrm{SO}^*(2N)/\mathrm{U}(N)$	N even	DIII-e	4	1	0
		N odd	DIII-o			4
chiral classes						
AIII	$\mathrm{GL}(N,\mathbb{C})/\mathrm{U}(N)$		A	2	0	0
BDI	$\mathrm{GL}(N,\mathbb{R})/\mathrm{O}(N)$		AI	1	0	0
CII	$\mathrm{U}^*(2N)/\mathrm{Sp}(2N)$		AII	4	0	0
Bogoliubov - de Gennes classes						
C	$\mathrm{Sp}(2p,2q)/\mathrm{Sp}(2p)\times\mathrm{Sp}(2q)$		CII	4	3	$4|p-q|$
CI	$\mathrm{Sp}(2N,\mathbb{C})/\mathrm{Sp}(2N)$		C	2	2	0
BD	$\mathrm{O}(p,q)/\mathrm{O}(p)\times\mathrm{O}(q)$		BDI	1	0	$|p-q|$
DIII	$\mathrm{SO}(N,\mathbb{C})/\mathrm{SO}(N)$	N even	D	2	0	0
		N odd	B			2

TABLE IV Transfer matrix spaces. First column: symmetry class of the Hamiltonian. Second and third columns: symmetric space for the transfer matrix and the corresponding Cartan symmetry class. Last three columns: multiplicities of the ordinary (m_o), long (m_l) , and short (m_s) roots.

the consecutive x_i are separated by intervals much larger than unity. One can thus approximate the hyperbolic sine functions in Eq. (5.5) by the exponentials. As a result, all the variables in the DMPK equation (5.4) fully decouple; the resulting Fokker-Planck equation for each of x_k reads

$$\frac{d\mathcal{P}(x_k)}{dL} = \frac{1}{2\gamma\ell} \frac{\partial^2 \mathcal{P}}{\partial x_k^2} - \frac{1}{\xi_k} \frac{\partial \mathcal{P}}{\partial x_k}, \tag{5.8}$$

where $\xi_k^{-1} = [1 + \beta(k-1)]/\gamma\ell$. This is an equation of the advection-diffusion type, with $1/2\gamma\ell$ playing the role of the diffusion constant and $1/\xi_1$ of the drift velocity. The solution has a Gaussian form with $\langle x_k \rangle = L/\xi_k$ and $\mathrm{var}(x_k) = L/\gamma\ell$. This immediately implies that the logarithm of the conductance $g \simeq d/\cosh^2 x_1$ has a Gaussian distribution with the following average and variance (Beenakker, 1997):

$$-\langle \ln g \rangle = 2L/\gamma\ell ; \qquad \mathrm{var}(\ln g) = 4L/\gamma\ell . \tag{5.9}$$

On the side of atypically large g this distribution is cut at $g \sim 1$. The average conductance is straightforwardly found to be determined by this cutoff (i.e. by rare events of $g \sim 1$), $-\ln\langle g \rangle = L/2\gamma l$. Defining the typical and the average localization length via

$$-\langle \ln g \rangle = 2L/\xi_{\mathrm{typ}} ; \qquad -\ln\langle g \rangle = 2L/\xi_{\mathrm{av}} , \tag{5.10}$$

we thus find

$$\xi_{\mathrm{typ}} = \gamma\ell ; \qquad \xi_{\mathrm{av}} = 4\gamma\ell . \tag{5.11}$$

These results are in full agreement with those obtained within the σ-model formalism (Mirlin, 2000b), which corresponds to $N \gg 1$, so that $\gamma = \beta N$.

A similar behavior is also found in the Bogoliubov–de Gennes classes C and CI (Brouwer *et al.*, 2000a). The same derivation yields the equation (5.8) with $\xi_k^{-1} = [3 + 4(k-1)]/\gamma\ell$ for class C and $\xi_k^{-1} = [2 + 2(k-1)]/\gamma\ell$ for class CI. Thus,

$$-\langle \ln g \rangle = 6L/\gamma\ell \; ; \quad \mathrm{var}(\ln g) = 4L/\gamma\ell \quad \text{(C)} \; ; \quad (5.12)$$

$$-\langle \ln g \rangle = 4L/\gamma\ell \; ; \quad \mathrm{var}(\ln g) = 4L/\gamma\ell \quad \text{(CI)} \; . \quad (5.13)$$

Calculating the average conductance, one gets $-\ln\langle g \rangle = 4L/\gamma l$ (class C) and $-\ln\langle g \rangle = 2L/\gamma l$ (class CI), so that

$$\xi_{\mathrm{typ}} = \gamma\ell/3 \; ; \qquad \xi_{\mathrm{av}} = \gamma\ell/2 \qquad \text{(C)} \; ; \quad (5.14)$$

$$\xi_{\mathrm{typ}} = \gamma\ell/2 \; ; \qquad \xi_{\mathrm{av}} = \gamma\ell \qquad \text{(CI)} \; . \quad (5.15)$$

A quasi-1D model of class C was also studied within the σ-model formalism in Bundschuh *et al.* (1998). It was found there that ξ_{av} is 8 times shorter than for class A. This agrees with the result of the DMPK approach, as is seen by comparison of ξ_{av} in Eq. (5.14) and Eq. (5.11).

C. Types of delocalization in disordered wires

Having discussed in Sec. V.B how conventional localization in disordered quasi-1D systems takes place, we now analyze how electrons in such a system can escape exponential localization. Table IV is very useful in this respect, showing that there are two distinct mechanisms.

First, we see that in five classes (in all three chiral classes AIII, BDI, and CII, as well as in the superconducting classes with broken spin-rotation invariance, BD and DIII) the multiplicity m_l of long roots in zero. This implies that there is no repulsion between the eigenvalue x_i and its mirror $-x_i$, so that the smallest (by absolute value) x_i can be close to zero. We will analyze the critical behavior that emerges in these classes in Sec. V.E and V.F.

The second type of delocalization is related to the multiplicity of short roots m_s in the Table IV. In the conventional situation it is equal to zero. However, there are five classes (A, C, BD, AII, and DIII), where it can be non-zero. A non-zero value of m_s implies a repulsion of x_i from zero, which is an indicator of the existence of exactly zero eigenvalues of the transfer-matrix. These zero eigenvalues imply perfectly transmitting channels, yielding a finite conductance in the limit of infinite system length. We will discuss this class of systems in Sec. V.D.

D. Models with perfectly conducting channels

In this subsection, we consider the models with perfectly transmitting channels, in which case $m_s \neq 0$, see Table IV. These models are in turn subdivided in two types.

In the classes A, C, and BD, the transfer-matrix spaces given in the Table IV correspond to a model with p channels propagating to the left and q channels propagating to the right. While in the conventional situation $p = q$, symmetric spaces with $p \neq q$ are allowed as well. It is not difficult to understand what is the physical realization for these models, if one recalls that these are exactly those classes whose 2D representatives show the quantum Hall effects, Sec. VI. When such a 2D system is on the quantum Hall plateau of order p, there are p edge channels that propagate on its boundary. These channels are chiral in the sense that they can propagate in one direction only. The edge of such a system represents thus a wire of the corresponding symmetry class with p modes propagating in one direction and zero in the opposite. Since there is no backscattering, the conductance of such a wire is identically equal to p. Let us consider now parallel edges of two quantum Hall systems with counterpropagating modes separated by a potential barrier. Assuming that there are p modes in one edge and q in the other and that they are coupled by tunneling, we get a wire of the (q, p) type from the corresponding class. In the long length limit, $|p - q|$ modes will then remain perfectly conducting, while the rest will be localized.

The situation with the classes AII and DIII is much more intricate. The systems of these classes may possess a single perfectly conducting channel. As we explain below, this reflects an underlying $\mathbb{Z}_2$ topological structure. A delocalization in the symplectic Wigner-Dyson class AII was obtained for the first time within the σ-model formalism in Mirlin *et al.* (1994); Zirnbauer (1992). It was found in these works that the average conductance and its variance remain finite in the long-wire limit, $\langle g \rangle \to 1/2$, $\mathrm{var}(g) \to 1/4$ due to a zero mode of the corresponding transfer-operator. The physical significance of these results was not understood at this stage. Further, it was shown in Brouwer and Frahm (1996) that the above zero mode is double-valued on the σ-model manifold and thus does not contribute in the case of a conventional wire with spin-orbit interaction. More recently, it was understood, however, that a model of symplectic symmetry with a perfectly conducting channel arises if one considers transport in carbon nanotubes (Ando and Suzuura, 2002; Suzuura and Ando, 2002). The problem is described by two species of Dirac fermions corresponding to two valleys in the graphene spectrum. If the scatterers are of long-range character and the intervalley scattering can be neglected, the problem acquires the symplectic (AII) symmetry, with the sublattice space taking the role of isospin (Sec. VI.G.2). Furthermore, in contrast to conventional wires of AII symmetry, where the number of channels is even, there is just a single channel here. (More precisely, its "partner" belongs to the other node, and they "do not talk to each other".) As a result, the channel remains perfectly transmitting independently of the length of the wire.

In subsequent works (Caselle and Magnea, 2006; Sakai and Takane, 2005; Takane, 2004a,b) quasi-1D sys-

tems of the AII symmetry class with odd number N of channels were studied within the DMPK approach. It was found that for any odd N a single perfectly transmitting channel remains in the limit $L \gg \gamma\ell$. As emphasized in Takane (2004c), these results are in full agreement with the earlier σ-model results of Mirlin et $al.$ (1994); Zirnbauer (1992), if the latter are complemented by the following interpretation. The Fourier expansion employed in Mirlin et $al.$ (1994); Zirnbauer (1992) contained eigenfunctions of the Laplace operator in the σ-model manifold of two types – with even and odd parity (the zero mode is of the odd-parity type). For systems with even (odd) number of channels one should keep only even-parity (resp. odd-parity) eigenmodes and include an overall factor of two. The original result of Mirlin et $al.$ (1994); Zirnbauer (1992) with $\langle g \rangle$, $\langle g^2 \rangle \to 1/2$ at $L \to \infty$ corresponds thus to an average over wires with even and odd number of channels.

In the problem with perfectly transmitting channels, one can determine the localization length for the remaining modes by considering the deviation δg of the conductance from its $L \to \infty$ limit. A straightforward generalization of the consideration sketched in Sec. V.B yields (Caselle and Magnea, 2006)

$$ -\langle \ln \delta g \rangle = (2m_l + m_s)L/\gamma\ell , \qquad (5.16) $$

so that $\xi_{\text{typ}} = \gamma\ell/(m_l + m_s/2)$. This implies for both the AII and DIII models with an odd number of channels

$$ \xi_{\text{typ}} = \gamma\ell/3 ; \qquad \xi_{\text{av}} = \gamma\ell/2 . \qquad (5.17) $$

The qualitative different behavior of class-AII (and DIII) wires with even and odd number of channels is intimately connected with a non-trivial topology of the corresponding σ-model manifold (or, more specifically, of its compact component $\mathcal{M}_F$): the first homotopy group $\pi_1(\mathcal{M}_F)$ is equal to $\mathbb{Z}_2$. This enables a topological θ-term with θ equal to 0 or π (Ostrovsky et $al.$, 2007a), in analogy with the 2D situation, see Sec. VI.A.5, VI.B.5 for these symmetry classes. The topological term with $\theta = \pi$ is present if the number of channels is odd.

Another realization of a symplectic-symmetry wire with an odd number of channels has recently emerged in the context of the quantum spin Hall (QSH) effect in systems of Dirac fermions with spin-orbit coupling (Bernevig et $al.$, 2006; Kane and Mele, 2005a,b). Such systems were found to possess two distinct insulating phases (with a transition between them driven by Rashba spin-orbit coupling strength), both having a gap in the bulk electron spectrum but differing by the edge properties. The topological distinction between the two insulating phases retains its validity in the presence of disorder (Essin and Moore, 2007; Obuse et $al.$, 2007a; Onoda et $al.$, 2007; Sheng et $al.$, 2005). While the normal insulating phase has no edge states, the QSH insulator is characterized by a pair of mutually time-reversed spin-polarized edge states penetrating the bulk gap. These edge states in the QSH phase, which do not

get localized by disorder, represent a realization of the class-AII wire with a non-trivial $\mathbb{Z}_2$ topology.

E. Chiral classes

For the chiral classes, the consideration analogous to that in Sec. V.B (Brouwer et $al.$, 2000b; Mudry et $al.$, 1999, 2000) yields $\langle x_k \rangle = (2k - 1 - N)\beta L/2\gamma\ell$. If the number of channels is even, then the smallest by absolute value eigenvalues x_k are separated by a large gap from zero: $-\langle x_{N/2} \rangle = \langle x_{N/2+1} \rangle = L/2\gamma\ell$. Therefore, the exponential localization is preserved, $-\langle \ln g \rangle = \beta L/\gamma\ell$, $\text{var}(\ln g) = 4L/\gamma\ell$, yielding the localization lengths

$$ \xi_{\text{typ}} = 2\gamma\ell/\beta ; \qquad \xi_{\text{av}} = 16\gamma\ell/\beta^2 . \qquad (5.18) $$

On the other hand, if N is odd, one of the eigenvalues is close to zero, $\langle x_{(N+1)/2} \rangle = 0$. This leads to a completely different behavior of the conductance,

$$ -\langle \ln g \rangle = \left(\frac{8L}{\pi\gamma\ell} \right)^{1/2} ; \quad \text{var}(\ln g) = \left(4 - \frac{8}{\pi} \right) \frac{L}{\gamma\ell} ; (5.19) $$

$$ \langle g \rangle = (2\gamma\ell/\pi L)^{1/2} ; \qquad \text{var}(g) = (8\gamma\ell/9\pi L)^{1/2}. (5.20) $$

It is seen from Eq. (5.19) that while the typical conductance decays in a stretched-exponential way, its fluctuations are very strong, so that the probability to have $g \sim 1$ is small as $L^{-1/2}$ only. This determines the very slow decay (5.20) of the average conductance, which is even slower than the in classical Ohm's law.

The delocalization takes place for arbitrary odd N, including $N = 1$. The single-channel model with chiral-class disorder has been studied, in its various incarnations, in a large number of works, starting form the pioneering paper by Dyson (1953). We list most salient features characterizing (in addition to the above results for the statistical properties of the conductance) this critical point.

i) $Localization$ $length$. If the energy E deviates from zero, the chiral symmetry is broken, and the exponential localization establishes. One can thus ask how the corresponding localization length diverges at $E \to 0$. It has been found that one should distinguish between average and typical observables (e.g. conductance) whose spatial dependence is governed by two parametrically different lengths (Balents and Fisher, 1997; Fisher, 1995),

$$ \xi_{\text{typ}} \sim |\ln E| ; \qquad \xi_{\text{av}} \sim |\ln E|^2 . \qquad (5.21) $$

ii) $Staggering$. An alternative way to drive the system out of criticality is to introduce a staggering M in the hopping strength which opens a gap around zero energy in the spectrum of a clean system. The corresponding localization lengths behave as follows (Balents and Fisher, 1997; Fisher, 1995; Mathur, 1997),

$$ \xi_{\text{typ}} \sim M^{-1} ; \qquad \xi_{\text{av}} \sim M^{-2} . \qquad (5.22) $$

iii) Wave function at criticality. The Hamiltonian of a single-chain problem can be written in a Dirac form (Balents and Fisher, 1997),

$$H = -i\sigma_z \partial_x + m(x)\sigma_y , \qquad (5.23)$$

where $m(x) = M + \tilde{m}(x)$ and $\tilde{m}(x)$ is the disorder (e.g. of the white-noise type). The zero-energy eigenfunction can then be found explicitly,

$$\Psi(x) = \begin{pmatrix} 1 \\ \pm 1 \end{pmatrix} \frac{\psi_\pm(x)}{\left[\int dx \, \psi_\pm^2(x) \right]^{1/2}},$$

$$\psi_\pm(x) = \exp\left[\pm \int^x dx' \, m(x') \right] . \qquad (5.24)$$

The properties of this wave function were analyzed in Balents and Fisher (1997). The following scaling of the spatial correlation function of the moments of $\psi(x)$ at criticality ($M = 0$) was found,

$$\langle |\psi(x)\psi(0)|^q \rangle \sim L^{-1}|x|^{-3/2} , \qquad (5.25)$$

for all $q > 0$. This result can be interpreted in terms of the following picture of wave functions at criticality (Balents and Fisher, 1997). The wave function is typically quasi-localized, showing a stretched-exponential decay with respect to its principal maximum. However, with a probability $\sim x^{-3/2}$ it shows a secondary maximum of a magnitude close to the primary one and separated from it by a distance x.

iv) Density of states. The DOS shows at criticality the Dyson singularity (Dyson, 1953; McKenzie, 1996; Titov *et al.*, 2001),

$$\rho(E) \sim 1/|E \ln^3 E| . \qquad (5.26)$$

When the system is driven away from criticality by a non-zero staggering parameter M, the singularity weakens and becomes non-universal, $\rho(E) \sim |E|^{-1+\delta}$ with $\delta > 0$.

Finally, it has been shown that a sufficiently strong staggering M can also drive a system with even N into a critical state (Brouwer *et al.*, 1998). More specifically, the staggering shifts all the variables x_k by a constant. With increasing M, the average values $\langle x_k \rangle$ consecutively cross zero; whenever this happens, the system is at criticality. Therefore, whether N is odd or even, changing M will drive the system through N transition points.

F. Bogoliubov-de Gennes classes with broken spin-rotation invariance

Analysis of the DMPK equation for the classes BD and DIII (Brouwer *et al.*, 2000a) leads to results identical to those obtained for chiral classes, Eq. (5.19), (5.20). Furthermore, the DOS was found to show the Dyson singularity (5.26), again in full analogy with the chiral classes.

On the other hand, Motrunich *et al.* (2001) studied certain single-channel models of the classes D and DIII

via a strong-disorder real-space RG. It was found that generically these systems are in localized phases and the DOS diverges in a power-law fashion with a non-universal exponent, $\rho(E) \sim E^{-1+\delta}$ with $\delta > 0$. Only at phase boundaries the system is critical and the DOS takes the Dyson form (5.26).

An apparent contradiction between the results of both papers was resolved in Gruzberg *et al.* (2005). It was shown there that, generically, quasi-1D systems of the classes BD and DIII are in a localized phase, in agreement with Motrunich *et al.* (2001). The terms that drive the system towards localization are usually neglected within the DMPK approach, as they are irrelevant at the short-distance (diffusive) fixed point. It was found, however, in Gruzberg *et al.* (2005) that these terms become relevant at the long-distance (critical) fixed point and drive the system away from it, into the localization fixed point. Only if the disorder is fine tuned, the system is at the critical point. On the other hand, the length at which the crossover from criticality to localization happens becomes exponentially large with increasing number of channels N. Therefore, in the thick-wire limit, $N \gg 1$, the system is essentially at criticality. An analogous conclusion was also reached in Brouwer *et al.* (2003).

It was also argued in Gruzberg *et al.* (2005); Motrunich *et al.* (2001) that critical points with Dyson singularities of all five symmetry classes (AIII, BDI, CII, BD, and DIII) belong to the same universality class. To establish this remarkable "superuniversality", Gruzberg *et al.* (2005) pointed out that all the universal properties can be obtained from $N = 1$ models and then constructed mappings between single-channel models of all the five classes.

VI. CRITICALITY IN 2D

A. Mechanisms of criticality in 2D

As was discussed in Sec. II.B.2, conventional Anderson transitions in the orthogonal and unitary symmetry classes take place only if the dimensionality is $d > 2$, whereas in 2D all states are localized. It is, however, well understood by now that there is a rich variety of mechanisms that lead to emergence of criticality in 2D disordered systems. Such 2D critical points have been found to exist for 9 out of 10 symmetry classes, namely, in all classes except for the orthogonal class AI. A nice summary of possible types of 2D criticality was given in (Fendley, 2000); we closely follow this work in our presentation in this subsection. We now list and briefly describe the mechanisms for the emergence of criticality; a detailed discussion of the corresponding critical points will be given in the remaining subsections of Sec. VI.

1. Broken spin-rotation invariance: Metallic phase

We begin with the mechanism that has been already mentioned in Sec. II.B.2 in the context of the Wigner-Dyson symplectic class (AII). In this case the β-function [(2.25) with $\epsilon = 0$] is positive for not too large t (i.e. sufficiently large conductance), so that the system is metallic (t scales to zero under RG). On the other hand, for strong disorder (low t) the system is an insulator, as usual, i.e. $\beta(t) < 0$. Thus, β-function crosses zero at some t_*, which is a point of the Anderson transition. Properties of this critical point will be discussed in detail in Sec. VI.B.

This mechanism (positive β-function and, thus, metallic phase at small t, with a transition at some t_*) is also realized in two of Bogoliubov-de Gennes classes – D and DIII, see Table III. All these classes correspond to systems with broken spin-rotation invariance. The unconventional sign of the β-function in these classes, indicating weak antilocalization (rather then localization), is physically related to destructive interference of time reversed paths for particles with spin $s = 1/2$.

2. Chiral classes: Vanishing β-function

Another peculiarity of the perturbative β-function takes place for three chiral classes – AIII, BDI, ad CII. Specifically, for these classes $\beta(t) \equiv 0$ to all orders of the perturbation theory, as was first discovered by Gade and Wegner (Gade, 1993; Gade and Wegner, 1991). As a result, the conductance is not renormalized at all, serving as an exactly marginal coupling. There is thus a line of critical points for these models, labeled by the value of the conductance. In fact, the σ-models for these classes contain an additional term (Gade, 1993; Gade and Wegner, 1991) that does not affect the absence of renormalization of the conductance but is crucial for the analysis of the behavior of the DOS. A detailed discussion of the chiral classes will be given in Sec. VI.F.

3. Broken time-reversal invariance: Topological θ-term and quantum Hall criticality

For several classes, the σ-model action allows for inclusion of a topological term, which is invisible to any order of the perturbation theory. This is the case when the second homotopy group π_2 of the σ-model manifold $\mathcal{M}$ (a group of homotopy classes of maps of the sphere S^2 into $\mathcal{M}$) is non-trivial.[10] From this point of view, only the compact sector $\mathcal{M}_F$ (originating from the fermionic part of the supervector field) of the manifold base matters.

___

[10] A pedagogical introduction of topological concepts in the context of condensed matter theory can be found in the recent monograph by Altland and Simons (2006).

There are five classes, for which $\pi_2(\mathcal{M}_F)$ is non-trivial, namely A, C, D, AII, and CII.

For the classes A, C, D the homotopy group $\pi_2(\mathcal{M}_F) = \mathbb{Z}$. Therefore, the action $S[Q]$ may include the (imaginary) θ-term,

$$iS_{\text{top}}[Q] = i\theta N[Q] \ , \qquad (6.1)$$

where an integer $N[Q]$ is the winding number of the field configuration $Q(\mathbf{r})$. Without loss of generality, θ can be restricted to the interval $[0, 2\pi]$, since the theory is periodic in θ with the period 2π.

The topological term (6.1) breaks the time reversal invariance, so it may only arise in the corresponding symmetry classes. The by far most famous case is the Wigner-Dyson unitary class (A). As was first understood by Pruisken (Pruisken, 1984, 1987), the σ-model of this class with the topological term (6.1) describes the integer quantum Hall effect (IQHE), with the critical point of the plateau transition corresponding to $\theta = \pi$. More recently, it was understood that counterparts of the IQHE exist also in the Bogoliubov-de Gennes classes with broken time-reversal invariance – classes C and D. They were called *spin* and *thermal* quantum Hall effects (SQHE and TQHE), respectively. The criticality at the IQHE, SQHE, and TQHE transitions will be discussed in detail in Sec. VI.C, VI.D, and VI.E, respectively.

4. $\mathbb{Z}_2$ topological term

For two classes, AII and CII, the second homotopy group is $\pi_2(\mathcal{M}_F) = \mathbb{Z}_2$. This allows for the θ-term but θ can only take the value $\theta = 0$ and $\theta = \pi$. It was shown very recently (Ostrovsky *et al.*, 2007a) that the σ-model of the Wigner-Dyson symplectic class (AII) with a $\theta = \pi$ topological angle arises from a model of Dirac fermions with random scalar potential, which describes, in particular, graphene with long-range disorder. Like in the case of quantum-Hall systems, this topological term inhibits localization. Whether the model then flows unavoidably into the ideal-metal fixed point or, else, there is also a novel attractive fixed point is a matter of ongoing research. The reader is referred to Sec. VI.B for more detail.

5. Wess-Zumino term

Finally, one more mechanism of emergence of criticalty is the Wess-Zumino (WZ) term. It is known that this term may appear in σ-models of the classes AIII, CI, and DIII. For these classes, the compact component $\mathcal{M}_F$ of the manifold is the group $H \times H/H = H$, where H is U(n), Sp($2n$), and O($2n$), respectively. The corresponding theories are called "principal chiral models". The WZ

term has the following form:

$$iS_{\rm WZ}(g) = \frac{ik}{24\pi} \int d^2r \int_0^1 ds\, \epsilon_{\mu\nu\lambda}$$
$$\times {\rm Str}(g^{-1}\partial_\mu g)(g^{-1}\partial_\nu g)(g^{-1}\partial_\lambda g), \qquad (6.2)$$

where k is an integer called the level of the WZW model. The definition (6.2) of the WZ term requires an extension of the σ-model field $g(\mathbf{r}) \equiv g(x,y)$ to the third dimension, $0 \le s \le 1$, such that $g(\mathbf{r},0) = 1$ and $g(\mathbf{r},1) = g(\mathbf{r})$. Such an extension is always possible, since the second homotopy group is trivial, $\pi_2(H) = 0$, for all the three classes. Further, the value of the WZ term does not depend on the particular way the extension to the third dimension is performed. (This becomes explicit when one calculates the variaton of the WZ term: it is expressed in terms of $g(\mathbf{r})$ only.) More precisely, there is the following topological ambiguity in the definition of $S_{\rm WZ}(g)$. Since the third homotopy group is non-trivial, $\pi_3(H) = \mathbb{Z}$, $S_{\rm WZ}(g)$ is defined up to an arbitrary additive integer n times $2\pi k$. This, however, does not affect any observables, since simply adds the phase $nk \times 2\pi i$ to the action.

The WZ term arises when one bosonizes certain models of Dirac fermions (Witten, 1984) and is a manifestation of the chiral anomaly. In particular, a σ-model for a system of the AIII (chiral unitary) class with the WZ term describes Dirac fermions in a random vector potential. In this case the σ-model coupling constant is truly marginal (as is typical for chiral classes) and one finds a line of fixed points. On the other hand, for the class CI there is a single fixed point. The WZW models of these classes were encountered in the course of study of dirty d-wave superconductors (Altland *et al.*, 2002; Nersesyan *et al.*, 1995) and, most recently, in the context of disordered graphene. We will discuss critical properties of these models in Sec. VI.G.3.

B. Symplectic Wigner-Dyson class (AII)

In metals with spin-orbit coupling the spin of a particle is no longer conserved. The spin-up and spin-down channels are coupled, and an electron needs to be represented as a two component spinor. If the time-reversal symmetry is preserved, the system belongs to the symplectic Wigner-Dyson class AII. The one-loop quantum correction at large conductance g takes then the form of weak antilocalization, see Sec. II.B.2, VI.A.1. At lower g the one-loop β-function is not sufficient anymore, and higher-order terms lead to localization, with the Anderson transition at some g_*. While the β-function has been calculated up to the four-loop order, see Eq. (2.25), this does not help to get quantitative predictions for critical properties. In particular, an attempt to use the four-loop β-function to extract the localization length exponent (Wegner, 1989) yields $\nu = \frac{1}{5}\left(\frac{3}{4}\zeta(3)\right)^{1/3} \approx 0.193$, which is an order of magnitude smaller than the numerical result (see below) and even violates the Harris criterion

$\nu \ge 2/d$ (Chayes *et al.*, 1986). This is not very surprising: the considered Anderson transition takes place at strong coupling, $g_* \sim 1$, so that keeping just the first few terms of the perturbative expansion is an uncontrolled procedure. In this situation, numerical simulations are particularly important. On their basis, a detailed quantitative picture of the transition has been developed; the key findings are summarized below.

1. Microscopic models

Most numerical studies employed a tight binding Hamiltonian. It is defined on a two dimensional square lattice with nearest neighbor coupling

$$H = \sum_{i,\sigma} \epsilon_i c_{i,\sigma}^\dagger c_{i,\sigma} + \sum_{\langle i,j\rangle,\sigma,\sigma'} V_{i,\sigma;j,\sigma'} c_{i,\sigma}^\dagger c_{j,\sigma'}. \qquad (6.3)$$

Here, $c_{i,\sigma}^\dagger$ ($c_{i,\sigma}$) denote creation (annihilation) operators of an electron with spin σ on site i. The on-site energies ϵ_i are taken to be random numbers drawn from the interval $[-W/2, W/2]$ with a homogeneous distribution. There exist various versions of the model, that differ by the choice of the hopping matrix $V_{i,\sigma;j,\sigma'}$.

Most studies employ the Ando model (Ando, 1989) characterized by non-random hopping between next neighbors only,

$$V_{i,\sigma;i+k,\sigma'} = (V_0 \exp(i\theta_k \sigma_k))_{\sigma,\sigma'}, \qquad k = x, y, \quad (6.4)$$

where σ_x, σ_y are the Pauli matrices. Conventionally, the spin-orbit energy scale is set to unity, $V_0=1$, and the mixing angles take constant values $\theta_k=\pi/6$. In the Evangelou-Ziman model (Evangelou, 1995; Evangelou and Ziman, 1987), the components of V that are proportional to $\sigma_{x,y,z}$, are chosen to be random with prefactors drawn independently from a box distribution of a width V_0. Recently, a third variant was introduced (Asada *et al.*, 2002, 2004) – the SU(2) model, in which the random matrix $\exp(i\theta_k \sigma_k)$ is chosen to be uniformly distributed on the SU(2) group. This last model was found particularly suitable for numerics, since finite size corrections appear to be very small.

2. Localization length exponent

The small magnitude of finite-size corrections in the SU(2) model has allowed Asada *et al.* (2002, 2004) to determine the localization length exponent with a high precision, $\nu=2.746 \pm 0.009$. Very recently, a similar result (though with somewhat higher uncertainty) was obtained (Markos and Schweitzer, 2006) in the context of the Ando model, $\nu = 2.8 \pm 0.04$. Asada *et al.* (2004) evaluated numerically the whole β-function and found that it has the expected shape, with a single zero determining the transition point.

3. Critical conductance

Since the transition takes place in the strong coupling regime, the mesoscopic conductance fluctuations at criticallity are comparable to the mean value, so that an ensemble of macroscopically identical coherent samples is to be characterized by the whole distribution function $\mathcal{P}(g)$. Quite generally speaking, critical conductance distributions are scale-invariant but depend on the shape of the sample (similar to the IPR distribution function, Sec. II.C.5 and the level statistics, Sec. II.E); a review of numerical results has been given by Markos (2006). The distribution $\mathcal{P}(g)$ for a square sample at the symplectic Anderson transition was determined in Ohtsuki *et al.* (2004) for the SU(2) model, see Fig. 28, and in Markos and Schweitzer (2006) for the Ando model, with essentially identical results. The average value $\langle g \rangle$ was found to be $\langle g \rangle = 1.42 \pm 0.005$ with a variance $\mathrm{var}g = 0.36$ (Markos and Schweitzer, 2006).

4. Multifractal spectrum

The spectrum τ_q can be calculated for the 2D symplectic transition with very good accuracy, because corrections to scaling turn out to be extremely small (Asada *et al.*, 2004; Mildenberger and Evers, 2007). Therefore, many generic features of the critical wavefunction statistics can be studied in great detail.

The results of a high-precision study of wave function multifractality at the symplectic Anderson transition (Mildenberger and Evers, 2007) are summarized in Fig. 25. In order to highlight the non-trivial features, the reduced anomalous dimensions $\delta_q = \Delta_q/q(1-q)$ are depicted. The key observations are as follows:

(i) One finds that $\delta_0 \equiv \alpha_0 - 2 = 0.172 \pm 0.002$. This result may be used as a check on the conformal invariance, which imposes the exact condition (Janßen, 1994, 1998)

$$\pi \delta_0 \Lambda_c = 1. \tag{6.5}$$

Here $\Lambda_c = \xi_M/M$, where ξ_M is the localization length in a quasi-1D strip of width L at criticality.) With the above value for δ_0 and with $\Lambda_c = 1.844 \pm 0.002$ (Asada *et al.*, 2004), the left-hand side of Eq. (6.5) becomes indeed very close to unity: 0.996 ± 0.013.

(ii) The function δ_q fulfills the symmetry relation Eq.(2.38), as demonstrated in the inset of Fig. 25 where the data for the range $-0.5 < q < 1.5$ are displayed.

(iii) δ_q has a small but non-zero curvature, implying that the the multifractal spectrum is not parabolic.

(iv) The results are essentially identical for the SU(2) and Ando models, confirming the universality of the transition. An abrupt change in the behavior of the data for the typical IPR in Fig. 25 at $q \simeq 2.5$ is related to the fact that at $q > q_+$, when the average IPR probes the tail of its distribution function, the exponents τ_q and τ_q^{typ} start to differ, see Eq. (2.42). In this range of q the statistical
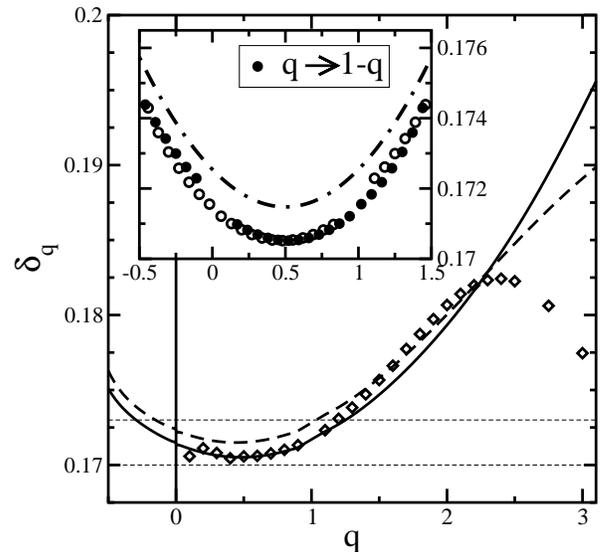

FIG. 25 Multifractal spectrum δ_q for the Ando model (dashed, $W_c = 5.84$) and the SU(2) model (solid, $W_c = 5.953$). To highlight deviations from parabolicity, reduced anomalous dimensions $\delta_q = \Delta_q/q(1-q)$ are plotted. Anomalous dimensions δ_q^{typ} obtained from typical IPR are also shown ($\diamond$). Dashed lines indicate the estimated error (2σ) in δ_0. *Inset:* blow up of the solid line behavior near $q = \frac{1}{2}$ is represented by empty circles ($\circ$). Filled symbols ($\bullet$) show original trace after reflection at $q = \frac{1}{2}$. Dot-dashed line is a fit (offset: 10^{-3}) $\delta_q = 0.1705 + 0.0043(q - \frac{1}{2})^2$. (Mildenberger and Evers, 2007)

uncertainty in determination of τ_q also increases, explaining some deviation between the data for both models.

Very similar results for the multifractality spectrum were obtained in (Obuse *et al.*, 2007b). In this work, the multifractality was also studied at the boundary and at the corner of the system. It was found that the multifractal exponents fulfill the relation (2.59), thus providing a further strong evidence for the conformal invariance at this critical point.

5. Symplectic-class theories with $\mathbb{Z}_2$ topology.

As was explained in Sec. VI.A.4, the σ-model of the symplectic class allows for an inclusion of a topological term with $\theta = \pi$. A microscopic realizations of such a non-trivial topology was for the first time identified in Ostrovsky *et al.* (2007a) where the model of Dirac fermions in disordered graphene was studied (see Sec. VI.G). It was found that for the case of long-range impurities, when two valleys in the spectrum are decoupled and the problem reduces to that of a single species of Dirac fermions in random potential, the field theory is the class-AII σ-model with $\theta = \pi$ topological term.

The fermionic sector of the corresponding σ-mode manifold is $\mathcal{M}_F = \mathrm{O}(4n)/\mathrm{O}(2n) \times \mathrm{O}(2n)$. In fact, for the "minimal" supersymmetric σ-model ($n = 1$) the sec-

ond homotopy group is richer:

$$\pi_2\big[\mathcal{M}_F|_{n=1}\big] = \mathbb{Z} \times \mathbb{Z}, \qquad \pi_2\big[\mathcal{M}_F|_{n\geq2}\big] = \mathbb{Z}_2. \quad (6.6)$$

For $n = 1$ the compact sector of the model is the manifold $(\mathrm{S}^2 \times \mathrm{S}^2)/\mathbb{Z}_2$ (product of the "diffuson" and "Cooperon" 2-spheres divided by $\mathbb{Z}_2$). Thus two topological invariants, $N_{1,2}[Q]$, counting the covering of each sphere, emerge in accordance with Eq. (6.6). The most general topological term is $iS_{\mathrm{top}} = i\theta_1 N_1 + i\theta_2 N_2$. However, the time-reversal symmetry requires that the action is invariant under interchanging the diffuson and Cooperon spheres, which yields $\theta_1 = \theta_2 \equiv \theta$ where θ is either 0 or π. Hence only a $\mathbb{Z}_2$ subgroup of the whole $\mathbb{Z} \times \mathbb{Z}$ comes into play as expected: the phase diagram of the theory should not depend on n. For the Dirac fermion problem (Ostrovsky *et al.*, 2007a), an explicit expression for $n = 1$ topological term can be written using $\mathbf{u} = T\nabla T^{-1}$ (where the σ-model field $Q = T^{-1}\Lambda T$, see Sec. II.B.1),

$$iS_2[Q] = \frac{\epsilon_{\alpha\beta}}{8}\mathrm{Str}\big[(\Lambda \pm 1)\tau_2 u_\alpha u_\beta\big] \equiv i\pi(N_1[Q] + N_2[Q]),$$

yielding $\theta = \pi$. The non-trivial value of the topological angle ($\theta = \pi$) holds for higher n as well. It implies that all configurations $Q(\mathbf{r})$ are subdivided into two topologically distinct classes ("even" and "odd"); the former give positive and the latter negative contribution to the σ-model partition function. This was confirmed numerically in Ryu *et al.* (2007b).

At large conductance g the contribution of topologically non-trivial configurations is exponentially small and can not affect the metallic phase in any essential way. On the other hand, at small g the topological term is expected to suppress localization, similarly to its role in the quantum Hall effect (Sec. VI.C) and in the quasi-1D symplectic model (Sec. V.D). This leaves room to two possibilities:

(i) The β-function changes sign twice. This would mean that, in addition to the conventional repulsive fixed point of the symplectic class, a new attractive fixed point arises. This scenario was proposed in Ostrovsky *et al.* (2007a). Then, if the RG flow starts with a sufficiently low conductivity, it ends up in this new critical point with a universal conductivity of order unity.

(ii) The β- function remains positive everywhere. The RG flow then necessarily leads the system into the ideal-metal fixed point with infinite conductivity.

In view of the strong-coupling nature of the problem, numerical simulations are needed to resolve this dilemma. Recent simulations of disordered graphene (Bardarson *et al.*, 2007; Nomura *et al.*, 2007; Nomura and MacDonald, 2007; Rycerz *et al.*, 2006) do confirm the suppression of localization in the symplectic class with $\mathbb{Z}_2$ topology. While the results of Nomura and MacDonald (2007); Rycerz *et al.* (2006) were consistent with the scenario (i), with a critical conductivity $\sim e^2/h$, most recent works (Bardarson *et al.*, 2007; Nomura *et al.*, 2007) appear to favor the second scenario.

It is worth reminding the reader of a different type of $\mathbb{Z}_2$ topology in 2D systems of the symplectic symmetry class (AII). It arises in the context of the quantum spin Hall (QSH) effect and is related to a non-trivial first homotopy group, $\pi_1(\mathcal{M}_F) = \mathbb{Z}_2$. This enables, in full similarity to the 2D situation, a θ-term with θ equal to 0 or π also in 1D case, inducing a $\mathbb{Z}_2$ topological classification of edge states in QSH systems, see Sec. V.D. Therefore, these systems possess in addition to the metallic phase, two distinct insulating phases, with different edge properties (normal insulator and QSH insulator). An important question is whether there is a direct, quantum-Hall-type transition between these two phases. Recent numerics (Essin and Moore, 2007; Obuse *et al.*, 2007a; Onoda *et al.*, 2007) on some models of QSH systems gives a negative answer: the insulating phases are found to be everywhere separated by the metallic phase. It would be interesting to find out whether such a direct transition is generically prohibited, independently of the microscopic model. More activity in this direction may be expected in near future.

C. The integer quantum Hall effect

Our presentation in this section complements the reviews (Huckestein, 1995; Kramer *et al.*, 2005).

1. Pruisken's σ-model

As was discovered in v. Klitzing *et al.* (1980), the Hall conductivity σ_{xy} of a 2D electron gas in a strong transverse magnetic field develops plateaus at values quantized in units of e^2/h. While the physics of the Hall plateau is fairly well understood by now, the theory of the quantum critical points separating the plateaus – the quantum Hall transition – remains a challenging issue.

From the field-theoretical point of view, the IQHE is described by the σ-model (2.17) with a topological term (6.1). It was first derived by Pruisken in the replica formalism (Levine *et al.*, 1983; Pruisken, 1984, 1987); a supersymmetric generalization was obtained in Weidenmüller (1987). The action of the model reads

$$S[Q] = \frac{1}{8}\mathrm{Str}[-\sigma_{xx}(\nabla Q)^2 + 2\sigma_{xy}Q\nabla_x Q\nabla_y Q], \quad (6.7)$$

where σ_{xx}, σ_{xy} are dimensionless conductivities. The Hall conductivity σ_{xy} is related to the topological angle as $\sigma_{xy} = \theta/2\pi$. There is strong evidence that the corresponding two-parameter flow diagram has the form shown in Fig. 26, as proposed in Khmelnitskii (1984); Pruisken (1985, 1987). The fixed point at $\theta = (2n + 1)\pi$ describes the QH transition. While the theory (6.7) is highly important for understanding of qualitative features of the problem, it allows to make only
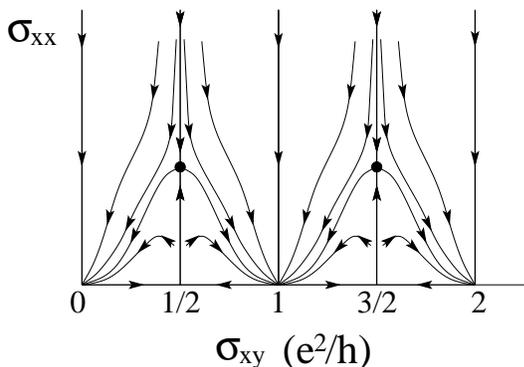
FIG. 26 Two-parameter flow diagram of the Pruisken σ-model, as first proposed in (Khmelnitskii, 1984).

rough predictions for parameters of the critical behavior (Pruisken and Burmistrov, 2005). This is because a controllable calculation in this framework can only be performed at weak coupling, $\sigma_{xx} \gg 1$, while the fixed points are at strong coupling, $\sigma_{xx} \sim 1$. In this situation, numerical simulations are particularly important; their results will be reviewed in Sec. VI.C.5–VI.C.7.

2. Further analytical approaches

A great deal of effort has been invested by many researchers in order to attack the problem of the QH transition from the analytical side. In addition to the Pruisken model, Sec. VI.C.1, several other analytical frameworks have been used. While this activity has not led to an ultimate success in the quantitative description of critical behavior, a variety of important connections between the models has been established. In particular, it has been shown that the σ-model (6.7) is also obtained as a continuum limit of the Chalker-Coddington network described in Sec.VI.C.4 (Zirnbauer, 1997). Further, either of these two models can be mapped onto a quantum antiferromagnetic superspin chain (Kondev and Marston, 1997; Lee, 1994; Marston and Tsai, 1999; Zirnbauer, 1994, 1997). Unfortunately, attempts to find an integrable deformation of this spin chain have failed. A further approach to QH criticality is based on the model of Dirac fermions; it will be reviewed in Sec. VI.G.2.

3. Quest for conformal field theory

Another line of activity is the search for a conformal field theory of the QH transition. The guiding principle is related to the fact that a relative of the Pruisken's model, the O(3) σ-model with $\theta = \pi$ topological term, describing a 1D quantum antiferromagnet with half-integer spin, flows under renormalization to a SU(2) WZW model. This means that the target space – which is the 2-sphere O(3)/O(2) = SU(2)/U(1)=S^2 for the O(3) σ-model –

is promoted to the group SU(2) (isomorphic to the 3-sphere S^3) at criticality. The idea is thus to identify the corresponding critical theory for the QH problem, with a hope that it is of the WZW type and is solvable by the methods of the conformal field theory. Such a proposal was made in Zirnbauer (1999), along with a detailed analysis of constraints on the sought fixed-point theory. The target space of the theory conjectured by Zirnbauer is a real form of the complex supergroup PSL(2|2). Its base $\mathcal{M}_F \times \mathcal{M}_B$ is a product of the 3-sphere $\mathcal{M}_F = $ SU(2) = S^3 and the 3-hyperboloid SL(2, $\mathbb{C}$)/SU(2) = H^3. A model of the same type was also proposed in (Bhaseen et $al.$, 2000) and most recently in (Tsvelik, 2007). The proposed theories have the form of the WZW model, see Sec. VI.A.5,

$$S[g] = \frac{1}{8\pi t} \int d^2 x \mathrm{Str} \partial_\mu g^{-1} \partial_\mu g + iS_{\mathrm{WZ}}[g], \qquad (6.8)$$

where iS_{WZ} is the WZ term (6.2). The peculiarity of the WZW models on the considered manifold is that they are critical at any value of the coupling constant t and level $k \in \mathbb{N}$. While (Zirnbauer, 1999) argues for $k = 1$, (Bhaseen et $al.$, 2000) considers the model with Kac-Moody symmetry, $k = 1/t$. The later condition restricts $1/t$ to be integer but facilitates the analysis of the model. Very recently, it was proposed (Tsvelik, 2007) that the later model with $k = 8$ may be the required fixed-point theory.

Both variants of the theory make a prediction for the statistics of critical eigenfunctions. Specifically, it is found that the multifractality spectrum is exactly parabolic,

$$\Delta_q = \gamma q(1 - q) ; \qquad (6.9)$$
$$f(\alpha) = 2 - (\alpha - \alpha_0)^2/4(\alpha_0 - 2) ; \quad \alpha_0 = 2 + \gamma , \quad (6.10)$$

with $\alpha_0 - 2 = 4t$ in the case of (Zirnbauer, 1999) and $\alpha_0 - 2 = 2t$ for (Bhaseen et $al.$, 2000). This prediction of parabolicity of Δ_q and $f(\alpha)$ indeed agrees with numerical simulations, Sec. VI.C.7, supporting this type of models. However, many questions related to the above conjectures remain open. In particular, if there is a whole line of fixed points (parametrized by t), then is there universality at the QH transition? If yes, how is it established? From the numerical point of view, there is no indication of non-universality at present.

4. Chalker-Coddington network

The Chalker-Coddington network (CCN) model was introduced in Chalker and Coddington (1988) as an effective description of the IQHE in a smooth random potential. In brief, the model is motivated in the following way. One considers electrons in a Landau level broadened by a potential with large correlation length. The electrons then drift along equipotential lines and tunnel between the lines near saddle points of the random
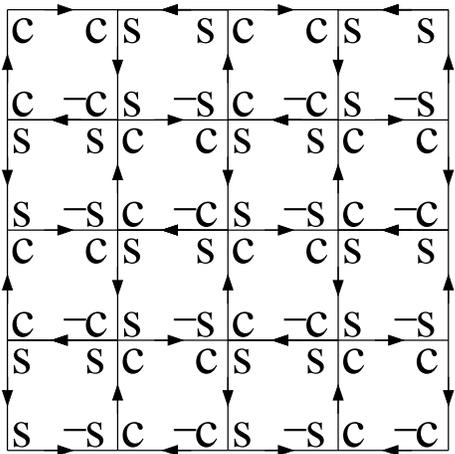
FIG. 27 Chalker-Coddington network model of the IQH transition (Chalker and Coddington, 1988). The symbols $\pm c$, $\pm s$ denote the components $\pm \cos\theta$, $\pm \sin\theta$ of scattering matrices at the nodes of the network.

potential. When the energy is sufficiently close to the band center (classical percolation threshold), the tunneling probability becomes ~ 1, and a random network with directed links is formed. At each node of the network two incoming and two ongoing links meet. In the CCN model, this geometrically random structure is replaced by a regular square network, as shown in Fig. 27; the disorder is accounted for by random phases associated with all links. A state Ψ of the network is defined by its amplitudes on the edges of the network. Originally (Chalker and Coddington, 1988) the network was characterized by a transfer matrix, as appropriate for finite-size scaling analysis of the localization length. Later (Klesse and Metzler, 1995) an equivalent description in terms of a scattering matrix was introduced. Each realization of the network is determined by a unitary operator $\mathcal{U} = \mathcal{U}_N\mathcal{U}_E$ acting on states Ψ and modelling the evolution of the state in a time step. Here $\mathcal{U}_N$ is an operator describing the unitary scattering at nodes with amplitudes $\pm\cos\theta$, $\pm\sin\theta$, as shown in Fig. 27. The second factor, $\mathcal{U}_E$, is a diagonal operator with random elements $e^{i\phi_e}$ on all edges e of the network. In the simplest formulation of the model, the angle θ is the same for all nodes, and the phases ϕ_e are independent random variables distributed uniformly over $[0; 2\pi]$. Changing the parameter θ allows one to drive the system through the IQH transition, with the critical point at $\cos^2\theta = 1/2$.

The CCN model has been extensively used for numerical simulations of the IQH transition point; it turned out to be particularly well suited for the analysis of statistical properties of energy levels and wave functions. Key results of computer simulations are reviewed below.

The model has been generalized to other symmetry classes. This is most naturally done for the counterparts of the IQHE in the superconducting classes C and D, namely, SQHE and TQHE. In these classes the symmetric spaces of the Hamiltonian (Table I) are the groups Sp(N) and O(N), and the required modification amounts to a replacement of the factors $e^{i\phi_e} \in U(1)$ by the elements of Sp(2)=SU(2) for the SQHE (in this case the amplitudes are spin doublets) and of O(1) for the TQHE, see Sec. VI.D, VI.E for more detail. For several other symmetry classes non-directed generalizations of the CCN have been constructed and used to study the corresponding critical behavior; specifically, this has been done for the chiral classes (AIII, BDI, CII) (Bocquet and Chalker, 2003), Sec. VI.F, and for the symplectic class AII (Merkt *et al.*, 1998; Obuse *et al.*, 2007a) considered in Sec. VI.B.

A further important aspect of the CCN model and its generalizations is that they can serve as a starting point for analytical work. We have already mentioned established equivalences between the CCN and other IQH models (Pruisken model and supersitin chain) in Sec. VI.C.2. Further, a connection with the models of disordered Dirac fermions has been established (Ho and Chalker, 1996). The network model of the SQHE has led to a number of exact analytical results, Sec. VI.D.

5. Localization length exponent

Several microscopic models have been used to study numerically the critical properties at the IQH transition. This includes tight-binding models, Landau-space models where the problem is projected on one or several Landau levels, and the CCN models, Sec. VI.C.4. For a more detailed review of the models the reader is referred to Huckestein (1995). The first high-precision determination of the localization length exponent ν has been achieved in the framework of the Landau-space model (Huckestein, 1995; Huckestein and Kramer, 1990; Huckestein *et al.*, 1992), with the result $\nu = 2.35 \pm 0.03$. Results of later simulations on different models are all in agreement with this value, thus favoring the universality of the IQH critical behavior. At present, the precise value of the leading irrelevant scaling index, y, is known with much less accuracy. While several authors find values close to y=0.4, e. g. (Evers and Brenig, 1998; Huckestein, 1995), in some cases values up to y=0.6 have been reported (Kramer *et al.*, 2005).

6. Critical conductivity and conductance distribution

In a number of works, the critical conductivity was found numerically in the range $0.5 - 0.6$. More specifically, the results are: from 0.50 ± 0.03 to 0.55 ± 0.05 for different types of disorder (Huo *et al.*, 1993); 0.50 ± 0.02 (Gammel and Brenig, 1994); 0.58 ± 0.03 (Schweitzer and Markos, 2005). Results in higher Landau levels are consistent with these values to the extent that the critical regime (of system sizes) could be reached
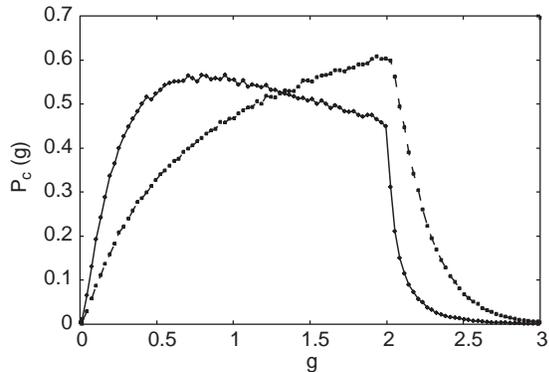
FIG. 28 Distribution function of the conductance at the IQH (solid) and the 2d symplectic (dashed) critical point using periodic boundary conditions and a square sample geometry (Ohtsuki *et al.*, 2004)

.

(Gammel and Evers, 1998).

Several authors also studied the conductance distribution $\mathcal{P}(g)$ of a square sample with periodic boundary conditions in the transverse direction; see Sec. VI.B.3 for a qualitative discussion of $\mathcal{P}(g)$ at criticality. As expected, a scale invariant distribution was found, see Fig. 28, with the average $\langle g \rangle = 0.58 \pm 0.03$ and the variance $\text{var}(g) = 0.081 \pm 0.005$ (Wang *et al.*, 1996); similar results were obtained in Cho and Fisher (1997b), in Kramer *et al.* (2005); Ohtsuki *et al.* (2004) where the average found to be $\langle g \rangle = 0.57 \pm 0.02$, as well as in Schweitzer and Markos (2005); the latter work yields $\langle g \rangle = 0.60 \pm 0.02$.

7. Wave function multifractality

A high-precision evaluation of the multifractal spectrum at the IQH transition was carried out in Evers *et al.* (2001) for the CCN model of a size $L \times L$ with L ranging from 16 to 1280. Figure 29 shows results for the $f(\alpha)$ spectrum. It is seen that after extrapolation to the thermodynamic limit, $L \to \infty$, the $f(\alpha)$ spectrum is well described by the parabolic form (6.10) with $\alpha_0 - 2 = 0.262 \pm 0.003$. One observes that deviations from parabolicity – if they exist – are too small to be resolved in this plot. In Fig. 30 reduced anomalous dimensions $\Delta_q/q(1-q)$ are plotted. This quantity is constant (equal to $\alpha_0 - 2$) for an exactly parabolic spectrum, Eq. (6.9). The observed deviations from the constant are very small ($\sim 1\%$) and within the error bars. Since there is no small parameter in the problem, it seems that an accidental closeness of the spectrum to a parabola with such a high accuracy is very improbable. So, the numerical results are in favor of exact parabolicity of the multifractal spectrum, thus supporting the possibility of
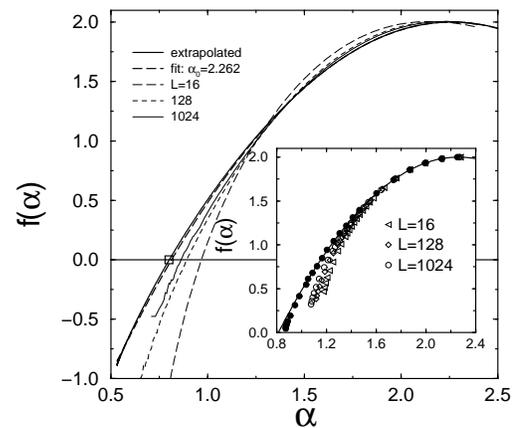

FIG. 29 Multifractal spectrum at the IQH transition. Fat solid line: numerical results for $f(\alpha)$ obtained from scaling of average IPR after extrapolation to $L \to \infty$. Datas for several finite values of $L = 16, 128, 1024$ are also shown. Dashed line: parabolic approximation, Eq. (6.9). Inset: data points from typical IPR from systems with sizes $L = 16, 128, 1024$ (open symbols) and extrapolation to infinite system size (full circles); data from average IPR are shown by solid line. (Evers *et al.*, 2001)

a conformal theory of the IQH critical point of the type discussed in Sec. VI.C.3.

It is worth mentioning that earlier studies of the IQH multifractality [the references can be found in (Evers *et al.*, 2001)] gave considerably different results, showing, in particular, strong deviations from parabolicity. As was shown in Evers *et al.* (2001), earlier numerics suffered strongly from the absence of ensemble averaging (its role was explained in Sec. II.C.5) and from finite-size effects. Importance of a careful analysis of the latter is illustrated in Fig. 29, where also data for finite sizes of a system are included.

A high-precision evaluation of multifractality allows to test the conformal invariance of the problem via Eq. (6.5). The parameter $\Lambda_c \equiv \xi_M/M$ was found to be $\Lambda_c = 1.22 \pm 0.01$ (Evers and Brenig, 1998; Evers *et al.*, 2001), implying, in combination with the above value of $\alpha_0 - 2$, that (6.5) is perfectly fulfilled and thus confirming the expectation that the IQH critical theory is conformally invariant.

8. Statistics of the two-point conductance

Closely related to wavefunction multifractality is the statistics of two-point conductances, Sec. II.C.9. In Klesse and Zirnbauer (2001) a relation between statistical properties of the wave functions and two-point con-
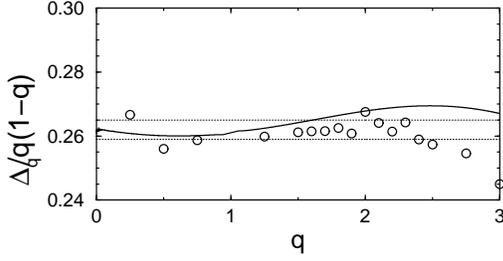
FIG. 30 Anomalous multifractal dimensions Δ_q [divided by $q(1-q)$] at the IQHE critical point, as obtained from extrapolation of the average inverse participation ratio (IPR). In the case of exact parabolicity, the plotted quantity should be constant. The dotted lines indicate the error bars obtained for $\alpha_0 - 2$. The circles give the $\Delta_q^{\mathrm{typ}}/q(1-q)$ as obtained from the typical IPR. As explained in Sec. II.C.5, $\Delta_q^{\mathrm{typ}} = \Delta_q$ for $q < q_+$; for IQHE with parabolic spectrum (6.9), (6.10) we find $q_+ = [2/(\alpha_0 - 2)]^{1/2} \simeq 2.76$. Thus, the last two data points for $\Delta_q^{\mathrm{typ}}/q(1-q)$ are in the range $q > q_+$, which explains their downward deviations from $\Delta_q/q(1-q)$. (Evers *et al.*, 2001)

ductances was derived,

$$2\pi\rho\langle y_m f(y_m/y_l)\rangle = \langle F(T_{lm})\rangle \; ;$$
$$F(T) = \int_0^{2\pi} \frac{d\phi}{2\pi} f\left(T^{-1}|1 - e^{i\phi}\sqrt{1-T}|^2\right) \; . \quad (6.11)$$

Here $f(x)$ is an arbitrary function, $y_l = |\Psi_l|^2$, $y_m = |\Psi_m|^2$ are wave function intensities at two links l and m for an eigenstate Ψ of a closed network, and $T_{l,m}$ is the two-point conductance defined for an open network with the edges l and m cut and attached to two terminals. This result was used in Evers *et al.* (2001) to derive the the relation (2.63) between the corresponding critical exponents. The parabolic spectrum for wave function multifractality, Eq. (6.9), found for IQHE translates thus into parabolic spectrum of exponents X_q for the two-point conductance,

$$X_{q\leq 1/2} = X_t q(1-q) \; ; \qquad X_{q\geq 1/2} = X_t/4 \; , \quad (6.12)$$

with $X_t = 2(\alpha_0 - 2) = 0.524 \pm 0.006$. In an earlier work (Janßen *et al.*, 1999) an explicit expression for the distribution of the two-point conductance on the CCN was derived under the assumption of the parabolic law (6.12) for X_q. In Klesse and Zirnbauer (2001) this result was used to test the conformal invariance of the theory, utilizing a numerical analysis of the moments of the two-point conductance in the quasi-1D (cylinder) geometry. The result of Janßen *et al.* (1999) for the distribution of the conductance T between the points $(0,0)$ and (x,y) in

this geometry reads

$$\mathcal{P}(T) = \frac{2\pi^{-1/2}\zeta^{-X_t/4}}{T^2(X_t\ln\zeta)^{3/2}} \int_{\mathrm{arcosh}\frac{1}{\sqrt{T}}}^{\infty} \frac{e^{-t^2/X_t\ln\zeta}\,t\,dt}{\sqrt{\cosh^2 t - T^{-1}}} \; ,$$
$$\zeta = (W/\pi a)|\sinh[\pi(x+iy)/W]| \; , \qquad (6.13)$$

where a is the non-universal microscopic scale that sets the length unit. The numerically determined moments of T were in perfect agreement with this formula, thus supporting the conformal invariance. The best fits yielded the values $X_t = 0.54 \pm 0.01$ from the analysis of the moments $\langle T^{n+1/2}\rangle$ and $X_t = 0.57 \pm 0.05$ from the analysis of the typical conductance, $\langle \ln T\rangle$. These values are consistent with the above result $X_t = 0.524 \pm 0.006$.

9. Classical percolation vs. quantum Hall effect

If the disorder correlation length is large, there is an intermediate, parametrically broad, range of energies where the physics is dominated by classical percolation. On corresponding length scales, tunneling between the percolating contours is exponentially small. This range of energies was studied in Mil'nikov and Sokolov (1988) where the scaling of the localization length with an exponent $\tilde{\nu} = \nu_{\mathrm{perc}} + 1 = 7/3$ was found ($\nu_{\mathrm{perc}} = 4/3$ is the correlation length index of the 2D percolation problem). In this regime quantum interference effects play no role. When energy approaches still closer the critical point, the probability of tunneling between the contours ceases to be small and the quantum interference becomes crucially important – the system enters the true critical regime of the quantum Hall transition. It is this latter regime that is described by the CCN model. While the "quasiclassical QHE" exponent $\tilde{\nu} = 7/3$ is remarkably close to the numerical value of the true QH exponent $\nu = 2.35 \pm 0.03$, this coincidence is apparently fully accidental, as the physics of the true QH critical regime and the intermediate quasiclassical regime of Mil'nikov and Sokolov (1988) is completely different.

It is worth mentioning that the physics of the intermediate, quasiclassical regime, where the physics is dominated by the vicinity of the percolation fixed point (Evers and Brenig, 1994, 1998; Gammel and Brenig, 1996; Klesse and Metzler, 1995; Kratzer and Brenig, 1994; Mil'nikov and Sokolov, 1988) is interesting in its own right. In particular, quasiclassical time evolution generates a long time tail in the velocity correlation function $\langle v_x(t)v_x(0)\rangle \sim t^{-2}$, which leaves $\sigma_{\mathrm{xx}}(\omega)$ with a nonanalytic ω-dependence inside an intermediate (quasiclassical) frequency window. The corresponding results may be relevant to experiments if the latter are performed on structures with smooth disorder, in which case the true QH criticality may in fact be totally unobservable for realistic temperatures.

10. Experiment vs. theory. Interaction effects

a. *Experimental results.* The IQH transition and the associated critical properties have been studied in numerous experiments. All the basic features — the existence of phase transitions with critical values $\sigma_{xy} = n + 1/2$ and σ_{xx} of the order of unity, as well as the power-law scaling behavior — are in agreement with the theoretical expectations. The situation with the values of critical exponents is not so simple, as we are going to discuss. To do this, we will have to touch the question of interaction effects, which is left out in the rest of this review, except for Sec. VII.A.

Experiments yield the following results for the critical exponents. First, the index ν of the localization length is found to be $\nu = 2.3 \pm 0.1$ (Koch *et al.*, 1991); this value was confirmed more recently in Hohls *et al.* (2001, 2002b). Second, the width of the critical region (peak in σ_{xx} and plateau transition in σ_{xy}) scales with the temperature T as $\Delta B \propto T^\kappa$ with $\kappa = 0.42 \pm 0.04$ (Wei *et al.*, 1988). While different values of κ were obtained in other works, it was emphasized in van Schaijk *et al.* (2000) that this results from macroscopic inhomogeneities that complicate observation of the true IQH critical behavior with $\kappa \simeq 0.42$. More recent work of the same group (Pruisken *et al.*, 2006; de Visser *et al.*, 2006) favors again $\kappa = 0.56 \pm 0.02$, however. On the other hand, the impact of density inhomogeneities was reconsidered by Li *et al.* (2005). It was found there, that for short-range disorder, when the true IQH criticality can be achieved, $\kappa = 0.42 \pm 0.01$, whereas the larger value $\kappa = 0.58$ was ascribed to impurity clustering. Finally, the frequency scaling of the transition width was found to be $\Delta B \sim \omega^\zeta$, with $\zeta = 0.41 \pm 0.04$ (Engel *et al.*, 1993). A more recent work (Hohls *et al.*, 2002a) yields a result consistent with this value, but with somewhat larger uncertainty, $\zeta = 0.5 \pm 0.1$. To summarize, the experiments yield ν that agrees with its numerical value (2.35 ± 0.03), as well as the dynamical exponents $z_T \equiv 1/\kappa\nu \simeq 1$ and $z \equiv 1/\zeta\nu \simeq 1$. The remarkable agreement in the value of ν is in fact surprising, in view of the electron-electron interaction.

b. *Finite-range interaction.* We consider first the case of a finite-range interaction $v(\mathbf{r} - \mathbf{r}')$, following Lee and Wang (1996); Wang *et al.* (2000). In this case the interaction is irrelevant. Indeed consider the Hartree-Fock interaction between the (close in energy) states α and β, normalized to the level spacing,

$$\lambda = \rho L^2 \int d^2 r d^2 r' \langle [|\psi_\alpha(\mathbf{r})|^2 |\psi_\beta(\mathbf{r}')|^2$$
$$- \psi_\alpha(\mathbf{r})\psi_\alpha^*(\mathbf{r}')\psi_\beta(\mathbf{r}')\psi_\beta^*(\mathbf{r}')] v(\mathbf{r} - \mathbf{r}') \rangle. \quad (6.14)$$

In the σ-model language, see Sec. II.B.1, the scaling of (6.14) with the system size L is governed by the scaling dimension of the operator

$$Q_{11}^{\rm bb}(\mathbf{r})Q_{22}^{\rm bb}(\mathbf{r}) - Q_{12}^{\rm bb}(\mathbf{r})Q_{21}^{\rm bb}(\mathbf{r}) . \quad (6.15)$$

While each of the two terms in (6.15) is relevant in the RG sense, having a dominant negative scaling dimension Δ_2 (which governs the IPR scaling, Sec. II.C.1,VI.C.7), the difference (6.15) is RG-irrelevant (Wegner, 1980), with a scaling dimension $x_2 > 0$. The numerical value of x_2 at the IQH critical point was estimated to be $x_2 = 0.66 \pm 0.04$ (Lee and Wang, 1996). With increasing L the interaction (6.14) scales as $\lambda \propto L^{-x_2}$, so that the fixed point is unaffected by it. This implies that the critical index ν of the localization length and the multifractality spectrum Δ_q remain the same as in the non-interacting problem. This is also true for the dynamical exponent z governing the destruction of localization by finite frequency: the corresponding scaling variable is $\omega\xi^z$ with $z = 2$. (In general, for a non-interacting transition with finite DOS in d dimensions the scaling variable is ω/q^d (Wegner, 1976)). The interaction cannot be fully discarded, however (it is said to be *dangerously irrelevant*), as the conductivity at finite T would be zero without the interaction-induced dephasing. The dephasing rate scales as $\tau_\phi^{-1} \propto T^p$ with $p = 1 + 2x_2/z$ (Wang *et al.*, 2000). Thus, the dephasing length is $L_\phi \propto \tau_\phi^{1/2} \propto T^{-1/z_T}$ with $z_T = 2/p = 2z/(2x_2 + z)$, yielding $z_T \simeq 1.2$ with the above estimate for x_2. Therefore, for a system with a metallic gate (which screens the interaction) one expects the exponents $\nu \simeq 2.35$, $z = 2$, and $z_T \simeq 1.2$.

c. *Coulomb interaction.* The situation with $1/r$ Coulomb interaction (as in typical experiments) is much less clear. In this case the interaction is RG-relevant and drives the system to a novel fixed point (Baranov *et al.*, 2002; Lee and Wang, 1996). While the conductivity and the screened compressibility $\partial n/\partial \mu$ remain finite at the transition (Belitz and Kirkpatrick, 1994; Finkelstein, 1990), much less is known theoretically about other critical properties. Several authors (Polyakov and Samokhin, 1998; Wang and Xiong, 2002) argued that charging effects analogous to those responsible for the linear Coulomb gap in the tunneling DOS of the insulator will lead to $z = z_T = 1$ (which is the natural scaling dimension of the $1/r$ interaction). The status of this argumentation is unclear, however, for the following reasons:

(i) These arguments essentially identify z and z_T with a dynamical exponent (z_3 in notations of Belitz and Kirkpatrick (1994)) governing the scaling of the density response function. It is known, however, that in metals the plasmon pole governed by this exponent, $z_3 = 1$, determines the interaction-induced quantum correction to tunneling DOS but not to conductivity (Altshuler and Aronov, 1984), in view of gauge invariance (Finkelstein, 1994). The conductivity correction is governed by the conventional diffusion pole in the *irreducible* density-density response function, which corresponds to the dynamical exponent $z_3^{\rm irr} = 2$.

(ii) Each Goldstone mode (or, equivalently, conserved quantity) is in general characterized by a dynamical exponent. For the QH transition this implies that, in

addition to the exponents related to the particle number conservation – $z_3 = 1$ and its irreducible counterpart, $z_3^{\text{irr}} = 2$, – there is another exponent associated with the energy conservation. This latter exponent, controlling the renormalization of the frequency term in the σ-model, is denoted by ζ in Finkelstein (1990), z_1 in Belitz and Kirkpatrick (1994), and by $2 + \gamma^*$ in Baranov et al. (2002). It is believed to govern the frequency scaling of the conductivity at the critical point of the Anderson transition in a system with Coulomb interaction and broken spin-rotation invariance in $2 + \epsilon$ dimensions (Belitz and Kirkpatrick, 1994; Finkelstein, 1990). One may thus expect that this dynamical exponent plays a central role at the quantum Hall transition as well (Baranov et al., 2002; Burmistrov, 2006).

The problem of the index ν of the localization length is also far from being solved. While it was found that ν is equal to its non-interacting value within the Hartree-Fock theory (Yang et al., 1995), it is not clear whether this should be applicable to the true fixed point in the problem with Coulomb interaction. To summarize, in our view, the theoretical problem of the critical behavior in the presence of Coulomb interaction remains open. In particular, it remains to be seen whether the remarkable agreement of ν with its non-interacting value as well as $z = z_T = 1$ — as suggested by experiments — are indeed exact properties of the interacting problem.

D. Spin Quantum Hall Effect (Class C)

1. Physical realization

The SQHE is a counterpart of the IQHE in superconductors with broken time-reversal but preserved spin-rotation invariance (Gruzberg et al., 1999; Kagalovsky et al., 1999; Senthil et al., 1999). The class-C Hamiltonian satisfies the symmetry (4.12) (with τ_y the Pauli matrix in the particle-hole space) and has the block structure (4.11). Several possible physical realization of SQHE systems have been proposed: (i) a d-wave superconductor with complex $d_{x^2-y^2} + id_{xy}$ pairing (Kagalovsky et al., 1999; Senthil et al., 1999) that was conjectured for high-T_c superconductors (Balatsky, 1998; Laughlin, 1998); (ii) granular superconducting film in a magnetic field (Kagalovsky et al., 1999); (iii) a state of composite fermions at filling fraction $\nu = 5/2$ with d-wave pairing (Read and Green, 2000), as proposed in Haldane and Rezayi (1988).

Similar to the case of the IQHE, the key signature of the SQHE is the quantization of the appropriate Hall conductance. Specifically, while the quasiparticle number is not conserved, the spin is, so that the relevant quantity is the spin Hall conductivity σ_{xy}^s. It describes the transverse spin current induced in response to a gradient of the Zeeman field,

$$j_x^z = \sigma_{xy}^s [-\partial B^z(y)/\partial y] \tag{6.16}$$

In the IQHE the step $\Delta\sigma_{xy}$ between the quantized values of the Hall conductivity is e^2/h per spin orientation. In the case of the SQHE, the elementary charge e is replaced by $\hbar/2$, yielding (Senthil et al., 1999)

$$\Delta\sigma_{xy}^s = 2n \cdot \hbar/8\pi , \tag{6.17}$$

where the factor 2 accounts for the spin and n for the valley degeneracy. In particular, for the case of Dirac fermions in a $d + id$ superconductor ($n = 2$), one finds two SQH phases with quantized values

$$\sigma_{xy}^s = \pm\hbar/4\pi . \tag{6.18}$$

In the presence of disorder, these two phases become Anderson insulators separated by the SQH transition. The field theory of this problem is analogous to Pruisken's theory of the IQHE (Sec. VI.C.1) — it is a σ-model of the class C with the topological term (6.1), possessing a critical point at $\theta = (2n + 1)\pi$ (Altland et al., 2002; Read and Green, 2000; Senthil et al., 1998, 1999). The corresponding flow diagram is expected to have qualitatively the same form as for the IQHE, Fig. 26. The critical behavior at the SQH transition is analyzed below. In the presence of a Zeeman term, the spin-rotation symmetry is broken, and the system crosses over to the symmetry class A of the IQHE transition (Cui et al., 2004; Kagalovsky et al., 1999; Senthil et al., 1998, 1999).

2. Mapping to percolation

The network model for the SQHE (Kagalovsky et al., 1999) is the SU(2) version of the Chalker-Coddington IQHE network, see Sec. VI.C.4 and Fig. 27. The directed links of the network carry doublets of complex fluxes representing propagation of spin-$1/2$ particle. The scattering at each node is spin-independent and defined in the same way as for the IQHE. Each realization of the network is characterized by a set of random 2×2 spin matrices U_e associated with all edges e of the network. In view of (4.12), the evolution operator of the network $\mathcal{U}$ satisfies the symmetry $\mathcal{U} = \tau_y \mathcal{U}^* \tau_y$, implying that $U_e \in \text{SU}(2)$. Starting with this network model, it turns out to be possible to establish a remarkable property of the SQH transition: some physical observables and critical indices can be calculated exactly via mapping to classical percolation. This was shown for the DOS and the conductance in Gruzberg et al. (1999) via the supersymmetry; an alternative derivation of these results was presented in Beamond et al. (2002). In Mirlin et al. (2003) the mapping was extended to all two- and three-point correlation functions describing, in particular, the wave function statistics. It was also shown there that the mapping breaks down for generic n-point correlation functions with $n > 3$.

We briefly sketch the idea of the approach of Beamond et al. (2002); Mirlin et al. (2003). The primary objects are Green functions on the network,

$$G(e', e; z) = \langle e'|(1 - z\mathcal{U})^{-1}|e\rangle ; \tag{6.19}$$
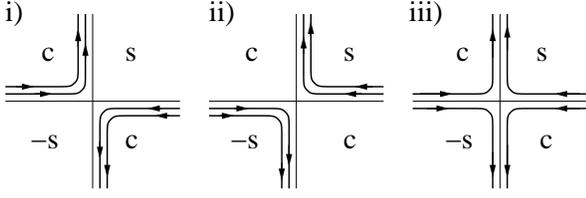
FIG. 31 Possible configurations of paths passing four times through a network node. The symbols c and $\pm s$ denote the elements $\cos\theta$, $\pm\sin\theta$ of the S-matrix at the node. The statement 2 in Sec. VI.D.2 allows one to get rid of the quantum interference contribution (iii) and to associate with the contributions (i) and (ii) the weights $\cos^2\theta$ and $\sin^2\theta$, respectively, yielding a mapping to the classical percolation.

for $z = \exp i(\epsilon \pm i\eta)$ they have a meaning of retarded (G_R, $|z| < 1$) and advanced (G_A, $|z| > 1$) Green functions at energy ϵ. The Green function is straightforwardly represented in the form of a sum over paths

$$G(e, e'; z) = \sum_{\text{paths } e' \to e} \ldots z U_{e_j} s_j \cdot z U_{e_{j+1}} s_{j+1} \cdot \ldots , \quad (6.20)$$

where s_j is the corresponding matrix element ($\cos\theta$, $\sin\theta$, or $-\sin\theta$) of the S-matrix between the edges e_j and e_{j+1}. Equation (6.20) generates a convergent expansion in powers of z when $|z| < 1$; otherwise the identity

$$G^\dagger(e, e'; z) = \mathbf{1} \cdot \delta_{ee'} - G(e', e; (z^*)^{-1}) \quad (6.21)$$

is to be used. As shown below, each of the sums over paths obtained by substituting (6.20), (6.21) in products of $n \leq 3$ Green functions can be reduced after disorder averaging to a sum over classical paths (hulls) in the percolation problem. This remarkable reduction crucially relies on the following two statements:

1. Only paths visiting each edge of the network either 0 or 2 times are to be taken into account; contributions of all the remaining paths sum up to zero.

2. Using the statement 1, it is easy to see that each node may be visited 0, 2, or 4 times. The second statement concerns the nodes visited four times. As illustrated in Fig. 31, there are three possibilities how this may happen; the corresponding contributions have weights (i) $\cos^4\theta$, (ii) $\sin^4\theta$, and (iii) $-\sin^2\theta\cos^2\theta$ from the scattering matrix at this node. The statement is that one can equivalently take into account only the contributions (i) and (ii) with the weights $\cos^2\theta$ and $\sin^2\theta$, respectively.

After application of the statement 2 to all nodes, the network is reduced to a weighted sum over all its possible decompositions in a set of closed loops (such that each edge belongs to exactly one loop). These loops can be viewed as hulls of the bond percolation problem. As a result, the correlation functions (averaged products of Green functions) are expressed in terms of classical sums over the percolation hulls. The results obtained in this way are listed below.

3. Density of states and localization length

The result for the average of a single Green function reads ($|z| < 1$) (Beamond et $al.$, 2002):

$$\langle \text{Tr} G(e, e, z) \rangle = 2 - \sum_{N>0} P(e; N) \, z^{2N} , \quad (6.22)$$

$$\langle \text{Tr} G(e, e, z^{-1}) \rangle = \sum_{N>0} P(e; N) \, z^{2N} , \quad (6.23)$$

where $P(e, N)$ is the probability that the edge e belongs to a loop of the length N. (In the bulk of a large system, $L \to \infty$, or for periodic boundary conditions, this probability does not depend on e, $P(e, N) = P(N)$.) This yields the DOS

$$\rho(E) = (1/2\pi)[1 - \sum_{N>0} P(N) \cos(2NE)] . \quad (6.24)$$

In the insulating phases ($t \equiv \cos^2\theta \neq 1/2$) this yields

$$\rho(E) \simeq \pi^{-1} \langle N^2 \rangle E^2, \quad (6.25)$$

which is the expected behavior of DOS in the class C. On approaching the percolation transition point, $t = 1/2$, the characteristic diameter of largest loops diverge,

$$\xi \sim |t - 1/2|^{-\nu} , \qquad \nu = 4/3. \quad (6.26)$$

At the critical point ($t = 1/2$)

$$P(N) \sim N^{-2/d_h} = N^{-8/7}, \quad (6.27)$$

where $d_h = 7/4$ is the fractal dimension of the percolation hull (Isichenko, 1992; Saleur and Duplantier, 1987), yielding (Beamond et $al.$, 2002; Gruzberg et $al.$, 1999)

$$\rho(E) \sim |E|^{1/7} . \quad (6.28)$$

The characteristic length of loops contributing to (6.28) is $N_E \sim E^{-1}$, yielding their characteristic "diameter" $\xi_E \sim |E|^{-1/d_h} = |E|^{-4/7}$, which is the localization length of the states with energy E. The percolation hull exponent d_h plays therefore a role of the dynamical exponent for the SQH transition.

4. Conductance

To define the two-terminal conductance g, one opens the system by cutting two subsets of links and attaching them to two reservoirs. The average dimensionless conductance is given by

$$\langle g \rangle = 2 \sum_{e \in 1_{\text{out}}; \ e' \in 2_{\text{in}}} P(e, e') , \quad (6.29)$$

where $P(e, e')$ is the probability that a path incident from the second reservoir on the link e' escapes to the first contact via the link e, and the sum goes over all such

links. Equation (6.29) was used in (Cardy, 2000) to calculate the critical conductivity by determining the conductance of a wide sample ($W \gg L$), $\langle g \rangle L/W = \sqrt{3}/2$. A very close result was earlier obtained by numerical evaluation of the Kubo formula, $\sigma_c = 2 \times (0.45 \pm 0.01)$ (Evers, 1997). It is worth stressing that, despite of the vanishing density of states, the critical conductance is finite. From the point of view of the Einstein relation, $\sigma = h\rho D$, this results from a mutual cancellation of the percolation exponents (Evers and Brenig, 1994; Ziff et $al.$, 1991), $\rho(E) \sim N_E/\xi_E^2 \sim E^{2/d_h-1} = E^{1/7}$ and $D(E) \sim \xi_E^2/N_E \sim E^{1-2/d_h} = E^{-1/7}$.

For the average two-point conductance (Sec. II.C.9), Eq. (6.29) yields (Gruzberg et $al.$, 1999)

$$\langle g(e,e') \rangle = 2P(e,e') \sim r^{-1/2} , \qquad (6.30)$$

where $r \gg 1$ is the distance between e and e'.

5. Higher correlation functions and multifractality

The results presented in this subsection were obtained in Mirlin et $al.$ (2003). To determine the fractal dimension Δ_2 governing the scaling of two-point correlations of wave functions (2.30), (2.32), one considers the correlation functions

$$\begin{aligned} \mathcal{D}(e',e;\gamma) &= (2\pi)^{-2} \langle \mathrm{Tr}[G(e',e;z) - G(e',e;z^{-1})] \\ &\quad \times [G(e,e';z) - G(e,e';z^{-1})] \rangle, \qquad (6.31) \\ \tilde{D}(e',e;\gamma) &= (2\pi)^{-2} \langle \mathrm{Tr}[G(e,e;z) - G(e,e;z^{-1})] \\ &\quad \times \mathrm{Tr}[G(e',e';z) - G(e',e';z^{-1})] \rangle, \quad (6.32) \end{aligned}$$

with a real $z = e^{-\gamma} < 1$ and $\gamma \ll 1$ playing a role of the level broadening. The mapping to percolation yields for the averaged products of two Green functions entering (6.31),

$$\begin{aligned} \langle \mathrm{Tr}G(e',e;z)G(e,e';z) \rangle &= \langle \mathrm{Tr}G(e',e;z^{-1})G(e,e';z^{-1}) \rangle \\ &= -2 \sum_N P(e',e;N)z^{2N}, (6.33) \\ \langle \mathrm{Tr}G(e',e;z)G(e,e';z^{-1}) \rangle &= -2 \sum_N P_1(e',e;N)z^{2N}, (6.34) \end{aligned}$$

where $P(e',e;N)$ and $P_1(e',e;N)$ are probabilities that the edges e and e' belong to the same loop of the length N (resp. with the length N of the part corresponding to the motion from e to e'). According to the classical percolation theory, P and P_1 scale as

$$P(e',e,N), \ P_1(e',e,N) \sim N^{-8/7}r^{-1/4} , \qquad r \lesssim N^{4/7} \tag{6.35}$$

and fall off exponentially fast at $r \gg N^{4/7}$, where r is the distance between e and e'. This yields for the correlation functions in (6.33) and (6.34) (which we abbreviate as $\langle G_R G_R \rangle$, $\langle G_A G_A \rangle$, $\langle G_R G_A \rangle$)

$$\begin{aligned} \langle G_R G_R \rangle = \langle G_A G_A \rangle &\simeq \langle G_R G_A \rangle \sim r^{-1/2}, \\ &r \ll \xi_\gamma \equiv \gamma^{-4/7} \qquad (6.36) \end{aligned}$$

in full agreement with the scaling argument of (Gruzberg et $al.$, 1999). However, these leading order terms cancel in (6.31), and the result is non-zero due to the factors z^{2N} only, implying that relevant N are $N \sim \gamma^{-1}$. As a consequence, $\langle (G_R - G_A)(G_R - G_A) \rangle$ scales differently compared to (6.36),

$$\begin{aligned} \mathcal{D}(e',e;\gamma) &= \frac{1}{\pi^2} \sum_N [P(r,N) - P_1(r,N)](1 - e^{-2N\gamma}) \\ &\sim P(r,\gamma^{-1})\gamma^{-1} \sim (\xi_\gamma r)^{-1/4}, \qquad r \lesssim \xi_\gamma. \ (6.37) \end{aligned}$$

The analysis of the correlation function (6.32) yields similar results. One thus finds the scaling of two-point wave function correlations for $r \lesssim \xi_E$,

$$\left. \begin{aligned} L^4 \langle \psi_{i\alpha}^*(e)\psi_{j\alpha}(e)\psi_{i\beta}(e')\psi_{j\beta}^*(e') \rangle \\ L^4 \langle |\psi_{i\alpha}(e)|^2 |\psi_{j\beta}(e')|^2 \rangle \end{aligned} \right\} \sim \left(\frac{\xi_E}{r} \right)^{\frac{1}{4}}. (6.38)$$

with α, β labeling the spin indices. This implies that the fractal exponent $\Delta_2 \equiv -\eta$ is

$$\Delta_2 = -1/4, \qquad (6.39)$$

at variance with what one might naively expect from the $r^{-1/2}$ scaling of the diffusion propagator $\langle G_R G_A \rangle$, Eq. (6.36). An analogous calculation for three-point correlation functions yields $\Delta_3 = -3/4$. For correlation functions of higher orders (determining, in particular, the exponents Δ_q with $q > 3$) the mapping to percolation breaks down.

The point $q = 3$ deserves special attention. It satisfies the relation

$$\Gamma(q) \equiv qx_\rho + \Delta_q = 0 , \qquad (6.40)$$

where $x_\rho = 1/4$ is the scaling dimension of DOS defined by $\rho(E) \sim \xi_E^{-x_\rho}$. It separates two regimes with different scaling of correlation functions. For smaller q, when $\Gamma(q) > 0$, the correlation functions

$$\begin{aligned} &\Pi_{s_1...s_q}^{(q)}(e_1,\ldots,e_q;E_1,\ldots,E_q) \\ &= \langle \mathrm{Tr}G_{s_1}(e_1,e_2;e^{iE_1})\ldots G_{s_q}(e_q,e_1;e^{iE_q}) \rangle, (6.41) \end{aligned}$$

where $s_j = R$ or A, show the scaling

$$\Pi_{s_1...s_q}^{(q)}(e_1,\ldots,e_q;E_1,\ldots,E_q) \sim r^{-qx_\rho} \qquad (6.42)$$

and are, to the leading approximation, independent of the indices s_i. However, when one calculates the wave-function correlations,

$$\begin{aligned} \mathcal{D}^{(q)}(e_1,\ldots,e_q;E_1,\ldots,E_q) &= (2\pi)^{-q} \\ \times \langle \mathrm{Tr}[(G_R - G_A)(e_1,e_2;e^{iE_1})(G_R - G_A)(e_2,e_3;e^{iE_2}) \\ \times \ldots \times (G_R - G_A)(e_q,e_1;e^{iE_q})] \rangle, \qquad (6.43) \end{aligned}$$

these leading-order terms cancel, yielding the multifractal behavior,

$$\mathcal{D}^{(q)}(e_1,\ldots,e_q;E_1,\ldots,E_q) \sim (r/\xi_E)^{\Delta_q}\xi_E^{-qx_\rho}, \qquad r \lesssim \xi_E. \tag{6.44}$$

On the other hand, for $q > 3$, when $\Gamma(q)$ is negative, the correlation functions $\Pi^{(q)}_{s_1,\dots,s_q}$ start to depend in a singular way on the infrared cutoff (ξ_E) and scale in the same way as $\mathcal{D}^{(q)}$, Eq. (6.44) (with a numerical prefactor depending on indices s_i), similarly to the conventional Anderson localization transition.

It is instructive to analyze this situation within the field-theoretical approach to the wave-function multifractality (Bernard and LeClair, 2002b; Bhaseen *et al.*, 2000; Duplantier and Ludwig, 1991; Mudry *et al.*, 1996; Wegner, 1980, 1985). In the renormalization-group language, $\Gamma(q)$ defined by Eq. (6.40) are scaling dimensions of operators of the type $\mathcal{O}^{(q)} \sim \psi_{s_1}\psi^\dagger_{s'_1}\dots\psi_{s_q}\psi^\dagger_{s'_q}$, where $\psi, \psi^\dagger$ are electronic fields. Averaged products of Green functions are expressed as correlation functions of the corresponding operators $\mathcal{O}^{(q)}$; in particular, (6.41) takes the form

$$\Pi^{(q)}_{s_1\dots s_q} \sim \langle \mathrm{Tr}\mathcal{O}^{(1)}_{s_1 s_2}(e_2)\mathcal{O}^{(1)}_{s_2 s_3}(e_3)\dots\mathcal{O}^{(1)}_{s_q s_1}(e_1)\rangle. \quad (6.45)$$

To calculate the scaling behavior of such correlation functions, one applies the operator product expansion (OPE) (Duplantier and Ludwig, 1991; Mudry *et al.*, 1996; Wegner, 1985). Generically, the identity operator will be among those generated by the OPE. Moreover, under the condition $\Gamma(q) > 0$ it will be the most relevant operator and will dominate the expansion, leading to the gap scaling $\Pi^{(q)} \sim r^{-q\Gamma(1)}$, in agreement with (6.42). On the other hand, if $\Gamma(q) < 0$, the operator $\mathcal{O}^{(q)}$ will give a dominant contribution to OPE, leading to a multifractal type of scaling, $\Pi^{(q)} \propto r^{-q\Gamma(1)}(r/\xi_E)^{\Gamma(q)}$, as in Eq. (6.44). What is, however, non-trivial from this point of view, is that the scaling of the wave function correlator (6.43) has the multifractal form (6.44) independently of the sign of $\Gamma(q)$. This means that in the regime $\Gamma(q) > 0$ the leading (gap scaling) terms (6.42) cancel in the particular combination of the functions $\Pi^{(q)}$ corresponding to $\mathcal{D}^{(q)}$, and subleading terms determine the result (6.44).

A related analysis can also be performed for the moments of the two-point conductance, Eq. (2.62). The corresponding exponents X_q are found to be linked to the wavefunction multifractal indices via (2.64).

6. Numerical results

The numerical simulations of the SQHE network (Mirlin *et al.*, 2003) have allowed to confirm the analytical predictions (Sec. VI.D.3–VI.D.5) as well as to determine some physical quantities that are not known analytically, – most notably, the whole spectrum of multifractality. We present a brief summary of the numerical results.

In Fig. 32 the numerically calculated DOS $\rho(E)$ for different system sizes L is displayed. After a proper rescaling all data collapse onto a single curve. The scale invariance of $\rho(E)$ at criticality is reminiscent of the analogous property of the level statistics at the conventional Anderson or QH transition, Sec. II.E. At $E \gg \delta$
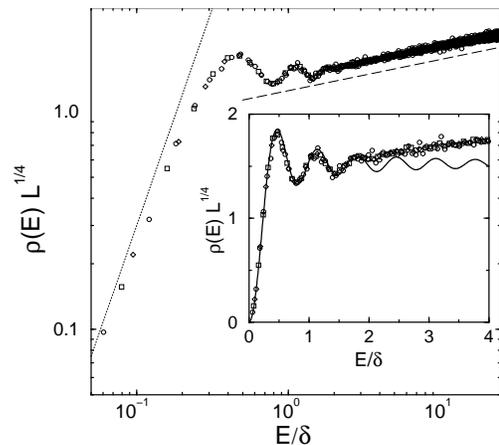

FIG. 32 Scaling plot of the density of states for system sizes $L = 16(\diamond), 32(\square), 96(\circ)$. Dashed and dotted lines indicate power laws (dashed: $E^{1/7}$, dotted: E^2), $\delta = 1/2\pi L^{7/4}$ denotes the level spacing at $E = 0$. *Inset:* same data on a linear scale and the RMT result (solid curve). (Evers *et al.*, 2003)

the critical DOS scales as $|E|^{1/7}$, in agreement with the analytical prediction (6.28). On the other hand, at $E \sim \delta$ one observes an oscillatory structure qualitatively analogous to the RMT behavior for the class C (Altland and Zirnbauer, 1997).

The anomalous multifractal dimensions Δ_q [divided by $q(1-q)$] are shown by a solid line in the upper panel of Fig. 33. They have been obtained from the scaling of the average IPRs. According to the analytical calculations (Sec. VI.D.5), $\Delta_q/q(1-q)$ is equal to $1/8$ for both $q = 2$ and $q = 3$; this value is marked by the dashed line in the figure. The numerical results agree perfectly well with the analytical findings at $q = 2$ and $q = 3$. Furthermore, the parabolic dependence may serve as a numerically good approximation,

$$\Delta_q \simeq q(1-q)/8. \quad \text{(approximate!)} \quad (6.46)$$

Nevertheless, Eq. (6.46) is not exact: at $0 < q < 2$ the numerically found Δ_q show clear deviations from exact parabolicity (6.46), which are of the order of 10% near $q = 0$. In particular, the deviation of the limiting value $\Delta_q/q(1-q)|_{q\to 0} = 0.137 \pm 0.003$ from $1/8$ well exceeds the estimated numerical uncertainty. The lower panel of Fig. 33 depicts the singularity spectrum $f(\alpha)$. The dashed line represents the parabolic approximation Eq. (2.37) with $\alpha_0 - 2 = 1/8$, corresponding to (6.46). The deviation of $\alpha_0 - 2 = 0.137 \pm 0.003$ from $1/8$ highlighted in the inset corresponds to non-parabolicity of τ_q discussed above. The numerical results for the multifractality at the SQH transition rule out conjectures of critical field theories that predict exactly parabolic spectra (Bernard and LeClair, 2001, 2002b).

In Fig. 34 the scaling of the average $\langle g \rangle$ and the typical $g_{\mathrm{typ}} = \exp\langle \ln g \rangle$ values of the two-point conductance is shown, along with analogous quantities $\langle |G|^2 \rangle$ and $|G|^2_{\mathrm{typ}} = \exp\langle \ln |G|^2 \rangle$ for a closed system, $|G|^2 \equiv$
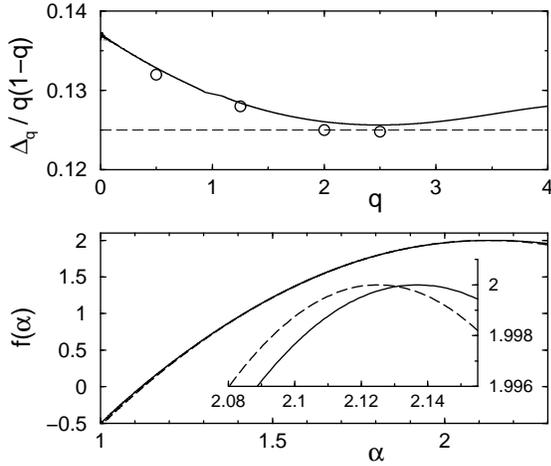
FIG. 33 *Upper panel:* anomalous dimensions Δ_q (solid line) and Δ_q^{typ} (circles) at the SQHE critical point. Numerical results agree very well with analytical findings $\Delta_2 = -1/4$ and $\Delta_3 = -3/4$. Data are presented in the form $\Delta_q/q(1-q)$ emphasizing deviations from exact parabolicity (dashed line). *Lower panel:* singularity spectrum $f(\alpha)$ (solid) and the parabolic approximation (dashed). *Inset:* magnified view of the apex region. (Mirlin *et al.*, 2003)

FIG. 34 Scaling of the two-point conductance with distance r between the contacts: average value (empty symbols), $\langle g \rangle$, and typical value (filled symbols), $g_{\mathrm{typ}} = \exp\langle \ln g \rangle$, in systems of sizes $L = 128(\square)$ and $L = 196(\circ)$. Also shown is scaling of the two-point Green function, $\langle |G|^2 \rangle$ and $|G|^2_{\mathrm{typ}} = \exp\langle \ln |G|^2 \rangle$ ($L = 128(\triangle), L = 196(\diamond)$). The lines correspond to the $r^{-1/2}$ (dotted) and $r^{-3/4}$ (dashed) power laws. Deviations from power-law scaling at large values of r are due to the finite system size. (Mirlin *et al.*, 2003)

$-\mathrm{Tr}G(e', e; 1)G(e, e'; 1)$. For the average values, $\langle g \rangle$ and $\langle |G|^2 \rangle$, the numerics fully confirm the theoretical results (6.30), (6.34) predicting that both quantities scale as $r^{-1/2}$ and, moreover, are equal to each other. A non-trivial character of the equality $\langle g \rangle = \langle |G|^2 \rangle$ is well illustrated by the data for typical quantities: g_{typ} and $|G|^2_{\mathrm{typ}}$ are not equal. Nevertheless, they are found to share a common scaling: $g_{\mathrm{typ}}, |G|^2_{\mathrm{typ}} \sim r^{-X_t}$, confirming the analytical expectations. Furthermore, the numerically obtained value of the exponent, $X_t \simeq 3/4$, is in agreement with the theoretical prediction based on the relation (2.64), $X_t = 2x_\rho + 2(\alpha_0 - 2) \simeq 0.774$.

E. Thermal quantum Hall effect (class D)

1. Physical realizations and general considerations

Systems belonging to the class D are disordered superconductors where both time reversal and spin rotation symmetries are broken. The corresponding Hamiltonian has the structure described in Sec. IV.D, see Eqs. (4.8), (4.9) and text below them. Possible physical realizations of this symmetry class include: (i) d-wave superconductors with strong spin-orbit scattering, (ii) p-wave paired states of spinless or spin-polarized fermions, e.g. paired states of composite fermions (Read and Green, 2000); (iii) triplet odd-parity (p- or f-wave) superconductors, like $SrRu_3O_4$ (Nelson *et al.*, 2004); (iv) type-II superconductors in a strong magnetic field in the presence of spin-orbit scattering impurities (Senthil and Fisher,

2000). While neither the quasiparticle number nor the spin are conserved for this symmetry class, one still can speak about thermal transport. The TQHE corresponds to the quantization of the ratio κ_{xy}/T of the thermal Hall conductance to the temperature in units of $\pi^2 k_B^2/6h$ (Senthil and Fisher, 2000).

For a combination of reasons, class-D systems show particularly rich behavior from the point of view of localization, quantum phases, and phase transition. First of all, class D allows for two mechanisms of 2D criticality, Sec. VI.A: (i) a topological θ-term associated with a quantum-Hall-type transition and (ii) a metallic phase, in view of broken spin-rotation invariance. Thus, generically, three phases are possible: metal, insulator, and quantized Hall conductor. A further striking feature of class D is that the type of disorder affects crucially the phase diagram. At the level of the σ-model, the reason is believed to be that the relevant target space has two disconnected pieces, and that, depending on the choice of the underlying microscopic model, it may or may not be necessary to consider configurations containing domain walls on which the σ-model field jumps between the two components (Bocquet *et al.*, 2000; Chalker *et al.*, 2002; Gruzberg *et al.*, 2005; Read and Ludwig, 2001). In the following we mainly concentrate on the Cho-Fisher (CF) network model (Cho and Fisher, 1997a) of the TQHE, which is generic in the sense that it displays all three possible phases. Other models of disorder will be briefly discussed in the end of Sec. VI.E.2.
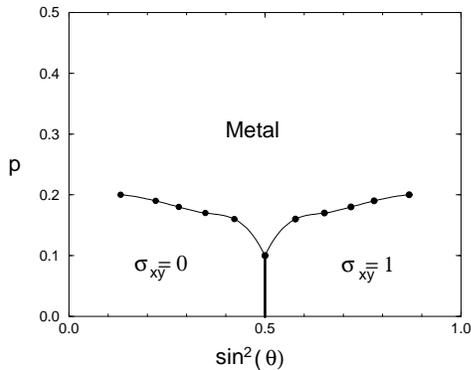
FIG. 35 Phase diagram of the Cho-Fisher model as obtained in (Chalker *et al.*, 2002) from transfer matrix calculations. The plane is spanned by the parameters $\sin^2\theta$, the interplaquette tunneling probability, and p, the concentration of vortex disorder: these control the short-distance values of the conductivity components σ_{xy} and σ_{xx} respectively.

2. Network model and phase diagram

To obtain a disordered network model of class D, one can start from the ordered network, Fig. 27, and then allow for independent fluctuations of the node parameters θ_i with some distribution function $\mathcal{P}(\theta)$. The CF model corresponds to the choice

$$\mathcal{P}(\theta) = (1-p)\delta(\theta-\theta_0)+\frac{p}{2}\delta(\theta+\theta_0)+\frac{p}{2}\delta(\theta+\theta_0-\pi), \quad (6.47)$$

implying that disorder is introduced as isolated defects by making the change $\theta \to -\theta$ or $\theta \to \pi - \theta$, for a subset of nodes randomly distributed with a concentration p. This amounts to flipping signs of either both $\sin\theta$ or both $\cos\theta$ associated with such a node. This procedure can be viewed as the insertion of two additional half-flux lines into two plaquettes adjacent to the node and belonging to the same sublattice. Note that the vortex pair appears with equal probability on the C- or S-sublattice. It is this feature that distinguishes the CF model from the random bond Ising model (RBIM) (Cho and Fisher, 1997a; Merz and Chalker, 2002), which is obtained if all the additional vortices are placed on the same sublattice.

The phase diagram of the CF model was established in Chalker *et al.* (2002), and it was found that all the three expected phases are indeed present, Fig. 35. The DOS in these phases and at transitions between them was studied in Mildenberger *et al.* (2007a), the results will be presented in Sec. VI.E.3, VI.E.4. It was also checked in Mildenberger *et al.* (2007a) that the CF model is indeed generic: the same behavior is obtained for a model with a Gaussian distribution $\mathcal{P}(\theta)$.

We briefly discuss now two other disorder models, with properties qualitatively different from the CF model:

(i) A fermionic version of the $\pm J$ RBIM is described by a disordered network model with (Chalker *et al.*, 2002;

Merz and Chalker, 2002; Read and Ludwig, 2001)

$$\mathcal{P}(\theta) = (1 - p)\delta(\theta - \theta_0) + p\delta(\theta + \theta_0). \quad (6.48)$$

This implies that all pairs of vortices are inserted in the same sublattice. It has been shown analytically (Read and Ludwig, 2001) and verified numerically (Chalker *et al.*, 2002) that the metallic phase is absent in the RBIM. Two phases with localized states (separated by the TQHE transition) correspond to the paramagnetic and ferromagnetic phases in the Ising spin language. The self-dual state of the disorder-free network ($p = 0$, $\sin^2\theta = 1/2$) maps onto the critical point of the clean Ising model.

(ii) The $O(1)$ model is obtained if one includes in the regular network factors (-1) for propagation along some links, randomly selected with a concentration p. The crucial feature of such a defect (that distinguishes it from the randomness in the nodal parameter such as the vortex pairs in the CF model and the RBIM) is that it cannot be "switched off" by any continuous transformation. Therefore, such a defect has the topological character of a vortex. It was found (Chalker *et al.*, 2002; Read and Ludwig, 2001) that such topological defects destroy completely the localization, so that the $O(1)$ model is always in the metallic phase. From the σ-model perspective, it was shown that the effect of vortices is in suppression of the second (disconnected) component of the target space (Bocquet *et al.*, 2000).

3. Thermal metal

The metallic phase can be treated analytically by using the σ-model approach. The corresponding RG analysis yields

$$dt/d\ln L = -t^2 , \quad (6.49)$$

where t is the running coupling constant inversely proportional to the dimensionless conductivity, $t = 1/\pi g$. The infrared behavior of the system is governed by the perfect-metal fixed point, $t \to 0$. Specifically, the conductance increases logarithmically with the system size, $g(L) = g_0 + (1/\pi)\ln L/\ell_0$ (ℓ_0 is the mean free path), justifying the perturbative RG. The RG equation for the second coupling constant ε, whose bare value is given by the energy E, reads

$$d\varepsilon/d\ln L = (2 + t)\varepsilon , \quad (6.50)$$

leading to a logarithmic increase of DOS (Bocquet *et al.*, 2000; Senthil and Fisher, 2000),

$$\rho(E) = \rho_0 + \frac{1}{4\pi^2 D} \ln \frac{D}{|E|\ell_0^2} , \quad (6.51)$$

where D is the diffusion constant (remaining unrenormalized to this order), $g_0 = 2\pi\rho_0 D$.
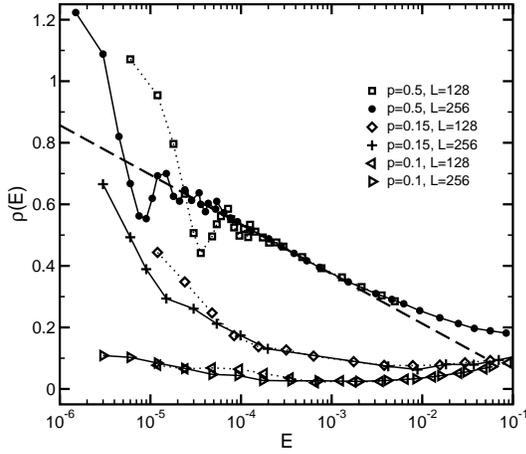
FIG. 36 Low-energy DOS in the metallic phase. Parameters (upper curves): p=0.5, $\alpha=\pi/4$, system sizes L=128 (squares) and L=256 (full circles). The straight dashed line represents the logarithmic asymptotics. For lowest energies the RMT oscillations are clearly visible; they can be collapsed on a single curve as shown in Fig. 37. For comparison, the results for $p = 0.15$ and $p = 0.1$ are also shown; the latter point is close to the expected boundary of the metallic phase, see Fig. 35. It is seen that when the system approaches the phase boundary, the logarithmic increase of the DOS disappears and the RMT oscillations get damped. (Mildenberger *et al.*, 2007a).

FIG. 37 Renormalized DOS at maximal disorder p=0.5 and on the symmetry line $\sin^2 \alpha$=1/2 for different system sizes vs. the energy measured in units of the level spacing δ_L. The RMT result, Eq. (6.53), is plotted as a dashed line for comparison. *Inset:* logarithmic dependence of $1/L^2\delta_L$ on the system size L, consistent with the data of Fig. 36. (Mildenberger *et al.*, 2007a).

Numerical results for the DOS in the metallic phase are shown in Fig. 36. The data exhibit a logarithmic increase of the DOS over almost three decades in E for the larger system size, L=256. It is worth stressing that the increase continues to be of logarithmic form even though the renormalized DOS at small energies becomes much larger than its bare (large-E) value $\rho_0 \simeq 0.1$. This is a signature of the fact that the RG flow is towards weak coupling, so that the one-loop result (6.51) is valid down to arbitrarily low energies in the thermodynamic limit.

At the smallest energies, pronounced oscillations in the DOS are observed. These are RMT oscillations due to finite system size and serve as another indication of the fact that we are dealing with a metallic phase. The RMT origin of these oscillations is demonstrated in Fig. 37, where these parts of DOS curves are replotted, with the energy rescaled to the mean level spacing δ_L at lowest energy for the corresponding system size. The data collapse on a single curve, which shows that the renormalized level spacing

$$\delta_L = \frac{1}{L^2\rho(E_{\rm Th})} = \frac{1}{L^2\rho_0[1 + t_0 \ln(L/\ell_0)]}, \qquad (6.52)$$

with $E_{\rm Th}$ being the Thouless energy, is indeed the only relevant energy scale in the regime $E \lesssim E_{\rm Th}$ where the RMT is applicable. As further seen in Fig. 37, the obtained curve agrees with the RMT prediction,

$$\rho(E) = \frac{1}{L^2\delta_L} \left[1 + \frac{\sin(2\pi E/\delta_L)}{2\pi E/\delta_L} \right], \qquad (6.53)$$

up to $E/\delta_L \sim$1.5–2; for larger energies the oscillations are strongly suppressed. This is fully consistent with the exponential vanishing of the RMT oscillations beyond the Thouless energy, see the review (Mirlin, 2000b). With increasing system size, the ratio $E_{\rm Th}/\delta_L$ increases (though only logarithmically), so that the RMT range includes progressively more oscillation periods. This tendency is clearly seen in Fig. 37.

4. Localized phases and TQH transition

An analytical approach to the problem alternative to the σ-model is based on the model of Dirac fermions with random mass, in the spirit of the analysis of the Ising model in Dotsenko and Dotsenko (1983). Being perturbative in the disorder strength, this approach is appropriate for the description of the localized phases and the transition between them. The disorder-free system has a transition, driven by tuning a uniform mass through zero, which in the CF model lies at p=0, $\sin^2 \theta$=1/2 and corresponds to the clean Ising transition. In the vicinity of the clean fixed point representing this transition the disorder strength g_M is marginally irrelevant. This implies for the critical DOS a logarithmic correction term of the form (Bocquet *et al.*, 2000; Mildenberger *et al.*, 2007a)

$$\rho(E) = \frac{|E|}{2\pi} \left(1 + \frac{2g_M}{\pi} \ln \frac{1}{|E|} \right). \qquad (6.54)$$

Slightly away from the critical value $\theta = \pi/4$, the system is in a localized phase with a large localization length $\xi \propto |\theta - \pi/4|^{-\nu}$. As the RG flow is towards the clean

Ising fixed point, the corresponding index should be the same as in the Ising model, $\nu = 1$. The behavior of the DOS in the localized phases can be also understood using the Dirac fermion RG (Mildenberger *et al.*, 2007a). Specifically, for energies that are not too small, behavior will be the same as at criticality, Eq. (6.54). However, for smallest energies, it is the localization length ξ (rather than E) that will terminate the RG process. In this sense, the role of ξ is fully analogous to that of finite system size L at criticality. This implies that $\rho(E)$ saturates at the value

$$\rho(E) \sim \frac{\ell_0}{\xi}\left(1 + 2\frac{g_M}{\pi}\ln\frac{\xi}{\ell_0}\right)^{1/2}, \qquad E \lesssim E_\xi, \quad (6.55)$$

The energy E_ξ at which the saturation takes place is

$$E_\xi \sim \frac{\ell_0}{\xi}\left(1 + 2\frac{g_M}{\pi}\ln\frac{\xi}{\ell_0}\right)^{-1/2}. \qquad (6.56)$$

The Anderson transition from the metallic to one of the localized phases should therefore be signalled by a transition from logarithmically diverging to finite $\rho(E \to 0)$. This has been verified by numerical simulations in Mildenberger *et al.* (2007a), Fig. 38.

A brief comment on the regions of localized phases where the interplaquette coupling is very weak ($\sin^2\theta$ close to zero or to unity), is in order here. As shown recently (Mildenberger *et al.*, 2006), in this situation the DOS of the RBIM acquires a non-universal power-law singularity, $|E|^{1/z-1}$ with $z > 1$ associated with Griffiths strings (Motrunich *et al.*, 2001, 2002). The same mechanism of the formation of divergent DOS in these parts of the localized phases is expected to be operative in the CF model as well.

We turn now to numerical results (Mildenberger *et al.*, 2007a) on the DOS at the line $\sin^2\theta = 1/2$, where the TQH phase boundary is located. They are shown in Fig. 39. While at sufficiently large p ($p \gtrsim 0.1$) the DOS shows a logarithmic increase characteristic for the metallic phase, for lower p the DOS behavior agrees with Eq. (6.54), as expected for the TQH transition. This is demonstrated in the inset of Fig. 39, where $\rho(E)/|E|$ as a function of $\log|E|$ is plotted for $p = 0.05$.

While at moderately low E the DOS at the TQH transition line is in good agreement with the Dirac-fermion RG, Eq. (6.54), the results for the lowest energies obtained in Mildenberger *et al.* (2007a) constitute a puzzle. Specifically, it was found that the DOS saturates at a very low energy scale and even shows a weak upturn. The reason for this behavior is not understood at present; several possible scenarios were proposed in Mildenberger *et al.* (2007a): (i) the position p_T of the tricritical point T is in fact not $p_T \simeq 0.1$ as in Fig. 35 but rather considerably smaller, $p_T < 0.05$; (ii) in addition to the tricritical point p_T there is a second, repulsive fixed point on the TQH transition line $\sin^2\theta = 1/2$, at some $p_N < p_T$. This point would then act as a "flow splitter" which is similar to the role of the Nishimori point in the RBIM; (iii) the
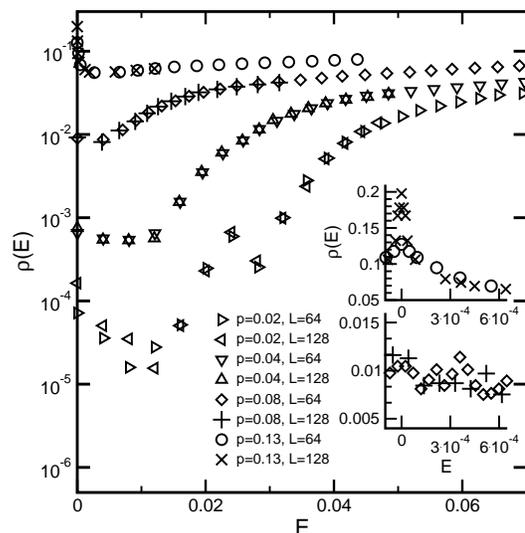

FIG. 38 DOS near $E = 0$ for disorder values $p = 0.13, 0.08, 0.04$, and 0.02 and for two system sizes $L = 64, 128$ at fixed interplaquette coupling $\sin^2(\theta) = 0.579$. The DOS diverges logarithmically as $E \to 0$ in the metallic phase ($p = 0.13$) and remains finite in the localized phase (other values of p). The results for the lowest impurity concentration, $p = 0.02$, show an oscillatory feature induced by the band structure of the clean system, as well strong scatter in the data at the lowest energies, which is due to insufficient ensemble averaging. *Upper inset:* Low-energy peak at $p = 0.13$; its amplitude increases with L, in agreement with Sec. III.A. *Lower inset:* Low-energy DOS at $p = 0.08$. No peak at $E \to 0$ is detected; $\rho(E \to 0)$ is a constant independent on L, indicating that the system is in the insulating phase. Statistical noise in the lower inset is more pronounced than in the upper one due to the smallness of the DOS. (Mildenberger *et al.*, 2007a).

RG treatment of the theory of Dirac fermions with Gaussian random mass is in fact insufficient, and some effects – possibly of non-perturbative origin – eventually drive the system away from the clean Ising fixed point. The clarification of this important issue remains a subject for future research.

F. Chiral classes (AIII, CII, BDI)

We have seen in Sec. V.E that quasi-1D systems of chiral symmetry show a criticality accompanied by a very slow ($L^{-1/2}$) decay of the average conductance and by a Dyson-type singularity ($1/|E\ln^3 E|$) in the DOS. As we discuss in the present subsection, a similar type of criticality takes place also in two dimensions.

1. Gade-Wegner σ-model

In their pioneering works, Gade (1993); Gade and Wegner (1991) derived σ-models for systems of the chiral classes and performed their RG analysis at and near two dimensions. They used the
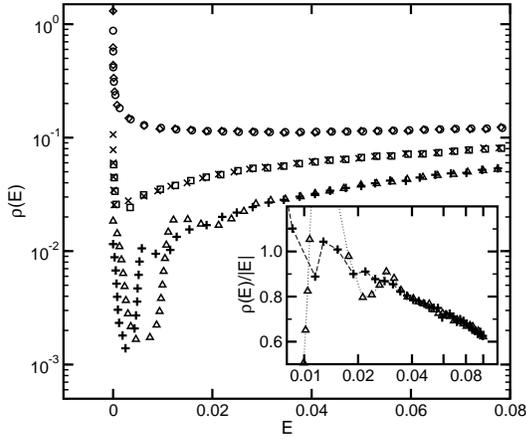
FIG. 39 DOS at low energy on the self-dual line $\sin^2(\alpha) = 0.5$ for disorder concentrations $p = 0.2$ ($\circ$, $\diamond$), 0.1 ($\square$, x), and 0.05 ($\triangle$, +), where in each case the first symbol is for $L = 128$ and the second is for $L = 256$. *Inset:* $\rho(E)/|E|$ at $p=0.05$ on a log-linear scale. The logarithmic correction is clearly observed, in agreement with Eq. (6.54). (Mildenberger *et al.*, 2007a).

fermionic replicas, so that the models are defined on the spaces U(N), U($2N$)/Sp($2N$), and U(N)/O(N) for the chiral unitary, orthogonal and symplectic classes, respectively. As usual, the supersymmetric generalization (see Table I for the symmetry classes of the corresponding models) is equivalent to the replica version on the level of the perturbation theory. For definiteness, we consider the chiral unitary class (AIII), the results for the other two are very similar. The action of the σ-model has the form

$$S[Q] = \int d^2 r \left\{ \frac{1}{16\pi t} \mathrm{Tr} \nabla Q^{-1} \nabla Q - \frac{1}{64\pi c} [\mathrm{Tr}(Q^{-1} \nabla Q)]^2 \right.$$
$$\left. + i \frac{\pi \rho_0}{4} \varepsilon \mathrm{Tr}(Q + Q^{-1}) \right\}, \qquad (6.57)$$

where $Q \in$ U(N), t and c are two coupling constants, the first of which is related to the conductivity in the usual way, $t^{-1} = 2\pi\sigma_{xx}$, ε is the running coupling whose bare value is the energy E (which breaks the chiral symmetry), and ρ_0 the bare density of states. A special feature of the σ-model for chiral classes is the existence of the second term (known as Gade term), which governs fluctuations of $\det Q$. This σ-model was later obtained and analyzed in a number of works (Altland and Simons, 1999; Fabrizio and Castellani, 2000; Fukui, 1999; Guruswamy *et al.*, 2000).

The one-loop RG equations in $2 + \epsilon$ dimensions read

$$-dt/\ln L = \epsilon t \qquad \text{(exact!)} ; \qquad (6.58)$$
$$-dc/d\ln L = \epsilon c + 2c^2 ; \qquad (6.59)$$
$$d\ln\varepsilon/d\ln L = (2+\epsilon) + t^2/2c . \qquad (6.60)$$

It is of central importance that in 2D ($\epsilon = 0$) the β-function (6.58) is identically zero (Gade and Wegner,

1991), i.e. the coupling constant t (and thus, the conductivity) is not renormalized. If one considers a system at non-zero (but small) energy, the chiral symmetry is broken down to that of the unitary Wigner-Dyson class (A), and the localization should happen at a sufficiently large scale. To find the scaling of the localization length with energy, one performs the RG transformation until the running energy $\varepsilon(L)$ ceases to be small (i.e. reaches a characteristic scale Δ of the problem; typically, the bandwidth). Beyond this scale, the RG takes the form characteristic for class A, driving the system towards the localized regime. The localization length $\xi(E)$ is thus given by the crossover length $L_c(E)$, up to an energy-independent factor $\sim \exp(-1/4t^2)$. Further, the DOS is given by

$$\rho(E) \sim 1/E L_c^2(E). \qquad (6.61)$$

Integration of Eqs. (6.59), (6.60) (with $\epsilon = 0$) yields

$$\ln L_c(E) \simeq \frac{1}{2t^2} \left(\sqrt{B^2 + 4t^2|\ln(E/\Delta)|} - B \right) , \quad (6.62)$$

where $B = 2 + t^2/c_0$ and c_0 is the bare value of the coupling c. For asymptotically low energies, $|\ln(E/\Delta)| \gg B^2/4t^2$, this reduces to

$$\xi(E) \propto \exp\left(t^{-1}|\ln(E/\Delta)|^{1/2}\right) , \qquad (6.63)$$
$$\rho(E) \propto E^{-1} \exp\left(-2t^{-1}|\ln(E/\Delta)|^{1/2}\right) . \quad (6.64)$$

The last formula is the 2D counterpart of the Dyson singularity. On the other hand, at intermediate energies, $|\ln(E/\Delta)| \ll B^2/4t^2$, the behavior is of the power-law type with a non-universal exponent,

$$\xi(E) \propto E^{-1/B} ; \qquad \rho(E) \propto E^{-1+2/B} . \qquad (6.65)$$

It is worth emphasizing that the bare coupling c_0 is of the order of unity even for a system with large conductance ($t \ll 1$). This means that $B \simeq 2$ and the asymptotic behavior (6.63), (6.64) establishes at exponentially low energies only, $\ln(\Delta/E) \ll 1/t^2$. For this reason it is very difficult to reach the true asymptotics in numerical simulations, whereras the intermediate power law regime (6.65) can be studied very well, see e.g. Markos and Schweitzer (2007).

Like in the 1D geometry, one can drive the system away from criticality by introducing a staggering in hopping strength ("dimerization") in a lattice model. The DOS in the localized phase was predicted to show a power-law behavior, $\rho(E) \sim E^{-1+2/z}$, governed by the Griffiths mechanism, with a non-universal dynamical exponent $z > 0$ (Motrunich *et al.*, 2002). In the work (Bocquet and Chalker, 2003) network models for all the chiral classes were constructed. A numerical study of the class-AIII network model confirmed the existence of the critical (Gade-Wegner) and the localized (Griffiths-type) phases. It was found that the DOS exhibits a non-universal $E^{-1+2/z}$ power-law behavior in the localized

2. Dirac fermions approach. Strong-coupling effects

The Gade-Wegner prediction of a critical state with a diverging DOS of the form (6.64) can also be reproduced by starting form a model of disordered Dirac fermions (Guruswamy *et al.*, 2000). Specifically, a model of fermions on a bipartite lattice with π flux and random real hopping (Hatsugai *et al.*, 1997), which belongs to the class BDI, is described by a two-flavor model of Dirac fermions subject to a random vector potential (coupling g_A) and a chiral random mass (g_m). This is a particular type of two-flavor disordered Dirac fermion models considered in Sec. VI.G.4; in the notations used there $g_A = \gamma_\perp/2$, $g_m = \beta_z/2$. For this model, the exact β-functions can be found (Guruswamy *et al.*, 2000) to all orders in g_m:

$$\frac{dg_A}{d\ln L} = \frac{2g_m^2}{(1+2g_m)^2}, \qquad \frac{dg_m}{d\ln L} = 0 \ . \tag{6.66}$$

Further, the dynamical scaling function was found to be

$$\frac{d\ln\varepsilon}{d\ln L} \equiv z = 1 + \frac{2g_A}{(1+2g_m)^2} + 2g_m + O(g_m^2) \ . \tag{6.67}$$

According to Eqs. (6.66), g_m is not renormalized, while g_A grows logarithmically with L. Assuming for simplicity weak disorder, $g_m \ll 1$, we have

$$g_A(L) \simeq g_A^{(0)} + 4g_m^2 \ln L \ . \tag{6.68}$$

For sufficiently large L the $\ln L$ term dominates. Substituting it in Eq. (6.67), one gets

$$\ln\varepsilon(L) \simeq 2g_m^2 \ln^2 L \ . \tag{6.69}$$

This reproduces Eqs. (6.63), (6.64) for the localization length and the DOS with $t \to g_m\sqrt{2}$.

As was shown in Motrunich *et al.* (2002), this result is, however, not fully correct, for the following reason. It is known that the multifractal spectrum of Dirac fermions in a random vector potential undergoes a transition from a weak-disorder to strong-disorder phase at $g_A = 1$ ("freezing transition"), see Sec. VI.G.3. As shown in Horovitz and LeDoussal (2002); Motrunich *et al.* (2002), this transition is accompanied by a change of the behavior of the dynamical exponent

$$z = \begin{cases} 1 + 2g_A \ , & g_A < 1 \ ; \\ 4\sqrt{g_A} - 1 \ , & g_A > 1 \ . \end{cases} \tag{6.70}$$

In the presence of the second coupling (g_m), $g_A(L)$ will flow according to (6.68), and z will develop following Eq. (6.70). While the first line of (6.70) agrees with

Eq. (6.67), it is only valid at short distances, $g_A(L) < 1$ (which corresponds to the ballistic regime). At sufficiently long (diffusive) scale, where the σ-model is applicable, g_A will become larger than unity. Using the second line of Eq. (6.70) instead of Eq. (6.67) yields

$$\rho(E) \sim E^{-1} \exp\left\{-\frac{1}{2}(3g_m^{-1}|\ln(E/\Delta)|)^{2/3}\right\} \ . \tag{6.71}$$

Therefore, the exponent $1/2$ in (6.63) and in the second (subleading) factor in (6.64) is replaced by $2/3$.

This result was also rederived in the framework of the RG approach. The key point is that, when the running coupling g_A ceases to be weak, it is not sufficient anymore to characterize the disorder by the lowest-order cumulants. Instead, one should take into account an infinite number of couplings. Such a functional RG method was developed in Carpentier and LeDoussal (1999) in the context of a related random XY model. For the problem of Dirac fermions with random mass and vector potential this program was carried out in Mudry *et al.* (2003): the results confirm the conclusion of Motrunich *et al.* (2002), Eq. (6.64). Analogous results were also obtained in Yamada and Fukui (2004).

G. Disordered Dirac Hamiltonians

Localization and criticality in models of 2D Dirac fermions subjected to various types of disorder have been studied in a large number of papers and in a variety of contexts, including the random bond Ising model (Dotsenko and Dotsenko, 1983), the quantum Hall effect (Ludwig *et al.*, 1994), dirty superconductors with unconventional pairing (Altland *et al.*, 2002; Bocquet *et al.*, 2000; Nersesyan *et al.*, 1995), and some lattice models with chiral symmetry (Guruswamy *et al.*, 2000). Recently, this class of problems has attracted a great deal of attention in connection with its application to graphene, see, in particular, Aleiner and Efetov (2006); Altland (2007); Khveshchenko (2006); McCann *et al.* (2006); Ostrovsky *et al.* (2006, 2007a,b).

In the presence of different types of randomness, Dirac Hamiltonians realize all ten symmetry classes of disordered systems; see (Bernard and LeClair, 2002a) for a detailed symmetry classification. Furthermore, in many cases the Dirac character of fermions induces non-trivial topological properties (θ-term or WZ term) of the corresponding field theory (σ-model). In Sec. VI.G.1 we review the classification of disorder in a two-flavor model of Dirac fermions describing the low-energy physics of graphene, the RG treatment of the problem, and types of criticality. The emergent critical theories will be discussed in Sec. VI.G.2–VI.G.4. In Sec. VI.G.5 we briefly discuss a four-node Dirac fermion model appropriate for a description of dirty d-wave superconductors.

1. Disordered two-node Dirac Hamiltonians: Symmetries of disorder, renormalization group, and types of criticality.

The presentation below largely follows the papers (Ostrovsky *et al.*, 2006, 2007b). We concentrate on a two-flavor model, which is in particular relevant to the description of electronic properties of graphene. Graphene is a semimetal; its valence and conduction bands touch each other in two conical points K and K' of the Brillouin zone. In the vicinity of these points the electrons behave as massless relativistic (Dirac-like) particles. Therefore, the effective tight-binding low-energy Hamiltonian of clean graphene is a 4×4 matrix operating in the AB space of the two sublattices and in the K–K' space of the valleys. We introduce the four-component wave function

$$\Psi = \{\phi_{AK}, \phi_{BK}, \phi_{BK'}, \phi_{AK'}\}^T , \qquad (6.72)$$

In this representation the Hamiltonian has the form

$$H = v_0 \tau_3 \boldsymbol{\sigma} \mathbf{k}. \qquad (6.73)$$

Here τ_3 is the third Pauli matrix in the K–K' space, $\boldsymbol{\sigma} = \{\sigma_1, \sigma_2\}$ the two-dimensional vector of Pauli matrices in the AB space, and v_0 the velocity ($v_0 \simeq 10^8$ cm/s in graphene). It is worth emphasizing that the Dirac form of the Hamiltonian (6.73) does not rely on the tight-binding approximation but is protected by the symmetry of the honeycomb lattice which has two atoms in a unit cell.

Let us analyze the symmetries of the clean Hamiltonian (6.73) in the AB and KK' spaces. First, there exists an SU(2) symmetry group in the space of the valleys , with the generators (McCann *et al.*, 2006)

$$\Lambda_x = \sigma_3 \tau_1, \qquad \Lambda_y = \sigma_3 \tau_2, \qquad \Lambda_z = \sigma_0 \tau_3 , \qquad (6.74)$$

all of which commute with the Hamiltonian. Second, there are two more relevant symmetries of the clean Hamiltonian, namely, time inversion operation (T_0) and chiral symmetry (C_0). Combining T_0, C_0, and isospin rotations $\Lambda_{0,x,y,z}$, one can construct twelve symmetry operations, out of which four (denoted as T_μ) are of time-reversal type, four (C_μ) of chiral type, and four (CT_μ) of Bogoliubov-de Gennes type:

$$
\begin{aligned}
T_0: \ & A \mapsto \sigma_1 \tau_1 A^T \sigma_1 \tau_1, & C_0: \ & A \mapsto -\sigma_3 \tau_0 A \sigma_3 \tau_0, \\
& CT_0: \ A \mapsto -\sigma_2 \tau_1 A^T \sigma_2 \tau_1, \\
T_x: \ & A \mapsto \sigma_2 \tau_0 A^T \sigma_2 \tau_0, & C_x: \ & A \mapsto -\sigma_0 \tau_1 A \sigma_0 \tau_1, \\
& CT_x: \ A \mapsto -\sigma_1 \tau_0 A^T \sigma_1 \tau_0, \\
T_y: \ & A \mapsto \sigma_2 \tau_3 A^T \sigma_2 \tau_3, & C_y: \ & A \mapsto -\sigma_0 \tau_2 A \sigma_0 \tau_2, \\
& CT_y: \ A \mapsto -\sigma_1 \tau_3 A^T \sigma_1 \tau_3, \\
T_z: \ & A \mapsto \sigma_1 \tau_2 A^T \sigma_1 \tau_2, & C_z: \ & A \mapsto -\sigma_3 \tau_3 A \sigma_3 \tau_3, \\
& CT_z: \ A \mapsto -\sigma_2 \tau_2 A^T \sigma_2 \tau_2.
\end{aligned}
$$

It is worth recalling that the C and CT symmetries apply to the Dirac point ($E = 0$), i.e. to undoped graphene, and get broken by a non-zero energy E. We will assume

the average isotropy of the disordered graphene, which implies that Λ_x and Λ_y symmetries of the Hamiltonian are present or absent simultaneously. They are thus combined into a single notation $\Lambda_\perp$; the same applies to $T_\perp$ and $C_\perp$. In Table V all possible matrix structures of disorder along with their symmetries are listed.

To derive the field theory of the problem, one introduces a superfield $\psi(\mathbf{r})$, see Sec. II.B.1 (or, alternatively, its replica counterpart). After the disorder averaging, the action containing all possible disorder structures from Table V reads ($\bar{\psi} = \psi^\dagger \Lambda$)

$$
\begin{aligned}
S[\psi] = & \int d^2 r \Big\{ i\bar{\psi} (\varepsilon + i v_0 \tau_3 \boldsymbol{\sigma} \nabla - i 0 \Lambda) \psi \\
& + \pi v_0^2 \Big\{ \alpha_0 (\bar{\psi}\sigma_0\tau_0\psi)^2 + \frac{\alpha_\perp}{2} \left[(\bar{\psi}\sigma_1\tau_3\psi)^2 + (\bar{\psi}\sigma_2\tau_3\psi)^2 \right] \\
& + \alpha_z (\bar{\psi}\sigma_3\tau_0\psi)^2 + \frac{\beta_0}{2} \left[(\bar{\psi}\sigma_3\tau_1\psi)^2 + (\bar{\psi}\sigma_3\tau_2\psi)^2 \right] \\
& + \frac{\beta_\perp}{4} \left[(\bar{\psi}\sigma_1\tau_1\psi)^2 + (\bar{\psi}\sigma_1\tau_2\psi)^2 + (\bar{\psi}\sigma_2\tau_1\psi)^2 + (\bar{\psi}\sigma_2\tau_2\psi)^2 \right] \\
& + \frac{\beta_z}{2} \left[(\bar{\psi}\sigma_0\tau_1\psi)^2 + (\bar{\psi}\sigma_0\tau_2\psi)^2 \right] + \gamma_0 (\bar{\psi}\sigma_0\tau_3\psi)^2 \\
& + \frac{\gamma_\perp}{2} \left[(\bar{\psi}\sigma_1\tau_0\psi)^2 + (\bar{\psi}\sigma_2\tau_0\psi)^2 \right] + \gamma_z (\bar{\psi}\sigma_3\tau_3\psi)^2 \Big\} \Big\}.
\end{aligned}
$$
$$(6.75)$$

A complete set of one-loop perturbative RG equations for nine disorder amplitudes has the form (Ostrovsky *et al.*, 2006)

$$
\begin{aligned}
\frac{d\alpha_0}{d\ln L} &= 2\alpha_0(\alpha_0 + \beta_0 + \gamma_0 + \alpha_\perp + \beta_\perp + \gamma_\perp \\
&\quad + \alpha_z + \beta_z + \gamma_z) 2\alpha_\perp\alpha_z + \beta_\perp\beta_z + 2\gamma_\perp\gamma_z; \\
\frac{d\alpha_\perp}{d\ln L} &= 2(2\alpha_0\alpha_z + \beta_0\beta_z + 2\gamma_0\gamma_z); \\
\frac{d\alpha_z}{d\ln L} &= -2\alpha_z(\alpha_0 + \beta_0 + \gamma_0 - \alpha_\perp - \beta_\perp - \gamma_\perp \\
&\quad + \alpha_z + \beta_z + \gamma_z) + 2\alpha_0\alpha_\perp + \beta_0\beta_\perp + 2\gamma_0\gamma_\perp; \\
\frac{d\beta_0}{d\ln L} &= 2[\beta_0(\alpha_0 - \gamma_0 + \alpha_\perp + \alpha_z - \gamma_z) \\
&\quad + \alpha_\perp\beta_z + \alpha_z\beta_\perp + \beta_\perp\gamma_0]; \\
\frac{d\beta_\perp}{d\ln L} &= 4(\alpha_0\beta_z + \alpha_z\beta_0 + \beta_0\gamma_0 + \beta_\perp\gamma_\perp + \beta_z\gamma_z); \\
\frac{d\beta_z}{d\ln L} &= 2[-\beta_z(\alpha_0 - \gamma_0 - \alpha_\perp + \alpha_z - \gamma_z) \\
&\quad + \alpha_0\beta_\perp + \alpha_\perp\beta_0 + \beta_\perp\gamma_z]; \\
\frac{d\gamma_0}{d\ln L} &= 2\gamma_0(\alpha_0 - \beta_0 + \gamma_0 + \alpha_\perp - \beta_\perp + \gamma_\perp \\
&\quad + \alpha_z - \beta_z + \gamma_z) + 2\alpha_\perp\gamma_z + 2\alpha_z\gamma_\perp + \beta_0\beta_\perp; \\
\frac{d\gamma_\perp}{d\ln L} &= 4\alpha_0\gamma_z + 4\alpha_z\gamma_0 + \beta_0^2 + \beta_\perp^2 + \beta_z^2; \\
\frac{d\gamma_z}{d\ln L} &= -2\gamma_z(\alpha_0 - \alpha_\perp + \alpha_z - \beta_0 + \beta_\perp - \beta_z + \gamma_0 \\
&\quad - \gamma_\perp + \gamma_z) + 2\alpha_0\gamma_\perp + 2\alpha_\perp\gamma_0 + \beta_\perp\beta_z. \quad (6.76)
\end{aligned}
$$

The RG equation for the running energy ε (whose bare

structure	coupling	AE	GLL	$\Lambda_\perp$	Λ_z	T_0	$T_\perp$	T_z	C_0	$C_\perp$	C_z	CT_0	$CT_\perp$	CT_z
$\sigma_0\tau_0$	α_0	$\gamma_0/2\pi v^2$		+	+	+	+	+	−	−	−	−	−	−
$\sigma_{\{1,2\}}\tau_{\{1,2\}}$	$\beta_\perp$	$2\beta_\perp/\pi v^2$		−	−	+	−	−	+	−	−	+	−	−
$\sigma_{1,2}\tau_0$	$\gamma_\perp$	$\gamma_\perp/\pi v^2$	$2g_A$	−	+	+	−	+	+	−	+	+	−	+
$\sigma_0\tau_{1,2}$	β_z	$\beta_z/\pi v^2$	$2g_m$	−	−	+	−	−	−	−	+	−	−	+
$\sigma_3\tau_3$	γ_z	$\gamma_z/2\pi v^2$		−	+	+	−	+	−	+	−	−	+	−
$\sigma_3\tau_{1,2}$	β_0		$2g_\mu$	−	−	−	−	+	−	−	+	+	−	−
$\sigma_0\tau_3$	γ_0			−	+	−	+	−	−	+	−	+	−	+
$\sigma_{1,2}\tau_3$	$\alpha_\perp$		$2g_{A'}$	+	+	−	−	−	+	+	+	−	−	−
$\sigma_3\tau_0$	α_z			+	+	−	−	−	−	−	−	+	+	+

TABLE V Disorder symmetries in graphene. The first five rows of the table represent disorders preserving the time reversal symmetry T_0; the last four — violating T_0. First column: structure of disorder in the sublattice (σ_μ) and valley (τ_ν) spaces. Second column: disorder strength according to the notations of (Ostrovsky *et al.*, 2006, 2007b) used in this review. Third (AE) and fourth (GLL) columns: disorders considered in (Aleiner and Efetov, 2006) and (Guruswamy *et al.*, 2000) and notations used there. The remaining columns indicate which symmetries of the clean Hamiltonian are preserved by disorder. (Ostrovsky *et al.*, 2006).

value is E) reads

$$\frac{d\ln\varepsilon}{d\ln L} = 1 + \alpha_0 + \beta_0 + \gamma_0 + \alpha_\perp + \beta_\perp + \gamma_\perp$$
$$+\alpha_z + \beta_z + \gamma_z . \qquad (6.77)$$

If all types of disorder are present (i.e. no symmetries is preserved), the RG flow is towards the conventional localization fixed point (unitary Wigner-Dyson class A). If the only preserved symmetry is the time reversal (T_0), again the conventional localization (orthogonal Wigner-Dyson class AI) takes place (Aleiner and Efetov, 2006). A non-trivial situation occurs if either (i) one of chiral symmetries is preserved or (ii) the valleys remain decoupled. In the Table VI we list those situations when the symmetry prevents the localization and leads to criticality and non-zero conductivity at $E = 0$ (in the case of decoupled nodes – also at nonzero E). Models with decoupled nodes will be analyzed in Sec. VI.G.2, and models with a chiral symmetry in Sec. VI.G.3 (C_0-chirality) and Sec. VI.G.4 (C_z-chirality).

2. Decoupled nodes: Disordered single-flavor Dirac fermions and quantum-Hall-type criticality

If the disorder is of long-range character, the valley mixing is absent due to the lack of scattering with large momentum transfer. The couplings that do not mix the valleys are α_0, $\alpha_\perp$, α_z, γ_0, $\gamma_\perp$, and γ_z. For each of the nodes, the system can then be described in terms of a single-flavor Dirac Hamiltonian,

$$H = v_0[\boldsymbol{\sigma}\mathbf{k} + \sigma_\mu V_\mu(\mathbf{r})]. \qquad (6.78)$$

Here disorder includes random scalar (V_0) and vector ($V_{1,2}$) potentials and random mass (V_3). The corresponding couplings are $g_V = \alpha_0 + \gamma_0$, $2g_A = \alpha_\perp + \gamma_\perp$,

and $\tilde{g}_m = \alpha_z + \gamma_z$ [11]. The clean single-valley Hamiltonian (6.78) obeys the effective time-reversal invariance $H = \sigma_2 H^T \sigma_2$. This symmetry ($T_\perp$) is not the physical time-reversal symmetry (T_0): the latter interchanges the nodes and is of no significance in the absence of internode scattering. The RG equations have the form

$$dg_A/d\ln L = 2g_V\tilde{g}_m ; \qquad (6.79)$$
$$dg_V/d\ln L = 2(2g_A + g_V)(g_V + \tilde{g}_m) ; \qquad (6.80)$$
$$d\tilde{g}_m/d\ln L = 2(2g_A - \tilde{g}_m)(g_V + \tilde{g}_m) ; \qquad (6.81)$$
$$d\ln\varepsilon/d\ln L = 1 + 2g_A + \tilde{g}_m + g_V . \qquad (6.82)$$

Remarkably, single-flavor Dirac fermions are never in the conventional localized phase! More specifically, depending on which of the disorders are present, four different types of criticality take place:

(i) The only disorder is the random vector potential (g_A). This is a special case of the symmetry class AIII. This problem is exactly solvable and has been studied in a great detail; we will discuss it in Sec. VI.G.3.

(ii) Only random mass ($\tilde{g}_m$) is present. The system belongs then to class D. The random-mass disorder is marginally irrelevant, and the system flows under RG towards the clean fixed point. This problem has been analyzed in Sec. VI.E.3.

(iii) The only disorder is random scalar potential (g_V). The system is then in the Wigner-Dyson symplectic (AII) symmetry class. As was found in Ostrovsky *et al.* (2007a), the corresponding σ-model contains a topological term with $\theta = \pi$, which leads to delocalization. This model has been discussed in Sec. VI.B.5.

---

[11] (i) The tilde in $\tilde{g}_m$ serves to distinguish it from the "chiral random mass" coupling g_m, see Table V and Sec. VI.F.2, VI.G.4; (ii) our couplings are related to those of Ludwig *et al.* (1994) via $g_A = \Delta_A/2\pi$, $g_V = \Delta_V/2\pi$, $\tilde{g}_m = \Delta_m/2\pi$.

Symmetries	Class	Criticality	Conductivity
C_z, T_0	BDI	Gade	$\approx 4e^2/\pi h$
C_z	AIII	Gade	$\approx 4e^2/\pi h$
C_z, T_z	CII	Gade	$\approx 4e^2/\pi h$
C_0, T_0	CI	WZW	$4e^2/\pi h$
C_0	AIII	WZW	$4e^2/\pi h$
Λ_z, C_0	2×AIII	WZW	$4e^2/\pi h$
$\Lambda_z, T_\perp$	2×AII	$\theta = \pi$	$4\sigma_{Sp}^{**}$ or ∞ (?)
$\Lambda_z, CT_\perp$	2×D	$\theta = \pi$	$4e^2/\pi h$
Λ_z	2×A	$\theta = \pi$	$4\sigma_U^*$

TABLE VI Possible types of disorder in graphene leading to criticality.[a] First column: preserved symmetries. Second column: symmetry class. Third column: type of criticality. The first three row correspond to C_z chiral symmetry leading to Gade-Wegner-type criticality, Sec. VI.G.4. The next three rows contain models with C_0 chiral symmetry (random gauge fields), inducing a WZ term in the σ-model action, Sec. VI.G.3. The last four rows correspond to the case of decoupled valleys (long-range disorder), see Sec. VI.G.2; from top to bottom: random vector potential, scalar potential, mass, and any of their combinations. For these models (except for the random vector potential, which is C_0 chiral at the same time) the σ-model acquires a topological term with $\theta = \pi$. Adapted from (Ostrovsky et al., 2007b).

[a]A further possible mechanism of delocalization is generation of the metallic phase due to broken spin- (or isospin-) rotation invariance, Sec. VI.A.1. If the only preserved symmetry is T_z, the system is in class AII, while if only CT_0 or CT_z invariance is preserved the system belongs to class D. (No topological term arises in these situations.) In both these classes, the system flows towards a perfect-metal fixed point if the bare conductivity is above the localization threshold.

(iv) At least two types of randomness are present. This is the same as to say that all of them are present, as the third one will be generated by RG, see Eqs. (6.79)–(6.81). The model belongs to the Wigner-Dyson unitary class A, and it was argued in Ludwig et al. (1994) that it flows into the IQH transition fixed point. This is confirmed by the derivation of the corresponding σ-model (Altland et al., 2002; Ostrovsky et al., 2007a,b), which contains a topological term with $\theta = \pi$, i.e. is nothing but the Pruisken σ-model at criticality. A particular consequence of this is that the conductivity of graphene with this type of disorder is equal to the value σ_U^* of the longitudinal conductivity σ_{xx} at the critical point of the IQH transition multiplied by four (because of spin and valleys). Note that the conclusion of IQH criticality formally holds for arbitrary energy ε, although in reality it only works near half-filling; for other ε the critical point would only be approached for unrealistic system sizes and temperatures.

If a uniform transverse magnetic field is applied, the topological angle θ becomes energy-dependent. However, at the Dirac point ($E = 0$), where $\sigma_{xy} = 0$, its value remains unchanged, $\theta = \pi$. This implies the emergence of the half-integer quantum Hall effect, with a plateau transition point at $E = 0$.

3. Preserved C_0 chirality: Random abelian and non-abelian vector potentials

a. Generalities. Let us consider a type of disorder which preserves the C_0-chirality, $H = -\sigma_3 H \sigma_3$; according to the Table V, the corresponding couplings are $\alpha_\perp$, $\beta_\perp$, and $\gamma_\perp$. The one-loop RG equations then read

$$\partial \alpha_\perp / \partial \log L = 0, \tag{6.83}$$

$$\partial \beta_\perp / \partial \log L = 4 \beta_\perp \gamma_\perp, \tag{6.84}$$

$$\partial \gamma_\perp / \partial \log L = \beta_\perp^2 . \tag{6.85}$$

The specifics of the C_0-chirality is that it corresponds to the more common meaning of the term "chirality", which refers to a distinction between "left" and "right" particles. The model takes then the form of the euclidean version of $1+1$ theory of massless Dirac fermions coupled to a gauge field. Indeed, according to (6.73) the matrices $\sigma_1 \tau_3$ and $\sigma_2 \tau_3$ play the role of Dirac γ-matrices, and the matrix σ_3 determining the C_0-chirality is nothing but γ_5. Depending on further symmetries, three different C_0-chiral models arise:

(i) The only coupling present is $\alpha_\perp$, which corresponds to the random abelian vector potential. In this case the nodes are decoupled, and the Hamiltonian decomposes in two copies of a model of the class AIII. This model has already been mentioned in Sec.VI.G.2.

(ii) If the time-reversal symmetry T_0 is preserved, only the couplings $\beta_\perp$ and $\gamma_\perp$ are allowed, and the problem is in the symmetry class CI. The model describes then fermions coupled to a SU(2) non-abelian gauge field, and is a particular case of analogous SU(N) models.

(iii) All three couplings are present. This describes Dirac fermions coupled to both abelian U(1) and non-abelian SU(2) gauge fields. This model is in the AIII symmetry class.

Remarkably, all these critical C_0-chiral models are exactly solvable: one can calculate exactly the spectra of multifractal exponents, the critical index of the DOS, and the value of conductivity. They have been studied in a large number of works, and we summarize the key ideas and results.

b. Abelian vector potential. The model of 2D Dirac fermions moving in a random vector potential,

$$H = v_0 \sigma_\mu (i \partial_\mu - A_\mu) , \tag{6.86}$$

is exactly solvable at zero energy and characterized by a line of fixed points (Ludwig et al., 1994). Decomposing the vector potential in the longitudinal (pure gauge) and transverse parts,

$$A_\nu = \epsilon_{\nu\rho} \partial_\rho \phi(\mathbf{r}) + \partial_\nu \chi(\mathbf{r}) , \tag{6.87}$$

and assuming that the total magnetic flux is zero[12], one can explicitly write the zero-energy wave functions (Castillo *et al.*, 1997; Ludwig *et al.*, 1994):

$$\Psi_+(\mathbf{r}) = \begin{pmatrix} 0 \\ \psi_+(\mathbf{r}) \end{pmatrix} ; \qquad \Psi_-(\mathbf{r}) = \begin{pmatrix} \psi_-(\mathbf{r}) \\ 0 \end{pmatrix} ; \quad (6.88)$$

$$\psi_\pm(\mathbf{r}) = B_\pm^{-1/2} e^{-i\chi(\mathbf{r})} e^{\pm\phi(\mathbf{r})} , \qquad (6.89)$$

where $B_\pm = \int d^2r e^{\pm 2\phi(\mathbf{r})}$ is the normalization factor. We consider the first of the functions (6.88) for definiteness and analyze the statistical properties of $|\psi_+(\mathbf{r})|^2$. They are governed by fluctuations of $\phi(\mathbf{r})$. Assuming a white-noise distribution of the random vector potential with $\langle A_\mu(\mathbf{r}))A_\nu(\mathbf{r}')\rangle = 2\pi g_A \delta_{\mu\nu}\delta(\mathbf{r}-\mathbf{r}')$, one gets the following statistics of $\phi(\mathbf{r})$,

$$\mathcal{P}[\phi] \propto \exp\left\{\frac{-1}{4\pi g_A} \int d^2\mathbf{r}(\nabla\phi)^2\right\} . \qquad (6.90)$$

Equation (6.90) implies that $\phi(\mathbf{r})$ is a free massless bosonic field characterized by the correlation function

$$\langle\phi(\mathbf{r})\phi(\mathbf{r}')\rangle = g_A \ln(L/|\mathbf{r}-\mathbf{r}'|) . \qquad (6.91)$$

c. Multifractality. To find the multifractal spectrum, one considers the moments $\langle|\psi_+(\mathbf{r})|\rangle^{2q}$, see Sec. II.C.1. For not too strong disorder ($g_A \leq 1$), it turns out to be sufficient to average separately the exponential $e^{2q\phi(\mathbf{r})}$ and each of the q normalization factors $\int d^2\mathbf{r} e^{\pm 2\phi(\mathbf{r})}$. The resulting spectrum (Ludwig *et al.*, 1994)

$$\tau_q = 2(q-1)(1-g_A q) \qquad (6.92)$$

has an exactly parabolic form. The corresponding $f(\alpha)$ spectrum is given by Eq. (2.37) with $d = 2$, $\gamma = 2g_A$:

$$f(\alpha) = 2 - (\alpha - 2 - 2g_A)^2/8g_A . \qquad (6.93)$$

In view of the exact parabolicity, the spectrum necessarily contains a termination point at $\alpha = 0$, see Sec. II.C.7. The corresponding value of q is $q_c = (1 + g_A)/2g_A$. Thus, Eq. (6.92) is only valid for $q \leq q_c$; for larger q the exponent τ_q saturates at a constant value, $\tau_{q \geq q_c} = -f(0) = (1-g_A)^2/2g_A$. It is worth recalling that we consider the spectrum describing the ensemble-averaged IPRs, $\langle P_q \rangle$, see Sec. II.C.5. If one looks at the scaling of the typical IPR, P_q^{typ}, the information about rare events encoded in the part of the spectrum with $f(\alpha) < 0$ gets lost, and only the range $\alpha_+ < \alpha < \alpha_-$ is probed, where $\alpha_\pm = 2(g_A^{1/2} \mp 1)^2$. The corresponding τ_q^{typ} spectrum reproduces τ_q in the range $q_- < q < q_+$, where

$q_\pm = g_A^{-1/2}$, and becomes linear outside this range, see Eq. (2.42). This behavior was found for the random vector potential problem in de C. Chamon *et al.* (1996); Carpentier and LeDoussal (2001); Castillo *et al.* (1997) where the spectrum τ_q^{typ} was studied (in these works the notation q_c is used for our q_+).

d. Freezing. As was found in de C. Chamon *et al.* (1996); Carpentier and LeDoussal (2001); Castillo *et al.* (1997), with increasing disorder the system undergoes a phase transition ("freezing") at $g_A = 1$. In the strong disorder phase, $g_A > 1$, the spectrum takes the form

$$\tau(q) = -2(1 - g_A^{1/2}q)^2 , \qquad q < q_c = g_A^{-1/2} ; \quad (6.94)$$

$$f(\alpha) = \alpha(8g_A^{1/2} - \alpha)/8g_A . \qquad (6.95)$$

In this phase $f(0) = 0$, which implies that there is a probability of order unity to find a point in the sample where the wave function is of order unity. Correspondingly, the saturation value of τ_q for $q > q_c$ is $\tau_{q>q_c} = 0$. At first sight, this may seem to imply that the wave functions are localized. The situation is, however, not so simple: a nontrivial multifractal spectrum shows a complex structure of the wave functions. Further, it can be shown that the probability to find a secondary spike in the wave function of approximately the same magnitude as the main one and separated by a distance comparable to the system size L is of order unity (Carpentier and LeDoussal, 2001; Fukui, 2003). The nature of these "quasilocalized" wave functions is therefore similar to that of critical states in 1D systems of chiral symmetry, see Sec. V.E.

e. Density of states. The scaling of the DOS is governed by the dynamical exponent z via

$$\rho(E) \propto E^{(2-z)/z} . \qquad (6.96)$$

In the weak-disorder phase ($g_A < 1$) the value of z is straightforwardly found to be $z = 1 + 2g_A$ (Altland *et al.*, 2002; Ludwig *et al.*, 1994; Nersesyan *et al.*, 1995). However, as was already discussed in Sec. VI.F.2, the freezing has also impact on the dynamical exponent; the value of z in the strong-disorder phase is given by the second line of Eq. (6.70).

f. Non-abelian random gauge field. The problem remains exactly solvable in the case of a SU(N) non-abelian gauge filed. However, in contrast to the abelian case, where one finds a line of fixed points, the theory flows now into an isolated fixed point, which is a WZW theory on the level $k = -2N$ (Caux, 1998; Caux *et al.*, 1998; Mudry *et al.*, 1996; Nersesyan *et al.*, 1995). The spectrum of multifractality is parabolic with $\gamma = (N-1)/N^2$ and is given by Eqs. (6.92), (6.93) with a replacement of $2g_A$ by $(N-1)/N^2$. The DOS is given by Eq. (6.96) with

---

[12] For a nonzero total flux there will be additional zero modes, in view of the Atiyah-Singer index theorem; see, e.g. Aharonov and Casher (1979).

a dynamical exponent $z = 2 - 1/N^2$. In the case $N = 2$ that arises in the two-node model one thus finds $z = 7/4$, yielding the DOS scaling $\rho(E) \propto E^{1/7}$.

When both abelian and non-abelian random gauge fields are present, they contribute additively to the exponents (in the non-frozen regime), as the two sectors of the theory decouple. This yields (Mudry *et al.*, 1996) the multifractal scaling (6.92), (6.93) with $\gamma = 2g_A \to 2g_A + (N-1)/N^2$ and the DOS scaling (6.96) with $z = 1 + 2g_A + (N^2 - 1)/N^2$.

g. Conductivity. A further remarkable feature of the models with C_0-chiral randomness is the independence of conductivity on the disorder strength. We sketch the proof of this statement given in Ostrovsky *et al.* (2006). The conductivity is given by the Kubo formula

$$\sigma = -\frac{1}{2\pi\hbar} \mathrm{Tr}\Big[j^x(G^R - G^A) j^x(G^R - G^A) \Big] , \quad (6.97)$$

where 'Tr' includes both the matrix trace and the spatial integration. The chiral symmetry implies the identity

$$\sigma_3 G^{R(A)}(E)\sigma_3 = -G^{A(R)}(-E) , \quad (6.98)$$

allowing one to trade all advanced Green functions in Eq. (6.97) for retarded ones and thus to present the conductivity at zero energy in terms of retarded Green functions. Further, in view of the Dirac character of the spectrum, the components of the current operator are related via

$$\sigma_3 j^x = -j^x \sigma_3 = i j^y . \quad (6.99)$$

By making use of Eqs. (6.98) and (6.99) the Kubo formula can be cast in the following form:

$$\sigma(E = 0) = -\frac{1}{\pi\hbar} \sum_{\alpha = x,y} \mathrm{Tr}\Big[j^\alpha G^R j^\alpha G^R \Big]. \quad (6.100)$$

At first glance, this expression may be thought to be zero due to gauge invariance. Indeed, the right-hand side of Eq. (6.100) is proportional to the second derivative of the partition function $Z[\mathbf{A}] = \mathrm{Tr}\log G^R[\mathbf{A}]$ (or, equivalently, first derivative of the current $\mathrm{Tr}\,j^\alpha G^R[\mathbf{A}]$) with respect to the constant vector potential $\mathbf{A}$. The gauge invariance implies that a constant vector potential does not affect gauge-invariant quantities like the partition function or the current, so that the derivative is zero. This argument is, however, not fully correct, in view of a quantum anomaly. The elimination of $\mathbf{A}$ amounts technically to a shift in the momentum space $\mathbf{k} \to \mathbf{k} - e\mathbf{A}$, which naively does not change the momentum integral. If we consider a formal expansion in the disorder strength, this argument will indeed hold for all terms involving disorder but not for the zero-order contribution. The momentum integral $\int d^2k\,\mathrm{Tr}\,j^\alpha G_0^R(\mathbf{k})$ is ultraviolet-divergent and the shift of variable is illegitimate. This anomaly was first identified in Schwinger (1962) for $1 + 1$-dimensional massless Dirac fermions. In the Schwinger model, the polarization

operator is not affected by an arbitrary external vector potential $\mathbf{A}(x, t)$ and is given by the anomalous contribution, yielding a photon mass in the $1 + 1$ electrodynamics (Peskin and Schroeder, 1995; Schwinger, 1962). In the present context, the role of $\mathbf{A}(x, t)$ is played by the chiral disorder. The explicit calculation of the zero-order (disorder-free) diagram yields (including a factor of two accounting for spin)

$$\sigma = -\frac{8e^2 v_0^2}{\pi\hbar} \int \frac{d^2k}{(2\pi)^2} \frac{\delta^2}{(v_0^2 k^2 + \delta^2)^2} = \frac{4e^2}{\pi h}. \quad (6.101)$$

Therefore, the dimensionless conductivity acquires the universal value $4/\pi$, with no corrections at any order in the disorder strength. This result was earlier obtained in Ludwig *et al.* (1994) for the abelian case and in Tsvelik (1995) for a certain model of non-abelian gauge field.

4. Disorders preserving C_z chirality: Gade-Wegner criticality

Let us now turn to the disorder which preserves the C_z-chirality, $H = -\sigma_3\tau_3 H\sigma_3\tau_3$; according to Table V, the corresponding coupling constants are β_0, $\alpha_\perp$, $\gamma_\perp$ and β_z. If no time-reversal symmetries are preserved, the system belongs to the chiral unitary (AIII) class. The combination of C_z-chirality and the time reversal invariance T_0 (only couplings $\gamma_\perp$ and β_z are present) corresponds the chiral orthogonal symmetry class BDI; this model has already been discussed in Sec. VI.F.2. Finally, the combination of C_z-chirality and T_z-symmetry (couplings $\gamma_\perp$ and β_0) falls into the chiral symplectic symmetry class CII. The RG flow and DOS in these models have been analyzed in Guruswamy *et al.* (2000) in notations $g_A = \gamma_\perp/2$, $g_m = \beta_z/2$, $g_\mu = \beta_0/2$, $g_{A'} = \alpha_\perp/2$. . In all the cases, the resulting theory is of the Gade-Wegner type, see Sec. VI.F.

In contrast to random gauge field models (C_0 chirality), the proof of the universality of the conductivity based on gauge-invariance argument does not apply to models with C_z chirality. Nevertheless, the zero-energy conductivity is found to have the same universal value, $\sigma = 4e^2/\pi h$, in the limit of weak disorder (Ostrovsky *et al.*, 2006; Ryu *et al.*, 2007a). In this case, however, there are corrections to this value perturbative in the disorder strength. In particular, the leading correction is found in the second order (Ostrovsky *et al.*, 2006), $\delta\sigma^{(2)} = (e^2/\pi h)(\beta_0 - \beta_z)^2$.

The following comment (applicable both to C_0 and C_z chiral models) on the infrared regularization of the problem is in order here. This role is played in Eq. (6.101) by δ, which is an infinitesimal imaginary part in the denominator of the Green function. Physically, it has a meaning of the inverse electron lifetime or, alternatively, a dephasing rate, and can be thought of as modelling processes of escape of electrons in some reservoir or some dephasing mechanism. As discussed in Ostrovsky *et al.* (2006), for a different type of the infrared regularizations (i.e.

by finite frequency) the critical conductivity will take a different value, while still being of order e^2/h.

5. Dirac Hamiltonians for dirty d-wave superconductors.

We briefly discuss the application of Dirac fermion theory to disordered d-wave spin-singlet superconductors with $d_{x^2-y^2}$ symmetry. In such systems the superconducting gap vanishes at four points in the Brillouin zone, and the dispersion relation near these points of the Dirac type. One is thus led to analyze the low-energy physics of the problem in terms of a four-flavor Dirac Hamiltonian. The investigation of symmetries of this problem in the presence of different types of impurities and the corresponding RG treatment were pioneered in Nersesyan *et al.* (1995); for a recent detailed analysis the reader is referred to Altland *et al.* (2002). The main physical quantity of interest for this problem is the low-energy behavior of DOS.

Following Altland *et al.* (2002); Nersesyan *et al.* (1995), we specialize on potential disorder, assume that the spin-rotation invariance is preserved, but allow for a possibility of time-reversal symmetry breaking (i.e. by magnetic field in vortices in type-II superconductors). In full analogy with the two-flavor model, Sec. VI.G.1, it is crucially important, whether the disorder couples the nodes or not. Depending on the range of disorder and the interval of energies considered, one can distinguish three different situations:

(i) short-range disorder: all four nodes are coupled;

(ii) long-range disorder: inter-node scattering is negligible, and the nodes are decoupled. The problem acquires then a single-node character;

(iii) each node is coupled to the opposite one but not to the other two. The system then decomposes in two parts – each of them describing a pair of the oppositely located nodes. It was shown in Nersesyan *et al.* (1995) that, in view of strong anisotropy of the nodal Dirac Hamiltonians, there is an intermediate energy range where this model becomes physically justified.

Combining these three types of disorder with possibilities of preserved or broken time-reversal invariance, one gets six distinct models. Their symmetries, emerging types of criticality, and the corresponding behavior of DOS are summarized in Table VII. When all four nodes are coupled, the system is in the conventional localized regime of symmetry classes CI and C describing spin-singlet superconductors (Senthil and Fisher, 1999; Senthil *et al.*, 1998). When only the opposite nodes are coupled, the T-invariant problem becomes a model of non-abelian random gauge field, and the theory acquires the WZ term, leading to the $E^{1/7}$ scaling of the DOS, see Sec. VI.G.3. For broken T-invariance, the two-node problem is described by the class-C σ-model with the $\theta = \pi$ topological term, i.e. it is in the SQH transition universality class, Sec. VI.D. The DOS scales as $E^{1/7}$ in this case as well. Finally, when the nodes are completely

nodes coupled	T	Class	Criticality	DOS
1	+	AIII	WZW	$|E|^{(1-2g_A)/(1+2g_A)}$
2	+	CI	WZW	$|E|^{1/7}$
4	+	CI	—	$|E|$
1	−	A	θ-term	non-critical
2	−	C	θ-term	$|E|^{1/7}$
4	−	C	—	E^2

TABLE VII Criticality and DOS in d-wave superconductors with preserved spin rotation invariance and different types of randomness. First column: number of nodes coupled. Second column: presence or absence of time-reversal invariance. Third column: symmetry class. Fourth column: type of criticality. Fifth column: low-energy scaling of DOS.

decoupled, the Hamiltonian for each of them takes the form analyzed in Sec. VI.G.2. More specifically, when T-invariance is preserved, the problem reduces to the class-AIII model of random (abelian) vector potential, Sec. VI.G.3, with the DOS following the non-universal power law (6.96), $\rho(E) \sim |E|^{(1-2g_A)/(1+2g_A)}$. In the case of broken T-invariance, the problem belongs to the class A and is described by the Pruisken σ-model with topological term, i.e. it is in the universality class of the IQH critical point. In the latter situation, the DOS is uncritical.

We also mention two further types of disorder that have been studied in detail in the literature. In the case of magnetic impurities botn T-invariance and spin rotation symmetry are broken and thus the system belongs to class D (Bocquet *et al.*, 2000; Senthil and Fisher, 2000), see Sec. VI.E. For the case of perfect nesting, where the chemical potential μ=0, and very strong potential scatterers one encounters the symmetry class AIII leading to the Gade phase (Altland, 2002).

VII. CONCLUDING REMARKS

This concludes our review of physics of Anderson transitions between localized and metallic phases in disordered electronic systems and of associated critical phenomena. In our opinion, during the recent years a quite detailed understanding of these transtions has emerged, including such salient features as symmetry and topology classification, mechanisms of criticality in quasi-1D and 2D systems, and wavefunction multifractality. We have attempted to give a systematic exposition of these issues and hope that this will help interested researchers to navigate in this remarkably rich field.

For several reasons (including limits in space, time, and – last but not least – our expertise), we were not able to discuss all aspects of the problem. The selection of material in the review certainly reflects the authors' personal perspective of the field. We apologize to all researchers whose work is not sufficiently discussed in the

review. Probably, the most important issue out of those that we largely left apart in the review is the effects of electron-electron interactions. (We only briefly discussed it in Sec. VI.C in the context of the IQH transition.) This by itself is a very rich and complicated problem; we restrict ourselves to just a few remarks and references.

A. A few words about interaction effects

Physically, the impact of interaction effects onto low-temperature transport and localization in disordered electronic systems can be subdivided into two distinct effects: (i) renormalization and (ii) dephasing.

a. Renormalization. The renormalization effects, which are governed by virtual processes, become increasingly more pronounced with lowering temperature. The importance of such effects in diffusive low-dimensional systems was demonstrated in by Altshuler and Aronov, see the review (Altshuler and Aronov, 1984). To resum the arising singular contributions, Finkelstein developed the RG approach based on the σ-model for an interacting system, see Finkelstein (1990) for a review. This made possible an analysis of the critical behavior at the localization transition in $2 + \epsilon$ dimensions in the situations when spin-rotation invariance is broken (by spin-orbit scattering, magnetic field, or magnetic impurities). However, in the case of preserved spin-rotation symmetry it was found that the strength of the interaction in spin-triplet channel scales to infinity at certain RG scale. This was interpreted as some kind of magnetic instability of the system; for a detailed exposition of proposed scenarios see the review (Belitz and Kirkpatrick, 1994).

Recently, the problem has attracted a great deal of attention in connection with experiments on high-mobility low-density 2D electron structures (Si MOSFETs) giving an evidence in favor of a metal-insulator transition (Abrahams *et al.*, 2001). Whether these results are due to a true metallic phase existing in these systems or, else, are explained by interaction effects at intermediate ("ballistic") temperatures remains a debated issue. In a recent work (Punnoose and Finkel'stein, 2005) the RG for σ-model for interacting 2D electrons with a number of valleys $N > 1$ was analyzed on the two-loop level. It was shown that in the limit of large number of valleys N (in practice, $N = 2$ as in Si is already sufficient) the temperature of magnetic instability is suppressed down to unrealistically low temperatures, and a metal-insulator transition emerges.

The interaction-induced renormalization effects become extremely strong for correlated 1D systems (Luttinger liquids). While 1D systems provide a paradigmatic example of strong Anderson localization, a sufficiently strong attractive interaction can lead to delocalization in such systems. An RG treatment of the corresponding localization transition in a disordered interacting 1D systems was developed in Giamarchi and Schulz (1988), see also the book (Giamarchi, 2004).

b. Dephasing. We turn now to effects of dephasing governed by inelastic processes of electron-electron scattering at finite temperature T. The dephasing has been studied in great detail for metallic systems where it provides a cutoff for weak localization effects (Altshuler and Aronov, 1984). As to the Anderson transitions, they are quantum (zero-T) phase transitions, and dephasing contributes to their smearing at finite T. This has been discussed in Sec. VI.C.10 in the context of dynamical scaling at the IQH transition. There is, however, an interesting situation when dephasing processes can create a localization transition. We mean the systems where all states are localized in the absence of interaction, such as wires or 2D systems. At high temperatures, when the dephasing is strong, so that the dephasing rate $\tau_\phi^{-1}(T)$ is larger than mean level spacing in the localization volume, the system is a good metal and its conductivity is given by the quasiclassical Drude conductivity with relatively small weak localization correction (Altshuler and Aronov, 1984). With lowering temperature the dephasing gets progressively less efficient, the localization effects proliferate, and eventually the system becomes an Anderson insulator. What is the nature of this state? A natural question is whether the interaction of an electron with other electrons will be sufficient to provide a kind of thermal bath that would assist the variable-range hopping transport (Fleishman *et al.*, 1978), as it happens in the presence of a phonon bath. The answer to this question was given by Fleishman and Anderson (1980), and it is negative. Fleishman and Anderson found that at low T the interaction of a "short-range class" (which includes a finite-tange interaction in any dimensionality d and Coulomb interaction in $d < 3$) is not sufficient to delocalize otherwise localized electrons, so that the conductivity remains strictly zero. In combination with the Drude conductivity at high-T this implies the existence of transition at some temperature T_c.

This conclusion was recently corroborated by an analysis (Basko *et al.*, 2006; Gornyi *et al.*, 2005) in the framework of the idea of Anderson localization in Fock space (Altshuler *et al.*, 1997). In these works the temperature dependence of conductivity $\sigma(T)$ in systems with localized states and weak electron-electron interaction was studied. It was found that with decreasing T the system first shows a crossover from the weak-localization regime into that of "power-law hopping" over localized states (where σ is a power-law function of T), and then undergoes a localization transition. The transition is obtained both within a self-consistent Born approximation (Basko *et al.*, 2006) and an approximate mapping onto a model on the Bethe lattice (Gornyi *et al.*, 2005). The latter yields also a critical behavior of $\sigma(T)$ above T_c, which has a characteristic for the Bethe lat-

tice non-power-law form $\ln \sigma(T) \sim (T - T_c)^{-1/2}$, see Sec. II.C.9. Up to now, this transition has not been observed in experiments[13], which indicate instead a smooth crossover from the metallic to the insulating phase with lowering T (Hsu and Valles, 1995; Khavin et al., 1998; Minkov et al., 2007; Van Keuls et al., 1997). The reason for this discrepancy remains unclear. A recent attempt to detect the transition in numerical simulations also did not give a clear confirmation of the theory (Oganesyan and Huse, 2007), possibly because of strong restrictions on the size of an interacting system that can be numerically diagonalized.

B. Experimental studies of localization transitions

Of all the localization transitions, the best studied experimentally is the IQH transition. We have discussed the corresponding experimental findings in Sec. VI.C.10. Its superconducting counterparts (SQH and TQH transitions) have not been observed yet, although several physical realizations of them were proposed, Sec. VI.D.1 and VI.E.1. Much effort has been invested in research on strongly interacting disordered 2D systems in zero magnetic field but it remains controversial whether what is observed there is a true metal-insulator transition, see Sec. VII.A.

Below we briefly review the situation with the experimental observation of the Anderson transition in 3D electronic and optical systems. For electronic systems (doped semiconductors, Sec. VII.B.1) the localization transition has been observed unambiguously. However, a theoretical analysis of the critical behavior is complicated by the presence of Coulomb interaction, which modifies the critical behavior. As a result, one can not expect that the experimentally extracted critical exponents agree with numerical values obtained from computer simulations on non-interacting systems. The localization of light (Sec. VII.B.2) has an advantage in this respect, since the photon-photon interaction is negligibly small. However, it turns out that implementation of sufficiently strong disorder so as to reach the Anderson transition and strong localization of light in 3D is a remarkably complicated endeavor. The second major difficulty is posed by the absorption.

1. Anderson transition in doped semiconductors

The 3D localization transition was extensively studied on doped semiconductor systems, such as Si:P, Si:B,

Si:As, Ge:Sb. In most of the works, samples with a substantial degree of compensation [i.e. acceptors in addition to donors, e.g. Si:(P,B)] were used, which allows one to vary the amount of disorder and the electron concentration independently. On these samples, values of the conductivity exponent s in the vicinity of $s \approx 1$ were reported (Field and Rosenbaum, 1985; Hirsch et al., 1988; Thomas et al., 1982; Zabrodskii and Zinov'eva, 1984) with scattering of values and the uncertainties of the order of 10%. A similar result was obtained for an amorphous material $Nb_x Si_{1-x}$. (Recall that in 3D s is expected to be equal in 3D to the localization length exponent ν according to the scaling relation $s = \nu(d - 2)$)

On the other hand, the early study of the transition in undoped Si:P (Paalanen et al., 1982; Rosenbaum et al., 1983; Thomas et al., 1983) gave an essentially different result, $s \approx 0.5$. A resolution of this discrepancy was proposed in Stupp et al. (1993, 1994) where it was found that the actual critical region in an uncompensated Si:P is rather narrow and that the scaling analysis restricted to this range yields $s \approx 1.3$. A more recent study (Waffenschmidt et al., 1999), which employed uniaxial stress to tune through the transition (as used in Paalanen et al. (1982); Rosenbaum et al. (1983); Thomas et al. (1983)), has essentially confirmed these conclusions, yielding $s = 1.0 \pm 0.1$, in agreement with the values obtained for samples with compensation. Further, in this work dynamical scaling near the transition with varying temperature was demonstrated; the corresponding dynamical exponent was found to be $z = 2.94 \pm 0.3$. Good scaling was also observed in a similar experiment on uncompensated Si:B (Bogdanovich et al., 1999), however with somewhat different critical exponents ($s \approx 1.6$, $z \approx 2$). A possible explanation for this discrepancy is that the temperatures reached in this work were not sufficiently low. Another possibility is that Si:B belongs to a different universality class, in view of stronger spin-orbit scattering.

The fact that the experimental value $s \approx 1$ found in the majority of works differs from what one would expect based on numerical studies for non-interacting systems is not surprising, since the Coulomb interaction affects the critical exponents. For a more detailed discussion of the experimental data and their comparison with theoretical expectations for the Anderson transitions in the presence of Coulomb interaction the reader is refered to Belitz and Kirkpatrick (1994).

2. Anderson localization of light

Experimental efforts to observe the Anderson localization with light turned out to be very challenging. The main difficulty is, that the characteristic signature of wave localization, the exponential decrease $e^{-\xi/L}$ of the transmission with the system size L, is often hard to disentangle from another exponential $e^{-\ell_a/L}$ originating from photon absorption.

---

[13] Of course, in a real system, phonons are always present and provide a bath necessary to support the hopping conductivity at low T, so that there is no true transition. However, when the coupling to phonons is weak, this hopping conductivity will have a small prefactor, yielding a "quasi-transition".

Garcia and Genack (1991); Genack and Garcia (1991) studied the transmission of microwave radiation through a random mixture of aluminum and Teflon spheres inside a copper tube. In the vicinity of the localization transition, they report power law scaling of the effective diffusion constant $D(L) \sim L^{-1}$. The presence of strong absorption in the microwave system, makes it complicated to interpret the data that were reported as evidence for the localization of light.

To diminish photon losses, Wiersma *et al.* (1997) used a powder from μm gallium arsenide crystals employing near infrared radiation. However, still the exponential signal of localization reported in this work is not undisputed, again due to the presence of residual absorption (Scheffold *et al.*, 1999). A similar study in silicon powders did not show any hint of localization (Rivas *et al.*, 1999).

In order to overcome the notorious problem of separating localization from absorption, an interesting proposal has been made by Chabanov *et al.* (2000). Localization is accompanied by very large mesoscopic fluctuations in the spectral function which carry over also to the frequency dependent transmission function $T(\omega)$. Hence, the measurement of the statistical properties of $T(\omega)$, e.g. its variance, could provide a sensitive means to uncover quantum interference effects. Using this method the authors were able to confirm localization in quasi-one-dimensional waveguides; an application to a three-dimensional system, a mixture of aluminum spheres, did not show signatures of strong localization.

To summarize, up to now there does not seem to be a convincing demonstration for the Anderson localization and transition in 3D systems. However, in very recent work Störzer *et al.* (2006) report the observation of an anomalous time dependency of the light diffusion in a TiO_2 powder indicating the vicinity of the Anderson critical point. Another very promising research direction has appeared with the advent of photonic crystals (Busch *et al.*, 2007), where in the presence of disorder a localization transition should take place for states near a photonic band edge (Busch and John, 1999; John, 1984, 1987).

VIII. ACKNOWLEDGMENTS

References

Abou-Chacra, R., P. W. Anderson, and D. J. Thouless, 1973, J. Phys. C **6**, 1734.

Abou-Chacra, R., and D. J. Thouless, 1974, J. Phys. C **7**, 65.

Abrahams, E., P. W. Anderson, D. C. Licciardello, and T. V. Ramakrishnan, 1979, Phys. Rev. Lett. **42**, 673.

Abrahams, E., S. V. Kravchenko, and M. P. Sarachik, 2001, Rev. Mod. Phys. **73**, 251.

Aharonov, Y., and A. Casher, 1979, Phys. Rev. A **19**, 2461.

Aleiner, I. L., and K. B. Efetov, 2006, Phys. Rev. Lett. **97**, 236801.

Altland, A., 2002, Phys. Rev. B **65**, 104525.

Altland, A., 2007, Phys. Rev. Lett. **97**, 236802.

Altland, A., and B. Simons, 2006, *Condensed Matter Field Theory* (Cambridge University Press).

Altland, A., and B. D. Simons, 1999, Nucl. Phys. B **562**, 445.

Altland, A., B. D. Simons, and M. R. Zirnbauer, 2002, Phys. Rep. **359**, 283.

Altland, A., and M. R. Zirnbauer, 1997, Phys. Rev. B **55**, 1142.

Altshuler, B. L., and A. A. Aronov, 1984, in *Electron-Electron Interaction in Disordered Systems*, edited by M. Pollak and A. Efros, p. 1.

Altshuler, B. L., Y. Gefen, A. Kamenev, and L. S. Levitov, 1997, Phys. Rev. Lett. **78**, 2803.

Altshuler, B. L., V. E. Kravtsov, and I. V. Lerner, 1986, Sov. Phys. JETP **64**, 1352.

Anderson, P. W., 1958, Phys. Rev. **109**, 1492.

Ando, T., 1989, Phys. Rev. B **40**, 5325.

Ando, T., and H. Suzuura, 2002, J. Phys. Soc. Jpn **71**, 2753.

Asada, Y., K. Slevin, and T. Ohtsuki, 2002, Phys. Rev. Lett. **89**, 256601.

Asada, Y., K. Slevin, and T. Ohtsuki, 2004, Phys. Rev. B **70**, 035115.

Balatsky, A. V., 1998, Phys. Rev. Lett. **80**, 1972.

Balents, L., and M. P. A. Fisher, 1997, Phys. Rev. B **56**, 12970.

Baranov, M. A., I. S. Burmistrov, and A. M. M. Pruisken, 2002, Phys. Rev. B **66**, 075317.

Bardarson, J. H., J. Tworzydlo, P. W. Brouwer, and C. W. J. Beenakker, 2007, arXiv:0705.0886 .

Basko, D. M., I. L. Aleiner, and B. L. Altshuler, 2006, Ann. Phys. (N.Y.) **321**, 1126.

Beamond, E. J., J. Cardy, and J. T. Chalker, 2002, Phys. Rev. B **65**, 214301.

Beenakker, C. W. J., 1997, Rev. Mod. Phys. , 731.

Belitz, D., and T. Kirkpatrick, 1994, Rev. Mod. Phys. **66**.

Berezinsky, V. L., 1974, Sov. Phys. JETP **38**, 620.

Bernard, D., and A. LeClair, 2001, Phys. Rev. B **64**, 045306.

Bernard, D., and A. LeClair, 2002a, J. Phys. A **35**, 2555.

Bernard, D., and A. LeClair, 2002b, Nucl. Phys. B **628**, 442.

Bernevig, B. A., T. L. Hughes, and S.-C. Zhang, 2006, Science **314**, 1757.

Bhaseen, M. J., I. I. Kogan, O. A. Soloviev, N. Taniguchi, and A. M. Tsvelik, 2000, Nucl. Phys. B **580**, 688.

Bocquet, M., and J. T. Chalker, 2003, Phys. Rev. B **67**, 054204.

Bocquet, M., D. Serban, and M. R. Zirnbauer, 2000, Nucl. Phys. B **578**, 628.

Bogdanovich, S., M. P. Sarachik, and R. N. Bhatt, 1999, Phys. Rev. Lett. **82**, 137.

Bouchaud, J. P., and A. Georges, 1990, Phys. Rep. **195**, 127.

Brezin, E., and S. Hikami, 1997, Phys. Rev. B **55**, R10169.

Brouwer, P. W., and K. Frahm, 1996, Phys. Rev. B **53**, 1490.

Brouwer, P. W., A. Furusaki, I. A. Gruzberg, and C. Mudry, 2000a, Phys. Rev. Lett. **85**, 1064.

Brouwer, P. W., A. Furusaki, and C. Mudry, 2003, Phys. Rev. B **67**, 014530.

Brouwer, P. W., C. Mudry, and A. Furusaki, 2000b, Nucl. Phys. B **565** [**FS**], 653.

Brouwer, P. W., C. Mudry, B. D. Simons, and A. Altland, 1998, Phys. Rev. Lett. **81**, 862.

Bundschuh, R., C. Cassanello, D. Serban, and M. R. Zirnbauer, 1998, Nucl. Phys. B **532**, 689.

Burmistrov, I., 2006, PhD thesis, Amsterdam, URL http://dare.uva.nl/document/23446.

Busch, K., G. von Freymann, S. Linden, S. F. Mingaleev, L. Tkeshelashvili, and M. Wegener, 2007, Phys. Rep. **444**, 101.

Busch, K., and S. John, 1999, Phys. Rev. Lett. **83**, 967.

de C. Chamon, C., C. Mudry, and X.-G. Wen, 1996, Phys. Rev. Lett. **77**, 4194.

Cardy, J., 2000, Phys. Rev. Lett. **84**, 3507.

Carpentier, D., and P. LeDoussal, 1999, Nucl. Phys. B **588**, 565.

Carpentier, D., and P. LeDoussal, 2001, Phys. Rev. E **63**, 026110.

Caselle, M., and U. Magnea, 2004, Phys. Rep. **394**, 41.

Caselle, M., and U. Magnea, 2006, J. Stat. Mech. **0601**, P013.

Castellani, C., and L. Peliti, 1986, J. Phys. A: Math. Gen. **19**, L429.

Castilla, G. E., and S. Chakravarty, 1993, Phys. Rev. Lett. **71**, 384.

Castillo, H. E., C. de C. Chamon, E. Fradkin, P. M. Goldbart, and C. Mudry, 1997, Phys. Rev. B **56**, 10668.

Caux, J.-S., 1998, Phys. Rev. Lett. **81**, 4196.

Caux, J.-S., N. Taniguchi, and A. M. Tsvelik, 1998, Nucl. Phys. B **525**, 621.

Chabanov, A. A., M. Stoytchev, and A. Z. Genack, 2000, Nature **404**, 850.

Chalker, J. T., and P. D. Coddington, 1988, J. Phys. C **21**, 2665.

Chalker, J. T., N. Read, V. Kagalovsky, B. Horovitz, Y. Avishai, and A. W. W. Ludwig, 2002, Phys. Rev. B **65**, 012506.

Chayes, J. T., L. Chayes, D. S. Fisher, and T. Spencer, 1986, Phys. Rev. Lett. **57**, 299.

Cho, S., and M. P. A. Fisher, 1997a, Phys. Rev. B **55**, 1025.

Cho, S., and M. P. A. Fisher, 1997b, Phys. Rev. B **55**, 1637.

Cuevas, E., 2003a, Phys. Rev. B **68**, 024206.

Cuevas, E., 2003b, Phys. Rev. B **68**, 184206.

Cuevas, E., 2005, Phys. Rev. B **71**, 024205.

Cuevas, E., M. Ortuno, V. Gasparian, and A. Perez-Garrido, 2002, Phys. Rev. Lett. **88**, 016401.

Cui, Q., X. Wan, and K. Yang, 2004, Phys. Rev. B **70**, 094506.

Derkachov, S. E., and A. N. Manashov, 1997, Phys. Rev. Lett. **79**, 1423.

Dorokhov, O. N., 1982, JETP Lett. **36**, 318.

Dotsenko, V. S., and V. S. Dotsenko, 1983, Advances in Physics **32**(2), 129.

Duplantier, B., and A. W. W. Ludwig, 1991, Phys. Rev. Lett. **66**, 247.

Dyson, F., 1953, Phys. Rev. **92**, 1331.

Dyson, F. J., 1962, J. Math. Phys. **3**, 140, 1199.

Efetov, K. B., 1983, Adv. Phys. **32**, 53.

Efetov, K. B., 1985, Sov. Phys. JETP **61**, 606.

Efetov, K. B., 1987, Sov. Phys. JETP **65**, 360.

Efetov, K. B., 1990, Physica A **167**, 119.

Efetov, K. B., 1997, *Supersymmetry in Disorder and Chaos* (Cambridge University Press).

Efetov, K. B., and A. I. Larkin, 1983, Sov. Phys. JETP **58**, 444.

Efetov, K. B., A. I. Larkin, and D. E. Khmeniskii, 1980, Sov. Phys. JETP **52**, 568.

Engel, L. W., D. Shahar, C. Kurdak, and D. C. Tsui, 1993, Phys. Rev. Lett. **71**, 2638.

Essin, A. M., and J. E. Moore, 2007, arXiv.org:0705.0172 .

Evangelou, S. N., 1995, Phys. Rev. Lett. **75**, 2550.

Evangelou, S. N., and T. Ziman, 1987, J. Phys. C **20**, L235.

Evers, F., 1997, Phys. Rev. E **55**, 2321.

Evers, F., and W. Brenig, 1994, Z. Phys. B **94**, 155.

Evers, F., and W. Brenig, 1998, Phys. Rev. B **57**, 1805.

Evers, F., A. Mildenberger, and A. D. Mirlin, 2001, Phys. Rev. B **64**, R241303.

Evers, F., A. Mildenberger, and A. D. Mirlin, 2003, Phys. Rev. B **67**, 041303.

Evers, F., and A. D. Mirlin, 2000, Phys. Rev. Lett. **84**, 3690.

Fabrizio, M., and C. Castellani, 2000, Nucl. Phys. B **583**, 542.

Fal'ko, V. I., and K. B. Efetov, 1995a, Europhys. Lett. **32**, 627.

Fal'ko, V. I., and K. B. Efetov, 1995b, Phys. Rev. B **53**, 1186.

Fendley, P., 2000, in *Lecture at the NATO Advanced Study Institute/EC Summer School on New Theoretical Approaches to Strongly Correlated Systems* (Cambridge, UK), cond-mat/0006360.

Field, S. B., and T. F. Rosenbaum, 1985, Phys. Rev. Lett. **55**, 522.

Finkelstein, A. M., 1990, Sov. Sci. Rev. A Phys. **14**, 1.

Finkelstein, A. M., 1994, Physica B **197**, 636.

Fisher, D., 1995, Phys. Rev. B **51**, 6411.

Fleishman, L., and P. W. Anderson, 1980, Phys. Rev. B **21**, 2366.

Fleishman, L., D. C. Licciardello, and P. W. Anderson, 1978, Phys. Rev. Lett. **40**, 1340.

Fukui, T., 1999, Nucl. Phys. B **562**, 477.

Fukui, T., 2003, Phys. Rev. B **68**, 153307.

Fyodorov, Y. V., 1995, in *Mesoscopic Quantum Physics (Les Houches 1994)*, edited by E. Akkermans, G. Montambaux, J.-L. Pichard, and J. Zinn-Justin (North-Holland, Amsterdam), p. 493.

Fyodorov, Y. V., 2003, JETP Lett. **78**, 250.

Fyodorov, Y. V., and A. D. Mirlin, 1994, Int. Journ. Mod. Phys. B **8**, 3795.

Fyodorov, Y. V., and A. D. Mirlin, 1995, Phys. Rev. B **51**, 13403.

Fyodorov, Y. V., A. D. Mirlin, and H.-J. Sommers, 1992, J. Phys. I France **2**, 1571.

Fyodorov, Y. V., and H.-J. Sommers, 1997, J. Math. Phys. **38**, 1918.

Gade, R., 1993, Nucl. Phys. B **398**, 499.

Gade, R., and F. Wegner, 1991, Nucl. Phys. B **360**, 213.

Gammel, B. M., and W. Brenig, 1994, Phys. Rev. Lett. **73**, 3286.

Gammel, B. M., and W. Brenig, 1996, Phys. Rev. B **53**, R13279.

Gammel, B. M., and F. Evers, 1998, Phys. Rev. B **57**, 14829.

Garcia, N., and A. Z. Genack, 1991, Phys. Rev. Lett. **66**(14), 1850.

Garcia-Garcia, A. M., 2006, Phys. Rev. E **73**, 026213.

Garcia-Garcia, A. M., and E. Cuevas, 2006, cond-mat/0612454 .

Garcia-Garcia, A. M., and K. Takahashi, 2004, Nucl. Phys. B **700**, 361.

Genack, A. Z., and N. Garcia, 1991, Phys. Rev. Lett. **66**(16), 2064.

Giamarchi, T., 2004, *Quantum Physics in One Dimension* (Oxford University Press, Oxford, 2004).

Giamarchi, T., and H. Schulz, 1988, Phys. Rev. B **37**, 325.

Girvin, S. M., and M. Jonson, 1980, Phys. Rev. B **22**, 3583.

Gopar, V. A., K. A. Muttalib, and P. Wölfle, 2002, Phys. Rev. B **66**, 174204.

Gor'kov, L. P., A. I. Larkin, and D. Khmel'nitskii, 1979, JETP Lett. **30**, 248.

Gornyi, I. V., A. D. Mirlin, and D. G. Polyakov, 2005, Phys. Rev. Lett. **95**, 206603.

Gruzberg, I. A., N. Read, and A. W. W. Ludwig, 1999, Phys. Rev. Lett. **82**, 4524.

Gruzberg, I. A., N. Read, and S. Vishveshwara, 2005, Phys. Rev. B **71**, 245124.

Guhr, T., A. Müller-Gröling, and H. A. Weidenmüller, 1998, Phys. Rep. **299**, 189.

Guruswamy, S., A. LeClair, and A. W. W. Ludwig, 2000, Nucl. Phys. B **583**, 475.

Haldane, F. D. M., and E. H. Rezayi, 1988, Phys. Rev. Lett. **60**, 956, 1886 (E).

Halsey, T. C., M. H. Jensen, L. P. Kadanoff, I. Procaccia, and B. I. Shraiman, 1986, Phys. Rev. A **33**, 1141.

Hatsugai, Y., X.-G. Wen, and M. Kohmoto, 1997, Phys. Rev. B **56**, 1061.

Heinzner, P., A. Huckleberry, and M. R. Zirnbauer, 2005, Commun. Math. Phys. **257**, 725.

Helgason, S., 1978, *Differential Geometry, Lie Groups, and Symmetric Spaces* (Academic Press, New York).

Hikami, S., 1981, Phys. Lett. **98B**, 208.

Hikami, S., 1983, Nucl. Phys. B **215 [FS7]**, 555.

Hirsch, M. J., U. Thomanschefsky, and D. F. Holcomb, 1988, Phys. Rev. B **37**, 8257.

Ho, C.-M., and J. T. Chalker, 1996, Phys. Rev. B **54**, 8708.

Hohls, F., U. Zeitler, and R. J. Haug, 2001, Phys. Rev. Lett. **86**, 5124.

Hohls, F., U. Zeitler, and R. J. Haug, 2002a, Phys. Rev. Lett. **88**, 036802.

Hohls, F., U. Zeitler, R. J. Haug, R. Meisels, K. Dybko, and F. Kuchar, 2002b, Phys. Rev. Lett. **89**, 276801.

Horovitz, B., and P. LeDoussal, 2002, Phys. Rev. B **65**, 125323.

Hsu, S.-Y., and J. M. Valles, Jr., 1995, Phys. Rev. Lett. **74**, 2331.

Huckestein, B., 1995, Rev. Mod. Phys. **67**, 357.

Huckestein, B., and B. Kramer, 1990, Phys. Rev. Lett. **64**, 1437.

Huckestein, B., B. Kramer, and L. Schweitzer, 1992, Surf. Sci. **263**, 125.

Huo, Y., R. E. Hetzel, and R. N. Bhatt, 1993, Phys. Rev. Lett. **70**, 481.

Isichenko, M. B., 1992, Rev. Mod. Phys. **64**, 961.

Ivanov, D. A., 2002a, in *Vortices in Unconventional Superconductors and Superfluids*, edited by R. P. Huebener, N. Schopol, and G. E. Volovik, p. 253.

Ivanov, D. A., 2002b, J. Math. Phys. **43**, 126.

Janßen, M., 1994, Int. J. Mod. Phys. B **8**, 943.

Janßen, M., 1998, Phys. Rep. **295**, 1.

Janßen, M., M. Metzler, and M. R. Zirnbauer, 1999, Phys. Rev. B **59**, 15836.

John, S., 1984, Phys. Rev. Lett. **53**, 2169.

John, S., 1987, Phys. Rev. Lett. **58**, 2486.

Jüngling, K., and R. Oppermann, 1980, Z. Phys. B **38**, 93.

Kagalovsky, V., B. Horovitz, Y. Avishai, and J. T. Chalker, 1999, Phys. Rev. Lett. **82**, 3516.

Kane, C. L., and E. J. Mele, 2005a, Phys. Rev. Lett. **95**, 226801.

Kane, C. L., and E. J. Mele, 2005b, Phys. Rev. Lett. **95**, 146802.

Khavin, Y. B., M. E. Gershenson, and A. L. Bogdanov, 1998, Phys. Rev. B **58**, 8009.

Khmelnitskii, D. E., 1984, JETP Lett. **38**, 552.

Khveshchenko, D. V., 2006, Phys. Rev. Lett. **97**, 036802.

Klesse, R., and M. Metzler, 1995, Europhys. Lett. **32**, 229.

Klesse, R., and M. Zirnbauer, 2001, Phys. Rev. Lett. **86**(10), 2049.

v. Klitzing, K., G. Dorda, and M. Pepper, 1980, Phys. Rev. Lett. **45**, 494.

Koch, S., R. J. Haug, K. v. Klitzing, and K. Ploog, 1991, Phys. Rev. Lett. **67**, 883.

Kogan, I. I., C. Mudry, and A. M. Tsvelik, 1996, Phys. Rev. Lett. **77**, 707.

Kondev, J., and J. B. Marston, 1997, Nucl. Phys. B **497**, 639.

Kottos, T., 2005, J. Phys. A: Math. Gen. **38**, 10761.

Kramer, B., and A. MacKinnon, 1993, Rep. Prog. Phys. **56**, 1469.

Kramer, B., T. Ohtsuki, and S. Kettemann, 2005, Phys. Rep. **417**, 211.

Kratzer, P., and W. Brenig, 1994, Z. Phys. B **94**, 147.

Kravtsov, V. E., I. V. Lerner, and V. I. Yudson, 1988, Sov. Phys. JETP **67**, 1441.

Kravtsov, V. E., and K. A. Muttalib, 1997, Phys. Rev. Lett. **79**, 1913.

Kravtsov, V. E., and A. M. Tsvelik, 2000, Phys. Rev. B **62**, 9888.

Kravtsov, V. E., O. Yevtushenko, and E. Cuevas, 2006, J. Phys. A: Math. Gen. **39**, 2021.

Laughlin, R. B., 1998, Phys. Rev. Lett. **80**, 5188.

Lee, D. H., 1994, Phys. Rev. B **50**, 10788.

Lee, D.-H., and Z. Wang, 1996, Phys. Rev. Lett. **76**, 4014.

Lee, P. A., and T. V. Ramakrishnan, 1985, Rev. Mod. Phys. **57**, 287.

Lerner, I. V., and F. Wegner, 1990, Z. Phys. B **81**, 95.

Levine, H., S. B. Libby, and A. M. M. Pruisken, 1983, Phys. Rev. lett. **51**, 1915.

Levitov, L. S., 1990, Phys. Rev. Lett. **64**, 547.

Levitov, L. S., 1999, Ann. Phys. (Leipzig) **8**, 697.

Li, W., G. A. Csathy, D. C. Tsui, L. N. Pfeiffer, and K. W. West, 2005, Phys. Rev. Lett. **94**, 206807.

Ludwig, A. W. W., M. P. A. Fisher, R. Shankar, and G. Grinstein, 1994, Phys. Rev. B **50**, 7526.

Mandelbrot, B. B., 1974, J. Fluid Mech. **62**, 331.

Markos, P., 2006, Acta Phys. Slov. **56**, 561.

Markos, P., and L. Schweitzer, 2006, J. Phys. A: Math. Gen. **39**, 3221.

Markos, P., and L. Schweitzer, 2007, arXiv:0705.0622v2 .

Marston, J. B., and S.-W. Tsai, 1999, Phys. Rev. Lett. **82**, 4906.

Mathur, H., 1997, Phys. Rev. B **56**, 15794.

McCann, E., K. Kechedzhi, V. I. Fal'ko, H. Suzuura, T. Ando, and B. L. Altshuler, 2006, Phys. Rev. Lett. **97**, 146805.

McKenzie, R. H., 1996, Phys. Rev. Lett. **77**, 4804.

Mello, P. A., P. Pereyra, and N. Kumar, 1988, Ann. Phys. (N.Y.) **181**, 290.

Mendez-Bermudez, J. A., and T. Kottos, 2005, Phys. Rev. B **72**, 064108.

Mendez-Bermudez, J. A., and I. Varga, 2006, Phys. Rev. B **74**, 125114.

Merkt, R., M. Janssen, and B. Huckestein, 1998, Phys. Rev. B **58**, 4394.

Merz, F., and J. T. Chalker, 2002, Phys. Rev. B **65**, 054425.

Mildenberger, A., and F. Evers, 2007, Phys. Rev. B **75**, 041303(R).

Mildenberger, A., F. Evers, and A. D. Mirlin, 2002, Phys. Rev. B **66**, 033109.

Mildenberger, A., F. Evers, A. D. Mirlin, and J. T. Chalker, 2007a, Phys. Rev. B **75**, 245321.

Mildenberger, A., F. Evers, R. Narayanan, A. D. Mirlin, and K. Damle, 2006, Phys. Rev. B **73**, 121301(R).

Mildenberger, A., A. R. Subramaniam, R. Narayanan, F. Evers, I. A. Gruzberg, and A. D. Mirlin, 2007b, Phys. Rev. B **75**, 094204.

Mil'nikov, G. V., and I. M. Sokolov, 1988, JETP. Lett. **48**, 536.

Minkov, G. M., A. V. Germanenko, O. E. Rut, A. A. Sherstobitov, and B. N. Zvonkov, 2007, Phys. Rev. B **75**, 235316.

Mirlin, A. D., 2000a, in *New Directions in Quantum Chaos (Proceedings of the International School of Physics "Enrico Fermi" Course CXLIII)*, edited by G. Casati, I. Guarneri, and U. Smilansky (IOS Press, Amsterdam), p. 493.

Mirlin, A. D., 2000b, Phys. Rep. **326**, 259.

Mirlin, A. D., and F. Evers, 2000, Phys. Rev. B **62**, 7920.

Mirlin, A. D., F. Evers, and A. Mildenberger, 2003, J. Phys. A: Math. Gen. **36**, 3255.

Mirlin, A. D., and Y. V. Fyodorov, 1991, Nucl. Phys. B **366**, 507.

Mirlin, A. D., and Y. V. Fyodorov, 1994a, Phys. Rev. Lett. **72**, 526.

Mirlin, A. D., and Y. V. Fyodorov, 1994b, J. Phys. I France **4**, 655.

Mirlin, A. D., Y. V. Fyodorov, F.-M. Dittes, J. Quezada, and T. H. Seligman, 1996, Phys. Rev. E **54**, 3221.

Mirlin, A. D., Y. V. Fyodorov, A. Mildenberger, and F. Evers, 2006, Phys. Rev. Lett. **97**, 046803.

Mirlin, A. D., A. Müller-Groeling, and M. R. Zirnbauer, 1994, Ann. Phys. (N.Y.) **236**, 325.

Moshe, M., H. Neuberger, and B. Shapiro, 1994, Phys. Rev. Lett. **73**, 1497.

Motrunich, O., K. Damle, and D. Huse, 2001, Phys. Rev. B **63**, 224204.

Motrunich, O., K. Damle, and D. A. Huse, 2002, Phys. Rev. B **65**, 064206.

Mudry, C., P. W. Brouwer, and A. Furusaki, 1999, Phys. Rev. B **59**, 13221.

Mudry, C., P. W. Brouwer, and A. Furusaki, 2000, Phys. Rev. B **62**, 8249.

Mudry, C., C. Chamon, and X.-G. Wen, 1996, Nucl. Phys. B **466**, 383.

Mudry, C., S. Ryu, and A. Furusaki, 2003, Phys. Rev. B **64**,

064202.

Muttalib, K. A., Y. Chen, and M. E. H. Ismail, 2001, in *Symbolic Computation, Number Theory, Special Functions, Physics and Combinatorics*, edited by F. G. Garvan and M. E. H. Ismail, p. 199.

Muttalib, K. A., Y. Chen, M. E. H. Ismail, and V. N. Nicopoulos, 1993, Phys. Rev. Lett. **71**, 471.

Muttalib, K. A., and P. Wölfle, 1999, Phys. Rev. Lett. **83**, 3013.

Muttalib, K. A., P. Wölfle, and V. A. Gopar, 2003, Ann. Phys. **308**, 156.

Nelson, K., Z. Mao, Y. Maeno, and Y. Liu, 2004, Science **306**, 1151.

Nersesyan, A. A., A. M. Tsvelik, and F. Wenger, 1995, Nucl. Phys. B **438**, 561.

Nomura, K., M. Koshino, and S. Ryu, 2007, arXiv:0705.1607 .

Nomura, K., and A. H. MacDonald, 2007, Phys. Rev. Lett. **98**, 076602.

Novoselov, K. S., A. K. Geim, S. V. Morozov, D. Jiang, M. I. Katsnelson, I. V. Grigorieva, S. V. Dubonos, , and A. A. Firsov, 2005, Nature **438**, 197.

Novoselov, K. S., A. K. Geim, S. V. Morozov, D. Jiang, Y. Zhang, S. V. Dubonos, I. V. Grigorieva, and A. A. Firsov, 2004, Science **306**, 666.

Obuse, H., A. Furusaki, S. Ryu, and C. Mudry, 2007a, cond-mat/0702199 .

Obuse, H., A. R. Subramaniam, A. Furusaki, I. A. Gruzberg, and A. Ludwig, 2007b, Phys. Rev. Lett. **98**, 156802.

Oganesyan, V., and D. A. Huse, 2007, Phys. Rev. B 75 **75**, 155111.

Ohtsuki, T., K. Slevin, and B. Kramer, 2004, Physica E **22**, 248.

Onoda, M., Y. Avishai, and N. Nagaosa, 2007, Phys. Rev. Lett. **98**, 076802.

Ossipov, A., and Y. V. Fyodorov, 2005, Phys. Rev. B **71**, 125133.

Ostrovsky, P. M., I. V. Gornyi, and A. D. Mirlin, 2006, Phys. Rev. B **74**, 235443.

Ostrovsky, P. M., I. V. Gornyi, and A. D. Mirlin, 2007a, Phys. Rev. Lett. **98**, 256801.

Ostrovsky, P. M., I. V. Gornyi, and A. D. Mirlin, 2007b, cond-mat/0702616 .

Paalanen, M. A., T. F. Rosenbaum, G. A. Thomas, and R. N. Bhatt, 1982, Phys. Rev. Lett. **48**, 1284.

Peskin, M. E., and D. V. Schroeder, 1995, *An Introduction to Quantum Field Theory* (Westview Press).

Polyakov, D. G., and K. V. Samokhin, 1998, Phys. Rev. Lett. **80**, 1509.

Potempa, H., and L. Schweitzer, 2002, Phys. Rev. B **65**, 201105.

Prigodin, V. N., and B. L. Altshuler, 1998, Phys. Rev. Lett. **80**, 1944.

Pruisken, A. M. M., 1984, Nucl. Phys. B **235**, 277.

Pruisken, A. M. M., 1985, Phys. Rev. **32**, 2636.

Pruisken, A. M. M., 1987, in *The Quantum Hall Effect*, edited by R. Prange and S. Girvin.

Pruisken, A. M. M., and I. S. Burmistrov, 2005, Ann. Phys. **316**, 285.

Pruisken, A. M. M., D. T. N. de Lang, L. A. Ponomarenko, and A. de Visser, 2006, Sol. State Comm. **137**, 540.

Punnoose, A., and A. M. Finkel'stein, 2005, Science **310**, 289.

Read, N., and D. Green, 2000, Phys. Rev. B **61**, 10267.

Read, N., and A. W. W. Ludwig, 2001, Phys. Rev. B **63**,

024404.

Rivas, J. G., R. Sprik, C. M. Soukoulis, K. Busch, and A. Lagendijk, 1999, Europhys. Lett. **48**, 22.

Rosenbaum, T. F., R. F. Milligan, M. A. Paalanen, G. A. Thomas, R. N. Bhatt, and W. Lin, 1983, Phys. Rev. B **27**, 7509.

Rycerz, A., J. Tworzydlo, and C. W. J. Beenakker, 2006, cond-mat/0612446 .

Ryu, S., C. Mudry, A. Furusaki, and A. W. W. Ludwig, 2007a, Phys. Rev. B **75**, 205344.

Ryu, S., C. Mudry, H. Obuse, and A. Furusaki, 2007b, cond-mat/0702529 .

Sakai, H., and Y. Takane, 2005, J. Phys. Soc. Jpn. **74**, 1521.

Saleur, H., and B. Duplantier, 1987, Phys. Rev. Lett. **58**, 2325.

Schaefer, L., and F. Wegner, 1980, Z. Phys. B **38**, 113.

van Schaijk, R. T. F., A. de Visser, S. M. Olsthoorn, H. P. Wei, and A. M. M. Pruisken, 2000, Phys. Rev. Lett. **84**, 1567.

Scheffold, F., R. Lenke, R. Tweer, and G. Maret, 1999, Nature **398**, 206.

Schreiber, M., and H. Grussbach, 1996, Phys. Rev. Lett. **76**, 1687.

Schweitzer, L., and P. Markos, 2005, Phys. Rev. Lett **95**, 256805.

Schweitzer, L., and H. Potempa, 1999, Physica A **266**, 486.

Schweitzer, L., and I. K. Zharekeshev, 1997, J. Phys. Condensed Matter **9**, L441.

Schwinger, J., 1962, Phys. Rev. **128**, 2425.

Seiberg, N., 1990, Prog. Theor. Phys. Suppl. **102**, 319.

Senthil, T., and M. P. A. Fisher, 1999, Phys. Rev. B **60**, 6893.

Senthil, T., and M. P. A. Fisher, 2000, Phys. Rev. B **61**, 9690.

Senthil, T., M. P. A. Fisher, L. Balents, and C. Nayak, 1998, Phys. Rev. Lett. **81**, 4704.

Senthil, T., J. B. Marston, and M. P. A. Fisher, 1999, Phys. Rev. B **60**, 4245.

Sheng, L., D. N. Sheng, C. S. Ting, and F. D. M. Haldane, 2005, Phys. Rev. Lett. **95**, 136602.

Slevin, K., and T. Nagao, 1993, Phys. Rev. Lett. **70**, 635.

Slevin, K., and T. Ohtsuki, 1999, Phys. Rev. Lett. **82**, 382.

Störzer, M., P. Gross, C. M. Aegerter, and G. Maret, 2006, Phys. Rev. Lett. **96**, 063904.

Stupp, H., M. Hornung, M. Lakner, O. Madel, and H. v. Löhneysen, 1993, Phys. Rev. Lett. **71**, 2634.

Stupp, H., M. Hornung, M. Lakner, O. Madel, and H. v. Löhneysen, 1994, Phys. Rev. Lett. **72**, 2122.

Subramaniam, A. R., I. A. Gruzberg, A. W. W. Ludwig, F. Evers, A. Mildenberger, and A. D. Mirlin, 2006, Phys. Rev. Lett. **96**, 126802.

Suzuura, H., and T. Ando, 2002, Phys. Rev. Lett. **89**, 266603.

Takane, Y., 2004a, J. Phys. Soc. Jpn. **73**, 9.

Takane, Y., 2004b, J. Phys. Soc. Jpn. **73**, 2366.

Takane, Y., 2004c, J. Phys. Soc. Jpn. **73**, 1430.

Thomas, G. A., Y. Ootuka, S. Katsumoto, S. Kobayashi, and W. Sasaki, 1982, Phys. Rev. B **25**, 4288.

Thomas, G. A., M. Paalanen, and T. F. Rosenbaum, 1983, Phys. Rev. B **27**, 3897.

Thouless, D., 1974, Phys. Rep. **13**, 93.

Titov, M., P. W. Brouwer, A. Furusaki, and C. Mudry, 2001, Phys. Rev. B **63**, 235318.

Tsvelik, A. M., 1995, Phys. Rev. B **51**, 9449.

Tsvelik, A. M., 2007, cond-mat/0702611 .

Van Keuls, F. W., H. Mathur, H. W. Jiang, and A. J. Dahm, 1997, Phys. Rev. B **56**, 13263.

Varga, I., 2002, Phys. Rev. B **66**, 094201.

Verbaarschot, J. J. M., H. A. Weidenmüller, and M. R. Zirnbauer, 1985, Phys. Rep. **129**, 367.

Verbaarschot, J. J. M., and I. Zahed, 1993, Phys. Rev. Lett. **70**, 3852.

de Visser, A., L. A. Ponomarenko, G. Galistu, D. T. N. de Lang, A. M. M. Pruisken, U. Zeitler, and D. Maude, 2006, J. Phys.: Conference Series **51**, 379.

Vollhardt, D., and P. Wölfle, 1980, Phys. Rev. B **22**, 4666.

Waffenschmidt, S., C. Pfleiderer, and H. v. Löhneysen, 1999, Phys. Rev. Lett. **83**, 3005.

Wang, Z., M. P. A. Fisher, S. M. Girvin, and J. T. Chalker, 2000, Phys. Rev. B **61**, 8326.

Wang, Z., B. Jovanovic, and D.-H. Lee, 1996, Phys. Rev. Lett **77**, 4426.

Wang, Z., and S. Xiong, 2002, Phys. Rev. B **65**, 195316.

Wegner, F., 1976, Z.Phys.B **25**, 327.

Wegner, F., 1979, Z. Phys. B **35**, 207.

Wegner, F., 1980, Z. Physik B **36**, 209.

Wegner, F., 1985, in *Localisation and Metal Insulator transitions*, ed. by H. Fritzsche and D. Adler (Plenum, N.Y. 1985) , 337.

Wegner, F., 1987, Nucl. Phys. B **280**, 210.

Wegner, F., 1989, Nucl. Phys. B **316**, 663.

Wegner, F., 1990, Z. Phys. B **78**, 36.

Wei, H. P., D. C. Tsui, M. A. Paalanen, and A. M. M. Pruisken, 1988, Phys. Rev. Lett. **61**, 1294.

Weidenmüller, H., 1987, Nucl. Phys. B **290**, 87.

Wiersma, D. S., P. Bartolini, A. Lagendijk, and R. Righini, 1997, Nature **390**, 671.

Wigner, E. P., 1951, Ann. Math. **53**, 36.

Witten, E., 1984, Commun. Math. Phys. **92**, 455.

Wölfle, P., and R. N. Bhatt, 1984, Phys. Rev. B **30**, 3542.

Yamada, H., and T. Fukui, 2004, Nucl. Phys. B **679**, 632.

Yang, S.-R. E., A. H. MacDonald, and B. Huckestein, 1995, Phys. Rev. Lett. **74**, 3229.

Yevtushenko, O., and V. E. Kravtsov, 2003, J. Phys. A: Math. Gen **36**, 8265.

Yevtushenko, O., and V. E. Kravtsov, 2004, Phys. Rev. E **69**, 026104.

Zabrodskii, A. G., and K. Zinov'eva, 1984, Sov. Phys. JETP **59**, 425.

Zamolodchikov, A. B., and A. B. Zamolodchikov, 1996, Nucl. Phys. B **477**, 577.

Zhang, Y., Y.-W. Tan, H. L. Stormer, , and P. Kim, 2005, Nature **438**, 201.

Ziff, R. M., X. P. Kong, and E. G. D. Cohen, 1991, Phys. Rev. A **44**, 2410.

Zirnbauer, M. R., 1986a, Phys. Rev. B **34**, 6394.

Zirnbauer, M. R., 1986b, Nucl. Phys. B **265**, 375.

Zirnbauer, M. R., 1992, Phys. Rev. Lett. **69**, 1584.

Zirnbauer, M. R., 1994, Ann. Phys. **3**, 513.

Zirnbauer, M. R., 1996, J. Math. Phys. **37**, 4986.

Zirnbauer, M. R., 1997, J. Math. Phys. **38**, 2007.

Zirnbauer, M. R., 1999, hep-th/9905054v2 .

Zirnbauer, M. R., 2004, math-ph/0404057 .